MONTH

ROYAL ASTR L

Geophysical Discussions

of the

ROYAL ASTRONOMICAL SOCIETY

at

Burlington House London, W.1

(Discussions start at $16^h\ 15^m$; tea at $15^h\ 45^m$)

The following discussions have been arranged :

1961 January 27.—The geological time scale.

1961 February 24.—Upper atmospheric ionization and aurorae.

1961 March 24.—Geodetic uses of artificial satellites.

No meeting for the discussion of papers submitted for publication has been arranged for this session. Fellows are reminded, however, that they may ask to read such papers at any ordinary meeting of the Society.

NOTICE TO AUTHORS

Presentation of Papers at Meeting

At some meetings of the Society the background and conclusions of selected papers are presented and then discussed. In order to assist the Secretaries in the selection of papers for such meetings, authors are asked to let the Society know, when submitting papers, whether they would be willing to give an account of their paper, if requested.

The attention of authors resident abroad is drawn to the fact that the Society welcomes information about their work. The Secretaries would be happy to consider having such work described at a meeting, in accordance with the author's wishes, either by a Secretary or other Fellow.

Publication of Papers

1. *General.*—It is the aim of the Society to be of the greatest possible service in disseminating astronomical results and ideas to the scientific community with the utmost possible speed. Contributors are accordingly urged to give the most careful consideration to the presentation of their work, for attention to detail will assuredly result in a substantial saving of time.

It is the practice of the Society to seek a referee's opinion on nearly every paper submitted for publication in *Monthly Notices*; experience has shown that frequently the comments of referees have enabled authors to improve the presentation of their work and so increase its scientific value.

2. *Communication.*—Papers must be communicated to the Society by a Fellow. They should be accompanied by a summary at the *beginning* of the paper conveying briefly the content of the paper, and drawing attention to important new information and to the main conclusions. The summary should be intelligible in itself, without reference to the paper, to a reader with some knowledge of the subject; it should not normally exceed 200 words in length. **Authors are requested to submit MSS. in duplicate.** These should be typed using double spacing and leaving a margin of not less than one inch on the left-hand side. Corrections to the MSS. should be made in the text and not in the margin. By Council decision, MSS. of accepted papers are retained by the Society for one year after publication; unless their return is then requested by the author they are destroyed.

3. *Presentation.*—Authors are allowed considerable latitude, but they are requested to follow the general style and arrangement of *Monthly Notices*. References to literature should be given either in the traditional form of a numbered list at the end of the paper, or as prescribed in *Notes on the Preparation of Papers to be Communicated to the Royal Society*.

4. *Notation.*—For technical astronomical terms, authors should conform closely to the recommendations of Commission 3 of the International Astronomical Union (*Trans. I.A.U.*; Vol. VI, p. 345, 1938). Council has decided to adopt the I.A.U. 3-letter abbreviations for constellations where contraction is desirable (Vol. IV, p. 221, 1932). In general matters, authors should follow the recommendations in *Symbols, Signs and Abbreviations* (London: Royal Society, 1951) except where these conflict with I.A.U. practice.

5. *Diagrams.*—**These should be designed to appear upright on the page, drawn about twice the size required in print and prepared for direct photographic reproduction except for the lettering, which should be inserted in pencil.** Legends should be given in the manuscript indicating where in the text the figure should appear. Blocks are retained by the Society for 10 years; unless the author requires them before the end of this period they are then destroyed. **Rough copies or prints of the diagrams should accompany each manuscript.**

6. *Tables.*—These should be arranged so that they can be printed upright on the page.

7. *Proofs.*—Authors are liable for costs of alteration exceeding 5 per cent of composition. It is therefore in their own and the Society's interests to seek the maximum conciseness and simplification of symbols and equations consistent with clarity.

CONTENTS

PAGE

M. W. Feast, A. D. Thackeray and A. J. Wesselink, The brightest stars in the Magellanic Clouds 337

Sidney van den Bergh, An analysis of the radial velocities of galaxies in the Virgo cluster 387

T. G. Cowling, Note on magnetic instabilities in stellar structure 393

A. J. Wickens and Harold E. Jones, Computing precise star co-ordinates ... 399

C. H. Costain and F. G. Smith, The radio telescope for 7·9 metres wavelength at the Mullard Observatory 405

J. E. Baldwin and C. H. Costain, The radio spectrum of the Andromeda nebula 413

H. E. Butler and H. Seddon, Spectroscopic measurements of early-type stars (Edinburgh paper summary) 419

Printed in London by Taylor & Francis, Ltd., 1960 November

MONTHLY NOTICES

OF THE

ROYAL ASTRONOMICAL SOCIETY

Vol. 121 No. 4

THE BRIGHTEST STARS IN THE MAGELLANIC CLOUDS

M. W. Feast, A. D. Thackeray and A. J. Wesselink

(Received 1960 March 30)

Summary

Spectroscopic and photoelectric observations of individual members of the Magellanic Clouds are presented (Sections 1–7). Table II includes spectral classifications of 50 Small Cloud objects and 105 Large Cloud objects; of these 93 have been observed photoelectrically (mostly in 3 colours), and 112 have measured radial velocities. Table III also lists 103 stars proved spectroscopically to be foreground galactic stars.

In Section 8 the observed colours of Cloud stars are compared with intrinsic colours of galactic supergiants by Johnson (O to A3) and Feinstein (A0 to K5). With the exception of Johnson's dip at A3 the least reddened Cloud stars agree well with these colours. Cloud stars are subject to a small amount of reddening ($\bar{E}_{B-V}=0{\cdot}10$) apparently arising partly in the Clouds and partly in the Galaxy. The Cloud reddening is greater for stars involved in nebulosity.

In Section 9 the HR diagram shows stars at A0 to A3 brighter visually than the early B and O supergiants. Bolometrically, however, the brightest stars ($M_b\sim-11$) cover this whole range of spectral types; these brightest stars all tend to show P Cyg characteristics in their spectra and are probably at the limit of stability for massive stars (mass $\sim100\odot$). Some peculiar emission-line stars resembling Eta Car are slightly less luminous. The few red super-supergiants (visually among the brightest Large Cloud members) are probably very rare objects. Photographically, the 18th brightest known LMC member has $B=10{\cdot}70$.

In Section 10, a detailed spectroscopic comparison between Cloud stars and galactic standards is made (together with a comparison of the gas in the Large and Small Cloud). Most of the small peculiarities noted can be attributed to very high luminosity (e.g. narrowness of the H lines) and lack of suitable galactic standards. In particular, no outstanding peculiarities are found in the 10 long-period Cloud Cepheids which have been studied. A list of 26 elements (including La II) identified in Cloud spectra is given.

In Section 11, a discussion of the *UBV* photometry shows that the reddening and intrinsic lines reinforce the essential similarity of stars (and dust) in both Clouds and the Galaxy.

In Sections 12 and 13 evidence is presented that interstellar lines due to Cloud and galactic gas occur in spectra of stars in both Clouds. Stars showing Cloud interstellar lines tend to be involved in nebulosity; our stars of type earlier than B1 are all involved in nebulosity, as in the Galaxy. The W stars and red super-supergiants also appear to be associated with nebulous regions.

In Sections 14 and 15 foreground stars are briefly discussed. Details of the photometric evidence for foreground galactic absorption are presented, and spectra of 3 peculiar galactic stars are described.

1. *Introduction.*—This paper presents spectroscopic and photo-electric observations of 155 objects (almost without exception individual stars) belonging

CONTENTS

PAGE

M. W. Feast, A. D. Thackeray and A. J. Wesselink, The brightest stars in the Magellanic Clouds 337

Sidney van den Bergh, An analysis of the radial velocities of galaxies in the Virgo cluster 387

T. G. Cowling, Note on magnetic instabilities in stellar structure 393

A. J. Wickens and Harold E. Jones, Computing precise star co-ordinates ... 399

C. H. Costain and F. G. Smith, The radio telescope for 7·9 metres wavelength at the Mullard Observatory 405

J. E. Baldwin and C. H. Costain, The radio spectrum of the Andromeda nebula 433

H. E. Butler and H. Seddon, Spectroscopic measurements of early-type stars (Edinburgh paper summary) 439

Printed in London by Taylor & Francis, Ltd., 1960 *November*

MONTHLY NOTICES

OF THE

ROYAL ASTRONOMICAL SOCIETY

Vol. 121 No. 4

THE BRIGHTEST STARS IN THE MAGELLANIC CLOUDS

M. W. Feast, A. D. Thackeray and A. J. Wesselink

(Received 1960 March 30)

Summary

Spectroscopic and photoelectric observations of individual members of the Magellanic Clouds are presented (Sections 1–7). Table II includes spectral classifications of 50 Small Cloud objects and 105 Large Cloud objects; of these 93 have been observed photoelectrically (mostly in 3 colours), and 112 have measured radial velocities. Table III also lists 103 stars proved spectroscopically to be foreground galactic stars.

In Section 8 the observed colours of Cloud stars are compared with intrinsic colours of galactic supergiants by Johnson (O to A3) and Feinstein (A0 to K5). With the exception of Johnson's dip at A3 the least reddened Cloud stars agree well with these colours. Cloud stars are subject to a small amount of reddening ($\bar{E}_{B-V}=0{\cdot}10$) apparently arising partly in the Clouds and partly in the Galaxy. The Cloud reddening is greater for stars involved in nebulosity.

In Section 9 the HR diagram shows stars at A0 to A3 brighter visually than the early B and O supergiants. Bolometrically, however, the brightest stars ($M_b\sim-11$) cover this whole range of spectral types; these brightest stars all tend to show P Cyg characteristics in their spectra and are probably at the limit of stability for massive stars (mass $\sim100\odot$). Some peculiar emission-line stars resembling Eta Car are slightly less luminous. The few red super-supergiants (visually among the brightest Large Cloud members) are probably very rare objects. Photographically, the 18th brightest known LMC member has $B=10{\cdot}70$.

In Section 10, a detailed spectroscopic comparison between Cloud stars and galactic standards is made (together with a comparison of the gas in the Large and Small Cloud). Most of the small peculiarities noted can be attributed to very high luminosity (e.g. narrowness of the H lines) and lack of suitable galactic standards. In particular, no outstanding peculiarities are found in the 10 long-period Cloud Cepheids which have been studied. A list of 26 elements (including La II) identified in Cloud spectra is given.

In Section 11, a discussion of the *UBV* photometry shows that the reddening and intrinsic lines reinforce the essential similarity of stars (and dust) in both Clouds and the Galaxy.

In Sections 12 and 13 evidence is presented that interstellar lines due to Cloud and galactic gas occur in spectra of stars in both Clouds. Stars showing Cloud interstellar lines tend to be involved in nebulosity; our stars of type earlier than B1 are all involved in nebulosity, as in the Galaxy. The W stars and red super-supergiants also appear to be associated with nebulous regions.

In Sections 14 and 15 foreground stars are briefly discussed. Details of the photometric evidence for foreground galactic absorption are presented, and spectra of 3 peculiar galactic stars are described.

1. *Introduction.*—This paper presents spectroscopic and photo-electric observations of 155 objects (almost without exception individual stars) belonging

to one or other of the two Magellanic Clouds. Proof of Cloud membership rests on (*a*) radial velocity, (*b*) supergiant characteristics in the spectrum. The same criteria have been used to weed out a number of foreground stars.

The observation of such stars is of obvious importance for various reasons. The absolute magnitudes of supergiants are at present only weakly known, and calibration by means of the Magellanic Cloud supergiants (both photoelectrically and spectroscopically) offers the most direct approach to this problem. Intrinsic colours of galactic supergiants are poorly determined on account of heavy absorption in the galactic plane; on the other hand, many supergiants in the Clouds, lying at high galactic latitudes, suffer very little absorption and their intrinsic colours are correspondingly easier to measure.

The spectroscopic comparison of Cloud and galactic stars enables one to say whether there are any gross differences in chemical composition; we can also compare absorbing properties of dust in the Clouds and Galaxy. Finally, the clear-cut spectroscopic distinction between Cloud members and foreground stars tells us something about just how bright stars can be; knowledge of the HR diagram of these extremely luminous objects, and their regional distribution in the Clouds (including involvement or otherwise in nebulosity) provide a pointer in theories of the evolution of very massive stars. As with so many other problems, the great ease with which the Magellanic Clouds can be resolved into individual stars means that we can study the bright end of the luminosity function with far greater *completeness* than in the Andromeda nebula and other nearby external systems.

Portions of this work have been published (**1**, **2**, **3**, **4**, **5**, **6**) at times during recent years, but this paper includes for the first time detailed results on individual stars. Analysis of the radial velocities, for rotation of the Clouds, etc., is postponed to a later paper.

2. *Selection of stars.*—Without slit-spectra, the surest criterion for membership of either Cloud for stars brighter than 13^m is blue colour or early type, since galactic stars are rarely found at the latitude of the Clouds with these characteristics. The HDE Catalogue (**7**) covering the Large Cloud is rich in stars classified as O, B, Con, and these are almost without exception Cloud members. The present investigation includes all such stars in the Catalogue with HDE magnitude 10·7 or brighter, and many considerably fainter. In addition, a number of anonymous stars, in the region of 30 Dor or selected as blue on blue-red pairs of photographs with the 74-inch reflector, have been observed.

The discovery of bright *red* stars in either Cloud is a far more difficult task. A few cases of red stars that appear to belong to Large Cloud associations or to nebulous regions have already been reported (**4**). The search for red stars was extended, the criterion for selection being primarily proximity to clusters; it was noted that the region of greatest density of K and M stars in the HDE lay in the Sf portion of the "bar" of the Large Cloud, and a number of these stars were investigated.

Since the HDE Catalogue does not cover the Small Cloud the list of bright SMC members was until recently restricted to 10 "B" stars in the HD Catalogue. Henize's (**8**) catalogue of emission-line stars proved to be a useful source of Cloud members, although it contains a few foreground stars. Many Cloud members have been observed in the region of the very large loose association NGC 371, some of them observed photoelectrically by Arp (**9**). Finally some

of the brighter Cepheids in both Clouds have been observed by Feast (**3**) and these observations, supplemented by later ones, are included in this paper.

The actual distribution of observed Cloud members among the criteria for selection is shown in the accompanying table:

SMC		LMC	
Source	Number	Source	Number
HD	11	HD	13
Henize	14	HDE	69*
NGC 371 (anon)	16	30 Dor (anon)	11
Arp	5	Blue (anon)	7
Cepheids	4	Cepheids	6
		R Cr B	1
		Henize	1
Total	50		108

* Including 3 clusters resolved visually or photographically, but not otherwise observed.

3. *Spectroscopic observations.*—All spectroscopic observations were made with the 2-prism Cassegrain spectrograph attached to the 74-inch Radcliffe reflector. All the brighter stars were observed at least once with the c camera (49 A/mm at $H\gamma$) with projected slit-width 0·024 mm. Fainter than $11^{m}\cdot0$ observations were made almost entirely with the d camera (86 A/mm at $H\gamma$) with projected slit-width 0·027 mm, except for emission-line objects. Many stars were observed with both these cameras. The customary width of spectrum was 0·2 mm with either camera; but with the brighter stars a width of 0·45 mm was often achieved and in some cases as great a width as 1·0 mm for accurate classification on the MK system. In a very few cases the b camera (29 A/mm at $H\gamma$) was used.

Over 300 spectra of Cloud members have been used in this investigation, involving over 800 hours of exposure time. This excludes a relatively small number of hours spent in obtaining exploratory single plates of foreground stars.

The spectral classifications were made by comparison with spectra of the standard stars of the MK system (**10**) taken under the same conditions as the programme stars. The list of standards was supplemented with a few early type stars of high luminosity whose types were kindly supplied privately by Dr W. W. Morgan. Comparison was generally made with a Hartmann spectro-comparator, kindly loaned by H.M. Astronomer, Royal Observatory, Cape.

Classifications were carried out in a short space of time at the conclusion of the observational programme in order to ensure uniformity. Luminosity classification was freed from any possible bias, because—with a few unavoidable exceptions—the classifier had no idea of the apparent magnitude of the star being classified.

The nomenclature employed is that normally used in the MK system. However, stars which give evidence of being brighter than class Ia are designated Ia-O. We adopted this designation on the recommendation of Dr W. W. Morgan and in conformity with the earlier procedure of Keenan. This class of stars has frequently been designated Ia+ in recent papers by

PLATE I (*see facing page*)

Sequence of Supergiants in the Magellanic Clouds (original dispersion 86 A/mm at Hγ). Region Hβ to K. Terrestrial Hg 4358 appears in some spectra. (See detailed remarks to Table II.)

1	R	14	5980	SMC	Pec	JD 2435389	Note change in width of emission in 1 and 2.
2	R	14	5980	SMC	Pec	JD 2435742	
3	R	64	32228	LMC	O8+WC6		
4	R	122	269810	LMC	O6		
5	R	78	269050	LMC	Bo Ia		Ca II K may be due to Cloud interstellar gas.
6	R	17	Arp h	SMC	Bo I		Ca II K may be due to Cloud interstellar gas.
7	R	9	5045	SMC	B3 Ia		
8	R	11	5291	SMC	B6 Ia		
9	R	62	32034	LMC	B9 Ia		
10	R	45	7583	SMC	Ao Ia–O		
11	R	80	269172	LMC	Ao Ia–O		
12	R	153	270086	LMC	A1 Ia–O:		
13	R	76	33579	LMC	A3: Ia–O(e)		
14	R	19	Arp g	SMC	A3 I		Absolute magnitude $2^{m}\cdot6$ fainter than 33579 (above).
15	R	151	269982	LMC	A5 Ia:		In 30 Dor region.
16	R	26		SMC	Fo Ia		Two different spectra of same star.
17	R	26		SMC	Fo Ia		
18	R	92	271182	LMC	F8 Ia		
19	R	1	HV 821	SMC	F8 Ia		JD 2436110 phase 0·83
20	R	1	HV 821	SMC	G1 Ib		JD 2435383 phase 0·10 Note the change in appearance of the G band in 19 and 20.
21	R	150	269953	LMC	Go Ia		
22	R	59	268757	LMC	G5 Ia		Two different spectra of same star.
23	R	59	268757	LMC	G5 Ia		
24	R	20	Hen S30	SMC	K5 Ia: e		The star of latest type yet found in either Cloud.
25	R	4	Hen S 6	SMC	Be		Note H emission and weak Fe II, [Fe II] emission.
26	R	66	268835	LMC	Aeq.		Typical P Cyg star (Beals' Type I).
27	R	50	Hen S65	SMC	Pec		Eta Car type, with [Fe II] emission.
28	R	99	269445	LMC	Pec		H, He I, He II emission.

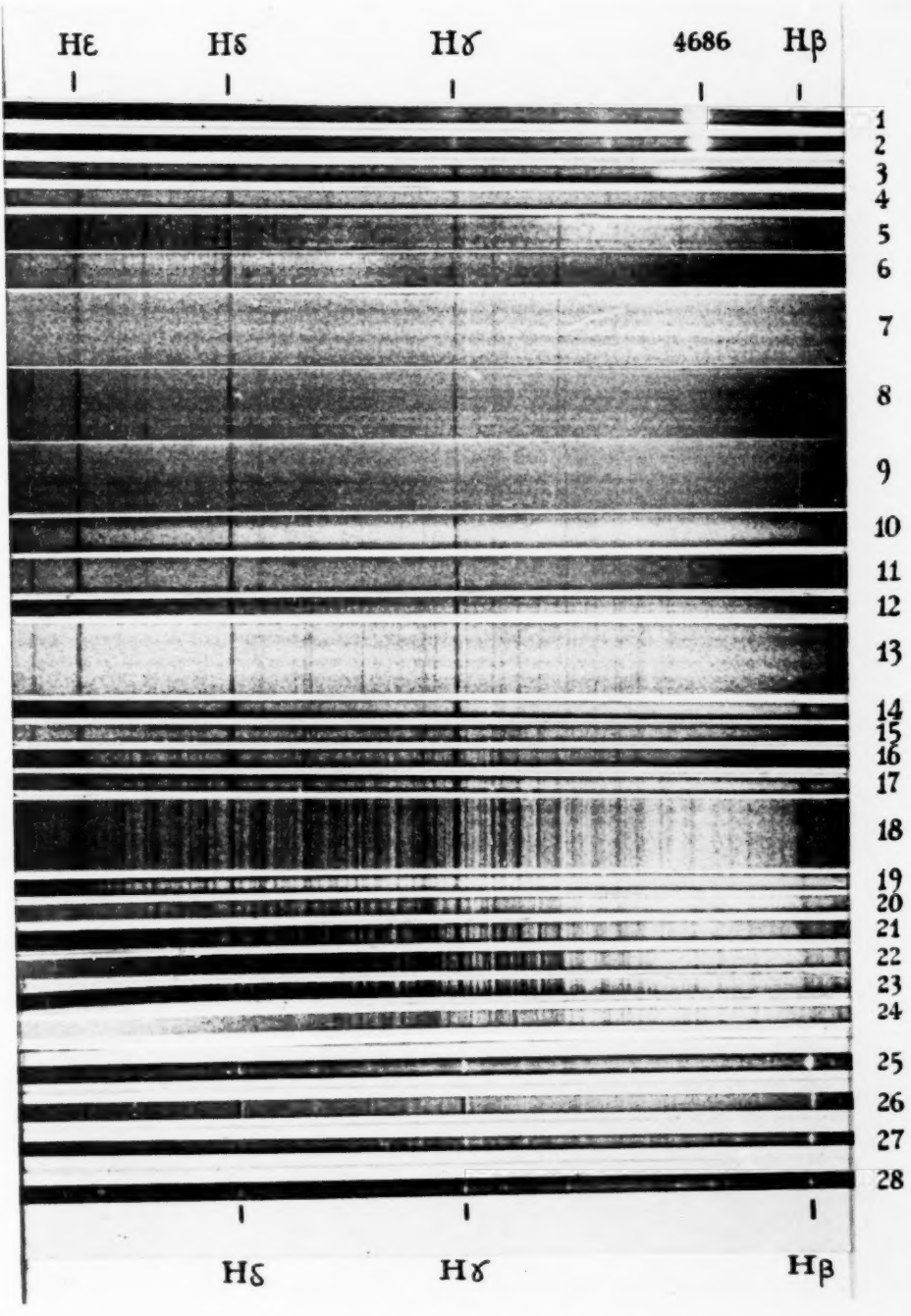

M. W. Feast, A. D. Thackeray and A. J. Wesselink, The brightest stars in the Magellanic Clouds

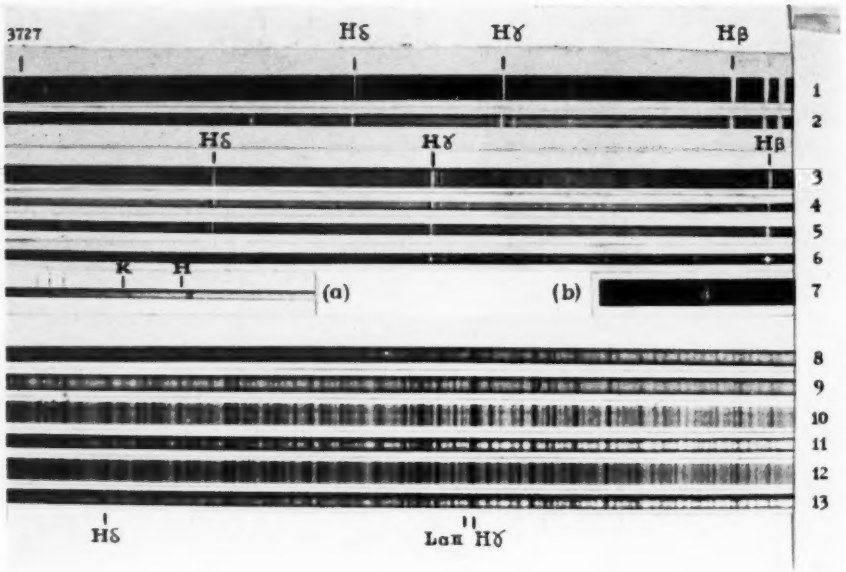

PLATE II

(*a*) *Gaseous nebulae in Magellanic Clouds;* 5010 *to* 3720 *A, original dispersion* 86 *A/mm at Hγ.*

1 Portion of 30 Dor nebulosity (LMC). Note terrestrial Hg 4358.

2 R 44 IC 1644 SMC.

(*b*) *Emission objects: Hβ to Ca II K, Hβ, γ, δ marked, original dispersion* 49 *A/mm at Hγ.*

3	R	88	S Dor	LMC	Aeq	Bright phase.
4	R	66	268835	LMC	Aeq	
5	R	126	37974	LMC	Pec	
6	R	67	32763	LMC	Pec	Eta Car type; 7b shows Hγ structure (original at 29 A/mm).
7(b)	R	67	32763	LMC	Pec	
7(a)	R	62	32034	LMC	B9 Ie	Galactic interstellar H and K marked.

(*c*) *Red super-supergiants in LMC compared with galactic MK standards; original dispersion* 49 *A/mm at Hγ; Hγ, La II* 4334, *Hδ marked.*

8	R	143	Anon	F7 Ia	30 Dor region
9	R	92	271182	F8 Ia	
10			δ C Ma	F8 Ia	MK standard
11	R	117	269723	Go Ia	
12			62058	Go Ia	MK standard
13	R	150	269953	Go Ia	

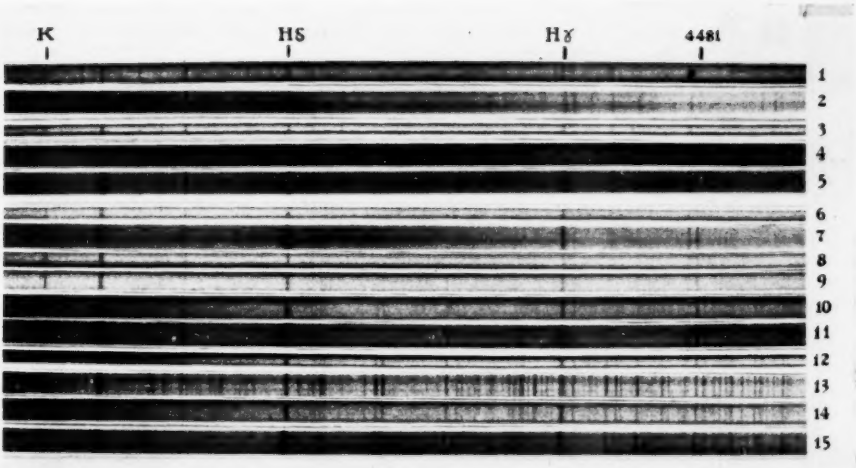

PLATE III

Magellanic Cloud supergiants compared with MK standards (types B to A). Original dispersion 49 A/mm at Hγ. Range 3910 to 4600 A

1	R 116	269700	LMC	B1·5	Iaeq	Terrestrial Hg 4358 visible
2		190603	MK	B1·5	Ia	
3	R 112	269660	LMC	B2	Ia:	Weak galactic interstellar K
4	R 42	7099	SMC	B2·5	I	
5		3 Gem	MK	B2·5	Ib	Strong galactic interstellar K
6	R 73	268907	LMC	B8	Ia	
7		β Ori	MK	B8	Ia	
8	R 40	6884	SMC	B8	Ie	Perhaps slightly later than B8
9	R 111	269661	LMC	B9	Ia–O:	
10	R 45	7583	SMC	A0	Ia–O	
11		167356	MK	A0	Ia	
12	R 153	270086	LMC	A1	Ia–O:	
13		160529	MK	A2	Ia–O	
14	R 76	33579	LMC	A3:	Ia–O(e)	
15		165784	MK	A2	Ia	

several authors, but this is objectionable since the plus sign has also been used among the giants to denote "less luminous than".

Radial velocities were measured in the usual way either with a Hilger micrometer or the Casella projection micrometer. For early-type stars, standard IAU wavelengths were adopted; since the Cloud members are all supergiants it was never necessary to apply Petrie's corrections to λλ4026, 4471 appropriate to main-sequence stars. Victoria wavelengths (**11**, **12**) were used for the relatively few stars of late type.

Comparison of velocities obtained with the c and d cameras of the same stars shows a mean difference $\Delta V(\text{c–d}) = +11{\cdot}4 \pm 2{\cdot}7$ km/s (s.e.) from 41 stars. This confirms the similar effect previously found from velocities of individual stars in 47 Tuc (**13**) in which $\Delta V(\text{c–d}) = +10{\cdot}0 \pm 3{\cdot}5$ km/s from 15 stars. As before, therefore, all d velocities have been corrected by +10 km/s, and in combining c and d velocities to form the mean velocity for any star double weight has been assigned to the velocities with the c camera. The origin of the systematic error is still unknown, but it must reside mainly in the low dispersion d plates, and the error apparently disappears near zenith. The sense of the error is accordant with a guiding error due to atmospheric dispersion. It can hardly be due to erroneous standard wavelengths since it affects both early- and late-type stars. Since the projected slit-width used with the d camera is as much as 160 km/s, the error must be regarded as relatively small.

4. *Photoelectric photometry.*—Photoelectric observations were also made at the Cassegrain focus of the 74-inch reflector. The beam from the aluminized Cassegrain secondary was deflected sideways by an aluminized flat (above the spectrograph slit) into the photometer.

The photometer was of conventional design. The beam of light was focused on a diaphragm, whose size was 12″ or 18″ of arc depending on whether or not close companions had to be isolated. Behind the diaphragm, the light passed a Fabry lens and filter slide before striking the cathode of an E.M.I. photomultiplier cell. The diameter of the image of the primary mirror formed by the Fabry lens on the cathode was 5·5 mm. The construction allowed a direct microscopic view of the diaphragm for the purpose of focusing. It was also possible to interrupt the beam by a flat mirror giving the observer a field of view 8′ of arc in diameter.

As a novel feature the Fabry lens was mounted on a slide that could be moved laterally. Further, the can containing the photo tube could be rotated around the photometer axis. By combining these two motions it was possible to find the most sensitive spot of the photo-cathode while the cell was on tension.

On the advice of Dr A. W. J. Cousins the photocell was fitted with a brass sleeve closely surrounding the cylindrical part of the cell. This sleeve was insulated by a plexiglass support from the can but being in electrical contact with the photocathode pin was on cathode potential. This device greatly improved the performance of the cell.

The output signal was amplified by a D.C. feedback amplifier and the voltage measured on a Brown recorder.

Prior to 1959 March 12, the primary mirror was silvered and the following filters were used: Omag 303, 1½ mm thick, for the yellow; Schott BG 12, 1 mm, and Schott GG 13, 2 mm, for the blue; and Corning 9863, 2 mm, for the ultraviolet.

The yellow filter gave natural magnitudes very close to the Cape SP_v system (14). The combination of BG12 and GG13 gave magnitudes that were close to the Cape S'Pg system. The observation prior to 1959 March 12 were all reduced to SP_v and S'CI, the system in which the Cape standard magnitudes in the E regions are given. The purpose of the GG13 filter is to eliminate any ultraviolet contribution beyond 3800A to the blue magnitudes, following the well-known advice of H. L. Johnson.

After 1959 March 12, when the primary mirror was aluminized, a slightly different set of filters was used: Omag 302, 2 mm thick, for the yellow; Schott BG 12, 1 mm, and Schott GG 13, 4 mm, for the blue; and the same filter, Corning 9863, 2 mm, for the ultraviolet.

The new yellow filter gives magnitudes which are close to Johnson's V, and the new blue combination gives a system close to Johnson's B; the thicker filter GG13 used in the 2nd set eliminates more efficiently the unwanted ultraviolet from the blue.

The earlier Radcliffe results in the yellow and blue, reduced to the Cape S system, were reduced to Johnson's V and $B-V$ by means of the formulae (14):

$$V - SP_V = -0{\cdot}06 + 0{\cdot}082\ S'CI + 0{\cdot}008\ (S'CI)^2$$

$$B - V = +0{\cdot}28 + 0{\cdot}87\ S'CI$$

and combined with the later Radcliffe results on the B, V system. In all, the different results proved to be quite consistent with one another. The mean results on Johnson's B, V system are given in the main Table.

The position with regard to our results for the ultraviolet is rather different. When the observations were started in 1955, with the then silvered primary, no standard ultraviolet colours were available that were suitable for the reduction of the Radcliffe natural ultraviolet colours. It was therefore decided to build up a new system of standard $U_R - B_R$ values representative for these Radcliffe observations made with the silvered primary. For about 40 stars in all the E regions $U_R - B_R$ values were derived that can be considered to form a homogeneous system without variations dependent on R.A. The system of $U_R - B_R$ standard colours just described was, however, not quite satisfactory in that it did not contain stars with as much ultraviolet as the Magellanic Cloud early supergiants.

During the work the further use of our photoelectric cell became impossible due to increased noise. A new tube giving excellent performance has been used since. However, this tube appeared relatively less ultraviolet sensitive than the former one. This difference in tube quality combined with the extrapolation required by the use of the E region standards resulted in a systematic difference in the results as obtained from these two tubes for the earliest Magellanic supergiants in $U_R - B_R$.

It proved possible, however, to derive a unique relation connecting the results from the two tubes, and the fewer early results were combined with the later ones after reduction on their system. It must be emphasised that *as regards B and V no systematic errors dependent on the cell were noted.*

In Table I are given magnitudes and colours for a number of bright foreground stars (in the direction of the Magellanic Clouds) that have been used as zero-point stars. The magnitudes and colours of most of these stars were kindly provided by the Royal Observatory, Cape, and were only slightly amended after observations were made by one of us at the Royal Observatory, Cape.

On a typical observing night it was standard practice to observe a zero-point star of Table I before and after the observation of any three Cloud members. Outside the interval of time devoted to the Clouds it was also standard practice to observe standard stars in the E regions.

Observations of E region standards ensured that the natural system of each night was tied in to the accurate E region system. This was particularly important in observing with a silvered primary having a gradually deteriorating coat (renewed every six months or more frequently). Further the frequent observation of zero-point standards at very nearly the same altitude as the Cloud stars proved useful in eliminating the extinction. The following mean extinction co-efficients have been used at the Radcliffe Observatory:

$$V,\ 0^{m}\cdot16;\quad B,\ 0^{m}\cdot33;\quad U,\ 0^{m}\cdot50.$$

All measures were reduced to the zenith with these coefficients. Slight variations from these mean values cannot be very important as the error is multiplied by the difference in sec z between Cloud members and zero-point stars, which is always very small.

The following standard errors for a single measure of a Cloud star were found: V, $\pm0\cdot03$; $B-V$, $\pm0\cdot015$; U_R-B_R, $\pm0\cdot03$. These errors are somewhat larger than have been met in photometry of galactic stars at Pretoria. Two reasons can be suggested:

(1) The supergiants studied here may be slightly variable. In fact, Cloud stars with total ranges in measured V and B of $0^{m}\cdot1$ or greater occur not infrequently and are quite probably variable; such stars have been excluded from the calculation of the above errors from the interagreement of individual measures.

(2) The Magellanic Clouds are in opposition during the summer season when climatic conditions are rarely as good as those prevailing in winter in Pretoria.

TABLE I

Zero point standards near Magellanic Clouds

HD	SP_V	S'CI	U_R-B_R	V	$B-V$
4651	9·78	+0·21	+0·88	9·74	+0·46
4725	10·79	+0·20	+0·89	10·74	+0·45
4852*	10·47	+0·35	+1·00	10·43	+0·58
5302	9·84	+1·48		9·92	+1·57
7187*	7·19	−0·23	+0·89	7·11	+0·08
7222	10·68	−0·25	+0·90	10·60	+0·06
25938	6·65	−0·22	+0·92	6·57	+0·09
31722	8·51	−0·08	+0·96	8·44	+0·21
32858	8·80	−0·26	+0·87	8·72	+0·05
33029	8·77	+0·26	+0·97	8·73	+0·51
33031	8·16	−0·02	+0·95	8·10	+0·26
33032	9·04	+0·22	+0·94	9·00	+0·47
38616	7·13	−0·35	+0·74	7·04	−0·02
39062	7·35	+1·19	+1·80	7·40	+1·32

* double

It was on account of the fear of variability of Magellanic Cloud supergiants that only galactic stars have been used as standards. It is realized, however, how extremely useful a few very blue constant Cloud members could be as standards for magnitude and colour. It may well be worth while to add as standards a few blue members which are least suspected of variability.

The present material has a few Cloud stars in common with those studied by Arp (**9**). Arp's results are quoted in the individual remarks to Table II. Only the V and $B-V$ measures can be directly compared and are generally in good agreement. The number in common is however too small to make a thorough comparison. A discussion of standards in common with Arp is postponed to a later paper.

Gascoigne (**15**) has published V, $B-V$ for seven SMC supergiants of the present paper. Gascoigne's V's average about $0^{m}\cdot14$ fainter than ours, whereas his $B-V$ values are $0^{m}\cdot02$ bluer than ours.

5. *Description of Table II.*—Table II presents individual observations of Cloud members in the following form:

(1) *Radcliffe serial number.*—The stars are arranged in order of R.A. (1975) (except for the last three entries referring to clusters rather than individual stars). This number is used on all identification charts and in the text (Figs. 1–10).

(2) *Star designation.*—The HD or HDE number is always given when available. Cepheids are identified by HV numbers. Henize numbers are used in the Small Cloud (and are frequently quoted as alternative designations in the Remarks). A few Arp (**9**) designations are also used.

(3) *R.A. and Dec.* (*epoch* 1975).—These have been computed from:

(*a*) CPD positions.

(*b*) Harvard x, y transformed according to Wesselink's (**16**) formulae.

(*c*) Henize positions.

(*d*) Interpolation from nearby stars with known coordinates.

(4) *Magnitude and colour*, based on Radcliffe photoelectric observations *unless asterisked.* V, $B-V$ columns correspond to the Johnson system. $U_{R}-R_{R}$ are Radcliffe ultraviolet colours whose relationship to the Johnson $U-B$ has not been finalised. A figure in the V column with asterisk is the HDE photographic magnitude corrected by $+0^{m}\cdot3$ which is found to be the average difference of these magnitudes from Radcliffe B magnitudes for stars for which both sets of magnitudes are available. Other magnitudes are quoted in the Remarks at the end of the Table.

(5) *Spectral classification* on MK system. e denotes emission lines of hydrogen, and possibly other elements. (e) means that though no emission lines are seen on Radcliffe plates, Hα has been recorded bright by Henize (**8**). Following Beals (**17**) q denotes P Cyg contours in at least one line. "Of" indicates at least He II 4686 emission and generally N II 4634, 4640 also. "Pec" means emission spectrum to which a normal type cannot be attached. Details of emission line stars are given in the Remarks.

In the classifications the colon refers only to the number or letter immediately preceding it. Thus B2 Ia: indicates a star considered to be certainly B2 I and less certainly Ia. Similarly A0 Ia–0: means that the star is probably but not certainly more luminous than A0 Ia.

(6) *Mean radial velocity* from Radcliffe spectra. Individual plate velocities will be found in the Remarks, together with the camera used. In taking the mean, half-weight was allotted to all d-camera plates, and further to uncertain measures marked with a colon.

(7) *Quality* of the observations in shorthand notation. First is given the number of Radcliffe photoelectric observations of V (in nearly every case identical to the number of observations of B and U). Second a capital letter A, B, C or D denotes decreasing quality of the spectral classification. Third appears a small letter c, d or e to denote the estimated quality of the radial velocity measures; these qualities correspond roughly to the qualities in Wilson's *General Catalogue of Radial Velocities*.

The remarks following the Table always include the following information:

(*a*) If the star appears in Henize's catalogue of emission-line stars, its Henize number is quoted (unless that already appears in the Table).

(*b*) If the star lies within an area of Henize emission nebulosity, the Henize nebula number is quoted.

(*c*) If the range of Radcliffe measures of magnitude exceeds $0^m.09$, the range is quoted.

(*d*) References to relevant Plate reproductions or identification charts.

(*e*) Individual plate velocities, followed by the letter denoting the camera used. If W follows the camera designation, it means that the plate was taken with telescope west of the pier; in all other cases the telescope was east of the pier.

Copious remarks on individual peculiarities and features in the spectral classification are added.

TABLE II

		Star	1975 α	1975 δ	V	$B-V$	U_R-B_R	Sp	RV	Q
			h m	° ′						
R	1	HV 821	0 40·9	−73 52	Var			F8 Ia		A
	2	Hen S2	0 42·3	−73 31				B6 Ie		C
	3	Hen S5	0 44·9	−72 06				A3: I: (e)	+153:	De
	4	Hen S6	0 46·0	−73 17				Be	+182	Dd
	5	4862	0 48·3	−73 30	11·0	−·02:	+·50:	B3 I	+152	1Bc
	6	4976	0 49·4	−73 16	10·96	+·14	+·54	B6 I	+168	9Cc
	7	HV 829	0 49·7	−72 53	Var			Go: I		D
	8	5030	0 49·8	−73 37	11·11	+·13	+·56	Ao Ia:	+168	9Bd
	9	5045	0 49·9	−73 36	10·98	·00	+·48	B3 Ia:	+168	8Bd
	10	5277	0 52·2	−73 15	10·91	+·14	+·65	Ao Ia:	+139	12Bc
	11	5291	0 52·3	−72 46	10·75	+·05	+·52	B6 Ia	+158	6Ac
	12	HV 834	0 52·9	−72 25	Var			F8 Ia		C
	13	Hen S27	0 58·1	−72 05				A3: Ia: (e)	+174:	Ce
	14	5980	0 58·6	−72 17	11·61	−·18	+·46	Wp		6B
	15	Hen S29	0 58·7	−72 09				(A−B)e	+128:	De
	16	Anon	0 58·9	−72 27				B	+162:	De
	17	Arp h	0 59·0	−72 54	12·12	−·09	+·46	Bo I	+169	2Bd
	18	Anon	0 59·2	−72 22				B 0·51	+181	Ce
	19	Arp g	0 59·8	−71 41				A3 Ia	+169	Bd
	20	Hen S30	0 59·8	−72 19	Var	+1·89	+1·65:	K5 Ia: e	+149:	5Ce

TABLE II (*continued*)

	Star	1975 α h m	δ ° ′	V	$B-V$	U_R-B_R	Sp	RV	Q
R	21 Anon	1 00·4	−72 26				Ao Ia:	+120	Bd
	22 Anon	1 01·0	−72 13	12·27	+ ·19	+ ·81	A3 I	+159	2Cd
	23 Anon	1 01·2	−72 09				A1 I	+149:	Ce
	24 Anon	1 01·2	−72 11	12·50	+ ·09	+ ·66	Ao:	+159:	3De
	25 Anon	1 01·4	−72 09				B1:	+169	Dd
	26 Anon	1 01·8	−72 16				Fo Ia:	+178	Bd
	27 Anon	1 01·9	−72 19	10·9	+ ·11:	+ ·57:	B9 Ia	+143	1Bd
	28 Anon	1 02·3	−72 11				Bo I	+180	Be
	29 Anon	1 02·4	−72 15	12·74	+1·18	+ ·80:	K:	+151:	3De
	30 Anon	1 02·5	−72 11	13·2	+ ·13:	+ ·83:	Be	+146:	1De
	31 Anon	1 02·5	−72 15	12·3	− ·19:	+ ·43:	O: f:	+141:	1De
	32 Anon	1 02·9	−72 12				B	+228: a +248: e	De
	33 Anon	1 03·0	−72 16				B	+189	Dd
	34 Hen S40	1 03·1	−72 02	12·83	+ ·41	+ ·77	Fo: I(e)	+195:	3Ce
	35 Anon	1 03·1	−72 11				B1 I:	+157:	De
	36 Arp e	1 04·0	−72 15	11·26	+ ·02	+ ·47	B3 I	+196	Bd
	37 Arp b	1 04·1	−72 17	11·20	+ ·11	+ ·54	B6 I	+180	2Bd
	38 Hen S46	1 05·0	−71 54				Pec		C
	39 Hen S45	1 05·2	−72 28				B2: I(e)	+144:	De
	40 6884	1 06·6	−72 36	10·73	+ ·08	+ ·53	B8 Ie	+181	5Ac
	41 Hen S53	1 08·0	−73 23				Be		D
	42 7099	1 08·4	−72 40	10·95	− ·04	+ ·50	B2·5 I	+247	9Ac
	43 Arp d	1 08·4	−73 11				A3 I	+175	Bd
	44 7113	1 08·5	−73 12				Neb	+166	Ad
	45 7583	1 12·8	−73 28	10·13	+ ·14	+ ·59	Ao Ia−O	+175	7Ac
	46 HV 2195	1 13·8	−72 48	Var			Go		D
	47 Hen S63	1 28·7	−72 50	11·56	+ ·38	+ ·90:	F Ie	+121:	2De
	48 Hen S62	1 29·7	−73 26				e		D
	49 Hen S64	1 30·7	−72 56				(A−B)e	+171:	De
	50 Hen S65	1 43·8	−74 47	11·56	+ ·19	+ ·64	Pec	+184	4Cc
	51 270754	4 47·0	−67 09	11·28	+ ·10	+ ·51	B1·5 Ia:	+306	6Bd
	52 268654	4 49·4	−69 30	10·49	+ ·18	+ ·60	B8 I	+266	4Bd
	53 268605	4 50·4	−67 42	11·33	− ·12	+ ·48	Bo Ia:	+309	3Bd
	54 31673	4 52·2	−69 26				Neb	+250	Bd
	55 268718	4 52·2	−69 28	10·69	+ ·25	+ ·58	B9 Ieq	+268	8Cd
	56 268623	4 52·3	−66 46	11·8•			B2 Ia	+312	Bd
	57 268653	4 53·4	−66 58	10·73	− ·03	+ ·52	B3 I	+301	5Bd
	58 268729	4 53·9	−68 45	11·0	+ ·12:		B5 I	+271	1Cd
	59 268757	4 54·4	−69 14	10·25	+1·55	+1·61	G5 Ia	+258	4Ad
	60 HV 873	4 54·8	−70 57	Var			F8: I		D
	61 268675	4 55·0	−66 47	10·80	+ ·05	+ ·54	Ao Ia	+286	5Bd
	62 32034	4 55·1	−67 12	9·65	+ ·10	+ ·54	B9 Ie	+295	3Ac
	63 HV 5497	4 55·6	−66 28	Var			G2 I		C
	64 32228	4 56·5	−66 31	10·8	− ·15:		WC6 +O8:	+275	1Bd
	65 268809	4 56·6	−69 18	11·89	− ·05	+ ·47	B1 Ia:	+258	4Bd

TABLE II (*continued*)

	Star	1975 α	1975 δ	*V*	*B*−*V*	U_R-B_R	Sp	RV	*Q*
		h m	° ′						
R	66 268835	4 56·9	−69 53	10·64	+ ·15	+ ·58	Aeq	+271e + 54a	3Bd
	67 32763	4 59·6	−70 14	11·4	+ ·20:		Pec	+244	1Ac
	68 270933	5 00·1	−65 48	10·95	− ·01	+ ·56	B8 I	+313	4Bd
	69 HV 883	5 00·3	−68 29	Var			G2: I		D
	70 270949	5 01·2	−65 51	11·15	− ·10	+ ·51	B3I	+300	5Bd
	71 269006	5 02·4	−71 22	10·91	+ ·01	+ ·48	B2·5 Iep	+192e +198a	5Cc
	72 268993	5 02·8	−70 43	11·98	+ ·05	+ ·55	Ao Ia	+237	3Bd
	73 268907	5 03·0	−66 59	10·62	− ·01	+ ·51	B8 Ia	+305	3Ad
	74 268939	5 04·2	−67 17	10·9*			BI e	+299	Bd
	75 268946	5 05·3	−66 46	10·30	+ ·09	+ ·55	Ao Ia	+297	3Bd
	76 33579	5 05·8	−67 55	9·11	+ ·18	+ ·62	A3: Ia−O(e)	+253	4Ac
	77 HV 2294	5 06·3	−66 43	Var			F7 I		C
	78 269050	5 07·5	−68 34	11·70	− ·07	+ ·48	Bo Ia	+238	5Ad
	79 269101	5 10·0	−68 48	12·01	·00	+ ·54	B5 I	+302	3Cd
	80 269172	5 10·0	−71 26	10·62	+ ·08	+ ·57	Ao Ia−O	+231	4Ad
	81 269128	5 10·6	−68 48	10·43	− ·01	+ ·49	B2·5 Ieq	+227	5Cd
	82 269217	5 13·8	−69 23	11·8	+ ·08:		Pec	+236	1Ce
	83 HV 2369	5 13·9	−67 05	Var			F−G		D
	84 269227	5 14·1	−69 33	11·7	+ ·33:		Pec	+262: e + 28: a	1Be
	85 269321	5 18·1	−69 17	10·87	+ ·09	+ ·53	B5 Iae	+292	6Ad
	86 35342	5 18·3	−69 14				Cluster		
	87 269333	5 18·4	−69 13	11·21	− ·09	+ ·53	W+B1: I	+286	3Cd
	88 35343	5 18·4	−69 16	Var			Aeq	+295e +213a	Ac
	89 35517	5 19·6	−69 40	11·3	− ·07:		Bo I	+285	1Ce
	90 Anon	5 19·6	−69 40	12·0	− ·21:		WC 6:		1C
	91 HV 2447	5 19·8	−68 42	Var			Go Ia		B
	92 271182	5 21·1	−65 49	9·74	+ ·57	+1·10	F8 Ia	+322	4Ad
	93 Anon	5 21·6	−65 46	12·61	− ·17	+ ·44	Bo:		3D
	94 271191	5 21·7	−65 46	10·03	+ ·75	+ ·61	B comp	+291	3Dd
	95 Anon	5 21·7	−65 46	12·72	− ·14	+ ·44	Bo I	+329:	3Ce
	96 271213	5 21·7	−71 58	12·29	− ·06	+ ·54	B3 I	+241	3Cd
	97 Anon	5 21·8	−65 48	12·33	− ·14	+ ·45	Bo·5 Ia:	+308	3Bd
	98 271192	5 21·8	−65 53	10·54	+ ·11	+ ·59	Ao Ia−O:	+308	3Bd
	99 269445	5 22·9	−68 03	11·5	+ ·27:	+ ·53:	Pec	+278	1Bd
	100 269475	5 23·2	−71 44	11·56	− ·02	+ ·53	B3 I	+251	3Bd
	101 269547	5 26·6	−71 35	11·61	+ ·05	+ ·56	B3 Ia:	+251	3Bd
	102 W Men	5 26·8	−71 12	Var			F8: Ip		D
	103 269546	5 27·0	−68 51	9·88	− ·02	+ ·53	B3 Ip	+298	3Bc
	104 271279	5 27·8	−65 42	11·25	+ ·09	+ ·69	Ao Ia:	+306	3Bc
	105 2695998	5 28·4	−69 10				B8: I	+268	1De
	106 269634	5 30·0	−67 29	12·5	+ ·10:		Ao I		1D
	107 269644	5 30·4	−67 33	11·2	− ·01:		B6 Ia	+336	1Bd
	108 Anon	5 30·6	−67 18	12·9	+1·19:		Pec	+318:	1De
	109 Anon	5 30·7	−67 17	12·0	− ·01:	+ ·52:	B6 I		1C
	110 269662	5 30·9	−69 04	11·1*			B9: Ieq		D

TABLE II (*continued*)

	Star	1975 α	1975 δ	V	$B-V$	U_R-B_R	Sp	RV	Q
		h m	° ′						
R 111	269661	5 31·0	−69 32	10·31	+ ·12	+ ·57	B9 Ia−O:	+260	3Ad
112	269660	5 31·2	−71 05	11·15	− ·01	+ ·51	B2 Ia	+237	3Bc
113	269676	5 31·6	−71 05	11·7*			O6 e	+244:	Ce
114	269692	5 31·7	−67 42	14·5	− ·14:		W		1D
115	269698	5 31·9	−67 39	12·2	− ·19:		O5 f		1B
116	269700	5 32·0	−68 34	10·55	·00	+ ·48	B1·5 Iaeq	+252	3Ad
117	269723	5 32·5	−67 43	9·91	+1·06	+1·37	G0 Ia	+317	4Ad
118	269781	5 34·3	−67 03	9·87	+ ·07	+ ·56	A0 Iae	+342	4Ac
119	269787	5 34·5	−67 00	11·3*			A0 Ia−O	+312:	Be
120	269797	5 34·9	−67 22	10·89	+ ·05		B8 Ia−O:	+288	3Ad
121	269801	5 34·9	−67 22	10·49	+ ·10		B9 Ia−O	+319	3Ad
122	269810	5 35·1	−67 34	12·22	− ·17	+ ·42	O6+Neb	+257	3Bd
123	37836	5 35·6	−69 41	10·7	+ ·12:		Pec	+267	1Bd
124	269841	5 35·9	−67 27	11·9	+ ·10:		A0		1D
125	269845	5 36·0	−67 28	11·80	+ ·01	+ ·48	B3 I	+292	3Cd
126	37974	5 36·6	−69 24	10·9	+ ·17:	+ ·55:	Pec	+258	1Ac
127	269858 f	5 36·9	−69 31	11·4*:			Pec	+284	Ce
128	269859	5 37·0	−69 31	11·2*			B1 I	+268	Cd
129	269896	5 37·9	−68 56	11·6*			B0 Ia:	+273	Bd
130	269891	5 37·9	−69 06	11·8*			B0: +W?		C
131	269902	5 38·2	−69 07	11·3*			B9 I	+269	Bd
132	Anon	5 38·3	−69 05				B−A		D
133	Anon	5 38·5	−69 06				O8	+235	Ce
134	Anon	5 38·5	−69 07				WN7		C
135	Anon	5 38·6	−69 06				WN7		C
136	38268	5 38·6	−69 07				O+WN	+274	Dd
137	Anon	5 38·7	−69 06				B0·5 Ia:		B
138	Anon	5 38·7	−69 07				A0: I:		D
139	Anon	5 38·8	−69 06				WN7: +O:		D
140	Anon	5 38·8	−69 06				WN6		C
141	Anon	5 38·8	−69 07				B0·5:		C
142	Anon	5 38·8	−69 07				B		D
143	Anon	5 38·9	−69 09				F7 Ia	+263	Ad
144	38283	5 39·0	−69 03	11·1	− ·11:		WN7		1C
145	269928	5 39·0	−69 07	12·1*			WN6−7		C
146	269926	5 39·1	−69 01	12·8*			WN5		C
147	38344	5 39·3	−69 02				WN5+		C
148	−69° 474	5 40·0	−69 45	11·98	+ ·24	+ ·57	B5 I+Neb		3B
149	−69° 476	5 40·3	−69 45	12·26	− ·05	+ ·40	Be+Neb		3B
150	269953	5 40·5	−69 41	9·96	+ ·94	+1·35	G0 Ia	+241	4Ac
151	269982	5 41·1	−69 16	11·4*			A5 Ia:		B
152	269992	5 41·8	−69 49	11·20	+ ·04	+ ·56	B2·5 Ia	+258	3Bd
153	270086	5 45·3	−69 00	10·28	+ ·24	+ ·71	A1 Ia−O:	+253	2Ad
154	270151	5 49·3	−70 03	12·0	+ ·10:		B1 I	+242	1Be
155	270196	5 51·7	−70 17	11·62	− ·08	+ ·48	B1·5 Ia	+248	3Bd
156	268807	4 56·3	−69 17	10·9*			Cluster		
157	268820	4 56·6	−69 26	10·3*			Cluster		
158	269578	5 27·7	−69 00	10·5*			Cluster		

Remarks to Table II

1. Cepheid variable 127^d period. $11^m.7 - 12^m.2$ V (**15**). Type at or near maximum light. Estimated types at five phases are F8 Ib (ph 0·91) G1 Ib (0·10) F8 Ia (0·83) F8 Ia (0·95) G1 Ib (0·11). See Feast (**3**) and text for discussion. Plate I, 19, 20. Chart, Fig. 2.

2. Emission at Hβ. Two plates of low quality suggest an absorption velocity of about +70, and H emission with considerably greater positive velocity. Probably a Cloud member.

3. Spectrum peculiar. Ca II too strong for A3; G band suspected. Possibly composite. No emission seen. 153d.

4. On border of N19. Velocity depends on Hγ, δ, ϵ emission. Ca II absorption present (+121: km/s). Si II suspected. Might be Ae. Apparently identical to Lindsay 15 (**18**). Plate I, 25. 183d, 180d.

5. Gascoigne (**15**) gives $V = 11{\cdot}06$; $B-V = -{\cdot}02$; $U-B = -{\cdot}74$. Ca II K measured on two plates (+146 km/s) may be stellar in origin.
154c, 154c, 146d.

6. ArpY. $V = 11{\cdot}00$. $B-V = +{\cdot}13$ (**9**). Gascoigne (**15**) gives $V = 11{\cdot}10$; $B-V = +{\cdot}14$; $U-B = -{\cdot}66$. Radcliffe observations of V show extreme range of 0·12.

Strong Ca II H and K apparently stellar, but shifted 30 km/s to violet (2 plates) relative to other absorption lines. Hβ invisible, possibly filled in by emission.
174c, 178c, 157: c, 141d, 171d.

7. Cepheid variable. Period $88^d.5$. $11^m.6$: $-12^m.4$ V (**15**). See Feast (**3**). Chart, Fig. 2.

8. Gascoigne (**15**) gives $V = 11{\cdot}22$: $B-V = +{\cdot}08$; $U-B = -{\cdot}50$. Ca II K measured on one plate (+158 km/s) is probably stellar. Hβ possibly weakened by emission.
178c, 166c, 151d.

9. Gascoigne (**15**) gives $V = 11{\cdot}10$, $B-V = -{\cdot}08$, $U-B = -{\cdot}94$. Radcliffe V, B show extreme ranges of ·13, ·14 respectively. All lines appear possibly somewhat weak compared with standard B3I. Plate I, 7.
179c, 147: c, 166d.

10. Fe II lines present.
153c, 127c, 140c, 133c, 130d, 158d.

11. On edge of Hen N50. HD has " This spectrum is nearly continuous and the hydrogen lines are suspected to be bright ". K line at +146 km/s is strong. Stellar line may be blended with Cloud gas component. Plate I, 8.
155c, 153c, 194: d.

12. Cepheid variable. Period $73^d.5$, $11^m.9 - 12^m.5$ V (**15**). Types at two epochs estimated as F8 Ia and F8 Iab. See Feast (**3**).

13. Fe II is present. H is displaced to violet relative to Fe II.
174d.

14. Hen S28, within N66 (NGC 346). Gascoigne (**15**) gives $V = 11{\cdot}77$, $B-V = -{\cdot}20$, $U-B = -{\cdot}99$. Radcliffe V shows extreme range of ·12.

Similar to W stars but definitely peculiar. Variations strongly suspected. He II 4686 emission strong and broad; He II 4541, 4200 sometimes quite strong in emission, the latter with a violet absorption edge. H lines also show occasional P Cyg structure. All emissions seem to vary in strength and width (see Plate I, 1, 2). H. J. Smith (**19**) noted 4686 and Hβ emission, and weak H and K absorption. Ca II K absorption (+153 km/s) measured on one dense plate, is presumably due to Cloud interstellar gas. Chart, Fig. 3.

15. The velocity depends solely on Hβ, γ, δ emission. Weak continuum present.
128c.

16. Fig. 3.
162d.

17. Arp (9) gives $V = 12{\cdot}04$, $B-V = -{\cdot}08$. Ca II K measured on one plate (+112 km/s) may originate in Cloud interstellar gas. Plate I, 6.
172d, 165d.

18. Near edge of Hen N66. Ca II K measured doubtfully on one plate (+112 km/s) may originate in Cloud interstellar gas. Fig. 3.
167d, 209: d.

19. Arp (9) gives $V = 11{\cdot}58$, $B-V = +{\cdot}15$. Fe II, Ti II present.
168c, 171d.

Remarks to Table II (continued)

20. Variable between $V = 11{\cdot}94 - 12{\cdot}56$. Ratio 4383/4406 indicates type later than K3. 4215/4226 indicates class brighter than Iab. No MK standards at K5 Ia.Hβ apparently in emission; Hγ probably weakened by emission. The Ia character indicates that the star must be at the distance of the Clouds and cannot be a foreground high velocity long period variable. Plate I, 24. Fig. 3.
149d.

21. Fig. 3.
128d, 105: d.

22. Galactic Ca II K very doubtfully measured on one plate (-76 km/s). Fe II present. Fig. 4.
160d, 157: d.

23. Fig. 4.
115: d, 182: d.

24. Fig. 4.
159: d.

25. Fig. 4.
167d, 172d.

26. Plate I, 16, 17. Fig. 4.
182d, 174d.

27. Ca II H and K measured ($+159$ km/s) on one plate, probably stellar. Sharp H lines indicate probably Ia–O. Fig. 4.
140c, 142d, 160: d.

28. On border of Hen N 76. Faint N1, Hβ emission suspected on the one plate available. Southern (brighter) component of double, separation about 9″ of arc. Fig. 4.
180d.

29. Within Hen N76. Radcliffe V, B show ranges of ·15, ·16 respectively. Late G or early K. Quality of spectra necessarily poor on this faint red star. Fig. 4.
151: d.

30. Within Hen N76. Ca II K doubtfully measured on one plate ($+74$ km/s) may be due to galactic or Cloud interstellar gas. Hβ, γ appear to have central emission. Fig. 4.
146d.

31. Within Hen N76. He II 4686 emission and Pickering absorption probably present. Fig. 4.
141d.

32. Within Hen 76. N1N2 emission superposed on B type absorption. Direct photographs show surrounding nebulosity (Hen N76A). The emission velocity refers to the nebula. Fig. 4.
228: d.

33. Near edge of Hen N76. ? Bo; Si IV suspected. Fig. 4.
194d, 179: d.

34. 222d, 140: d.

35. On border of Hen N76. Double star separation abour 4″·5 of arc, with following component the brighter. Fig. 4.
157: d.

36. Arp (9) gives $V = 11{\cdot}38$, $B - V = -{\cdot}02$. Ca II H and K give 152 km/s on one plate, and may originate in Cloud interstellar gas. O II, Si II present. Fig. 4.
204c, 180d.

37. Arp (9) gives $V = 11{\cdot}22$, $B - V = +{\cdot}10$. Ca II K absorption with measured low velocity appears too strong to be a galactic interstellar line at this latitude.
193c, 154d.

38. P Cyg (Beals' type I). One plate shows Hβ, γ, δ emission with mean velocity $+179$ km/s. For Hγ, Hδ the absorption is shifted 190 km/s to the violet of the emission. Fe II 4233 suspected bright.

39. 144: d.

40. Hen S52. V shows extreme range of 0·10m. Hβ emission. Hγ apparently filled in by emission. Hδ absorption. Perhaps slightly later than B8. Ca II absorption ($+162$ km/s) on two plates probably stellar; second component to K (-17 km/s) on one plate presumably due to interstellar galactic gas. Plate III, 8.
180c, 173c, 205: c, 168: d.

Remarks to Table II (continued)

41. Hβ, γ appear in emission. A poorly determined velocity of +153 km/s indicates Cloud membership.

42. Gascoigne (**15**) gives $V=11\cdot19$; $B-V=-\cdot07$; $U-B=-\cdot84$. The high velocity appears to be constant. All lines appear possibly weak. Plate III, 4.
246c, 247c, 247d.

43. Arp (**9**) gives $V=11\cdot30$, $B-V=+\cdot12$.
169c, 187d.

44. Hen N81. IC 1644. Nebular emission H, He I, [O II], [O III], [Ne III]. Direct examination shows a nebulous disk about 8″ of arc in diameter. Matches well with nebular spectrum of 30 Dor in Large Cloud, including ratio of [O II] 3726/3729. See Plate II, 2 and adjacent spectrum of 30 Dor. Object included in this list primarily for detection of faint lines. Velocity (168 km/s) previously determined by Lick Observatory (**20**).
158c, 181d, 168d.

45. Hen S57 near N83. "Emission doubtful". Gascoigne (**15**) gives $V=10\cdot26$; $B-V=+\cdot16$; $U-B=-\cdot40$.

Brightest known member of Small Cloud. Stellar Ca II K appears to be accompanied by galactic interstellar line on two plates (−13: km/s). Fe II lines present. Sharp H lines indicate Ia−O. Plates I, 10: III, 10.
180c, 178c, 168d, 180d, 164d.

46. Cepheid variable. Period $41^{d}\cdot78$, $12^{m}\cdot6-14^{m}\cdot2$ pg. Phase of observation 0·94. See Feast (**3**).

47. Probably near F5 I. Hβ emission (+222 km/s) appear fairly strongly on the one available plate. The velocity depends on absorption lines (chiefly Ti II), with wavelengths from α Per. Fe II may be weakened by emission. The star deserves examination for possible variation in light.
121: d.

48. Hβ, γ emission plus continuum on one weak plate.

49. Hβ, γ are sharp bright lines, and are used with Mg II and Si II absorption to yield a fairly accordant velocity on one plate.
171d.

50. Emission spectrum plus continuum, resembling Eta Car [Fe II] lines appear with 4244 stronger than Fe II 4233. The velocity is determined from [Fe II] and Fe II emission. Hydrogen emission (+238 km/s) is accompanied by violet displaced absorption. Plate I, 27.
191c, 176d, 187d, 175dW.

51. Radcliffe V, B show extreme ranges of ·12, ·15 respectively. O II, Si III absorption present.
307c, 316d, 283: d.

52. Near edge of Hen N79. Hβ appears rather weak, possibly weakened by emission. Perhaps B9.
270c, 249: d.

53. Within Hen N3. Galactic interstellar K suspected at +2: km/s on one plate.
306cW, 309d, 322: d.

54. Within Hen N 79. Star-like nucleus of NGC 1722; emission H, [O III], [Ne III], He I, on very faint continuum. Hβ intermediate between N1 N2.
245cW, 260d.

55. Hen S69 in N79. V, B show extreme ranges of ·11, ·16 respectively. Spectrum also varies. 1955 Dec, P Cyg structure (Beals Type I) noted at Hγ; 1959 Nov, almost pure continuum with scarcely any lines visible.
272c, 280: d, 239: d.

56. N II 3995 strong.
323d, 322: dW, 281: d.

57. Within Hen N4D and loose association of bright stars. V, B show extreme ranges of ·20, ·21 respectively. Emission suspected to red of Hγ on one plate, but the absorption is not significantly displaced to violet. Possibly as late as B5.
286c, 323d, 310dW.

58. Hβ invisible, faint Hγ emission suspected on one plate.
279c, 241: dW.

Remarks to Table II (continued)

59. Within N83, close to HD 31947 (nebula). *V*, *B* show gradual brightening by ·22, ·16 respectively in 4 years. Classified in HDE as Mo, this red star is of considerably earlier type, but is the latest type known among LMC members. See text. Plate I, 22, 23.
260d, 253d, 285: d, 236: d.

60. Cepheid variable. Period $34^{d}\cdot34$, $12^{m}\cdot6-15^{m}\cdot0$ pg. Phase of observation 0·03. See Feast (**3**).

61. *V*, *B* show extreme ranges of ·13, ·15 respectively. The HD classification (Oe) is much too early. Possibly Ia–O; sharp H absorption. Hβ appears rather weak, perhaps weakened by emission.
282c, 294d.

62. Hen S7 within N9. HD has " The spectrum appears very hazy and no lines are clearly seen. It may belong to Class Oe5 ". Hβ bright. Elements identified include H, He, Mg II, Si II, Ti II, Fe II. Plate I, 9; II, 7a.
294c, 296c, 292c, 299c. Galactic K appears on two plates (+6).

63. Cepheid variable. Period $98^{d}\cdot86$, $12^{m}\cdot3-13^{m}\cdot6$ pg. Calculated phase of observation 0·52 but may not have been as faint as indicated by this figure. Match with G2 Ib is good. See Feast (**3**).

64. Within Hen N11. Multiple Star (Mich 835) (**21**). He II 4686 emission (half width about 4000 km/s) possibly stronger than C III 4650, hence suggesting type earlier than WC 6. Normal O8 absorption spectrum but faint O II absorption possibly present indicating an additional B type component. H. J. Smith (**19**) gives WC 6+O6 I. Plate I, 3.
265dW, 302: d, 268: d.

65. O II prominent. Most plates show very large scatter in velocities from individual lines and the range of the mean velocities suggests that the velocity is variable.
265d, 272: d, 199: dW, 305: d, 242: dW.

66. Hen S73. P Cyg structure (Beals' type I) to H lines, Fe II 4233. Mg II 4481 measured in absorption (1959 Jan) with velocity +234, much closer to emission velocities, than other P Cyg absorptions. Plate I, 26, II, 4.
Emission: 264: c, 280: c, 268: d.

67. Hen S149 within N186. The spectrum resembles Eta Car, with Fe II (permitted and forbidden) represented by 48 sharp lines between 6300 and 4100A. [N II], [S II] and [Fe III] also appear to be present. Hβ and Hγ are double (red components nearly twice as strong as the violet) with separation about 135 km/s. This places star in Beals' Type III P Cyg. Plate II, 6 and 7b (Hγ only).
248c, 244c, 241·6b.

68. Galactic Ca II K appears to be present, rather diffuse, on one plate (+19: km/s).
305c, 328d.

69. Cepheid variable. Period 134^{d}, $11^{m}\cdot7-12^{m}\cdot8$ *V* (**15**). Calculated phase of observation 0·22. See Feast (**3**).

70. 284c, 346d, 273: d.

71. Hen S155. The HDE magnitude of 9·2 is much brighter than Radcliffe observations which show extreme ranges in *V* and *B* of ·15 and ·17 respectively. The star is to be regarded as probably variable.

Normal B 2·5 absorption with strong [Fe II] and ? [Ni II] emission, but not Fe II. Hβ weak emission, Hγ invisible, Hδ absorption. Diffuse Ca II absorption, presumed stellar, measured on one plate (+143 km/s), probably subject to P Cyg displacement.
Emission 191d, 194c, 193c, 188c.

72. 226d, 241d, 253: d.

73. Weak H; ? Class Ia–O. Weak galactic Ca II K measured (+18 km/s) on one plate, as well as stellar component. Plate III, 6.
300c, 324: c, 295d.

74. Hen S17. Outside N17, in cluster, NGC 1820. Hβ, Hγ emission, Hδ absorption.
289c, 339: dW.

75. H lines weak; ? due to emission or high luminosity. Fe II present. Galactic Ca II K suspected on one plate (+48: km/s). HD classification (Oe) much too early.
287c, 335: d.

Remarks to Table II (continued)

76. Hen S171. The brightest known member of either Magellanic Cloud still exceeding S Dor in its recent bright phase. In no recognised nebulosity. The following metals have been identified: Fe II, Ti II, Cr II, Sc II, Ni II. The spectrum does not match exactly any MK standard (see Plates I, 13; III, 14). The best overall match for metal lines is probably with A2 Ia. However the ratio Si II (4128−30) and the Fe II, Ti II, Y II blends (4172−79) which is generally sensitive to type in the early A's, indicates a type near A3 (Si II too weak for A2). The relative strength of Mg II 4481 to other metal lines also indicates a type near A3, but the overall metal line intensities are too weak for an A3 supergiant. The H lines are weaker than in an A2 Ia star. This may probably be taken as an indication of high luminosity. A preliminary measure of one plate (29A/mm) gives 2·6A for the equivalent width of Hγ. However the match with HD 160529, classed as A2 Ia−O (Morgan, private communication) is poor (H lines of comparable strength but metals much stronger in 160529). Clearly the later type suggested for 33579 increases rather than diminishes this discrepancy. It is extremely suggestive that the lines Mg II 4481 and Si II (4128−30) whose weakness suggests a type as late as A3, contrary to other evidence, are just those subject to conspicuous weakening in shell stars (**22**). It is not possible to determine at this stage, whether 33579 is actually a shell star or whether the dilution of radiation within the very extensive atmosphere that this star must have could satisfactorily account for the observations. However it is interesting to note that it is an Hα emission object (Henize). In the circumstances any exact spectral type is of doubtful significance and a detailed investigation of the spectrum is extremely desirable.
258·2b, 249c, 254c, 246d.

77. Cepheid variable. Period $36^{d}\cdot53$, $12^{m}\cdot3-13^{m}\cdot7$ *V* (**15**). Calculated phase of observation 0·13. Appears to be between F5 Ia and F8 Ia. See Feast (**3**).

78. Central star in Hen N100. *V*, *B* show extreme ranges of ·15, ·13 respectively. Hβ weak, ? emission. Ca II K absorption may be due to Cloud interstellar gas (+207: from one plate). Plate I, 5.
224d, 243: d, 267d, 220d.

79. Not in Hen nebulosity, but follows N 103A by 2′ of arc.
314d, 292d, 298: d.

80. *V*, *B* show extreme ranges of ·11, ·10 respectively. H lines weaker and sharper than Ia. Si II, Fe II, ? Sc II present. Ca II K treated as stellar. Plate I, 11.
235c, 225d, 228d.

81. Hen S86, not in nebulosity. *V*, *B* both show extreme ranges of ·11. Hβ, γ, δ show P Cyg structure (Beals' type I) and have not been used in determining the velocity. The mean velocity of H absorption is +154 km/s. Galactic Ca II K absorption is found at 0 km/s on one plate.
266d, 196: c, 224c.

82. Hen S89 within N113. Velocity depends on Fe II and faint [Fe II] emission. Hβ, Hγ have P Cyg structure (Beals' type III), separation of components 174 km/s; the velocity of H absorption is measured as +247 km/s.
236c.

83. Cepheid variable. Period $48^{d}\cdot27$, $12^{m}\cdot0-14^{m}\cdot2$ pg. Calculated phase of observation 0·35. Type estimated as late F or early G. See Feast (**3**).

84. Hen S91, not in nebulosity.

Hγ, δ and He 4471 show P Cyg structure (Beals' Type I) with rather broad emission bands. He II 4686 in emission, with suspected violet displaced absorption. N III also present in emission. H. J. Smith (**19**) also records Si IV, Si III in emission.
262: c.

85. Brighter component of wide double near S Dor within N119. *V*, *B* show extreme ranges of ·16, ·13 respectively. The north following star is not a member of the Cloud. Hβ emission, Hγ, δ absorption N II 3995 and stellar Ca II present. Galactic Ca II K is suspected at −9: km/s on one plate.
292c, 291d.

86. Within Hen N119. Cluster NGC 1910.

HD has " Con. . . . . No lines are seen ". Of four bright central stars, the northern and southern pairs both show early type (probably O) absorption.

Remarks to Table II (continued)

87. Bright star in Cluster within N119. Broad 4686 emission, ? WN5. Hβ invisible, Hγ suspected emission to red. Hδ pure absorption. Galactic Ca II K measured at +43: km/s on one plate.
289c, 279d.

88. S Dor. Hen S96, within N119. See Wesselink (**2**). Since 1957 September photoelectric observations show the variable to have been as bright as 9·2 (V) following a prolonged minimum at 10·0. We find $B-V=+\cdot22$ at maximum and $B-V=+\cdot10$ at minimum. In this bright phase the P Cyg absorption and emission lines (Beals' Type I) of the metals have intensified, especially for Ti II, for which the intensity ratio absorption/emission is much larger than for Fe II. See Plate II, 3 (the reproduction shows the emission clearer than the absorption). Sc II 4246, not recorded in Wesselink's paper, has appeared quite strongly; Sr II 4215 is also present. He I is invisible. The ionization temperature is lower in 1958–1959 (corresponding perhaps to A5eq) than it was in 1951–1952. The match of absorption lines with HD 164514 (A5 Ia) is good except that Sr II 4215 is weaker in S Dor.

At minimum phase emission lines due to [Fe II] were visible, and these were last seen clearly in February 1957 (JD 2435888). The velocities tabulated are taken from Wesselink (**2**).

89. Within Hen N120. CPD −69°361, a multiple star in NGC 1918, of which this is the brightest component. A faint star distant 3″·3 of arc is recorded by the Michigan observers (M936) (**21**). The one photoelectric observation was made with 12″ of arc diaphragm and should have excluded more distant companion (R90).
273dW, 309: d.

90. This star is 9″ Spr 35517 (R89). The W emission is responsible for the HD classification of 35517 as Oa. 4686 possibly stronger than 4650, suggesting type earlier than WC6 (cf. R64). The one photoelectric observation was made with 12″ of arc diaphragm and should have excluded 35517.

91. HD 269362 (K5). Cepheid variable. Period $118^{d}\cdot6$, $11^{m}\cdot9-12^{m}\cdot7$ V (**15**). Calculated phase of observation 0·34. See Feast (**3**).

92. B shows extreme range of ·14. See text for discussion of spectrum. Plates I, 18; II, 9. Fig. 5.
322c, 322d.

93. Within N43. Blue star picked out on direct photographs. Lines appear rather diffuse on one available plate. Fig. 5.

94. Within N43. Michigan double 946 (10·3 − 12, 0″·65) (**21**). V shows extreme range of ·10. The weak spectra show a predominantly early type Cloud member in the blue, together with some features of a late type companion probably also a Cloud member. The red component is recorded on one low dispersion plate which does not prove Cloud membership. This star lies 6′ of arc Sf 271182 (R92), a late type super-supergiant. The exposures required in the blue prove that the blue star is the fainter of the two. Fig. 5.
293: c, 286: d.

95. Within N43. Selected as very blue star on direct photographs. Fig. 5.
329d.

96. Possibly as late as B5.
221d, 228d, 263d, 262: d.

97. Within N43. Selected as very blue star on direct photographs. Fig. 5.
310d, 305d.

98. Not involved in nebulosity, but near N43 and within scattered cluster NGC 1925. Sharp H lines suggest Ia–O. Fig. 5.
302c, 321d.

99. Hen S30 in N44. Emission lines of H, He II 4686, He I 4713, 4471, 4388, 4026 on continuum.
No absorption seen. Plate I, 28.
281d, 285d, 258: d.

100. Not in nebulosity but near Hen N198.
260c, 233d.

101. Near edge of Hen N 205B.

Ca II K measured on two plates (+260 km/s) is probably stellar but was not used for velocity. A second weak component (+21 km/s) is presumably a galactic interstellar line.
254c, 238d, 259d.

Remarks to Table II (continued)

102. R CrB type variable ($13^m{\cdot}8 - 16^m$pg). Type in range F5 – Go, probably near F8. H lines weak for the type (a characteristic of RCrB variables). A velocity of about +260 km/s indicates Cloud membership. See Feast (**3**). Fig. 6.

103. In Hen N144. Very wide faint emission band at 4686 suggests that spectrum is composite with a faint W component. Ca II K measured on two plates (+260 km/s) may be due to Cloud interstellar gas.
302c, 295c.

104. 308c, 314:c, 293d.

105. Within N135 but not in specific nebulosity.

Hen S 111 is identical to HD 269599 (classified as 'Pec') and apparently to CPD – 69°383. This latter "star" is a compact cluster, and the single Radcliffe spectrum refers to the southern edge of the cluster and no emission lines are seen. A single Radcliffe photo-electric observation gives $V = 10{\cdot}2$, $B - V = +{\cdot}33$: but this refers to the cluster, not to an isolated star.
268d.

106. The HDE classification is F8, but a pair of direct photographs of the area showed it to be blue, and the single spectrum proves it to be a Cloud member of early type.

107. 333d, 327d, 360: dW.

108. Hen S43. This faint red star on edge of cluster NGC 2004 shows [Fe II] emission on a continuum with no certain absorption due to H or other elements in the one spectrum available. Fig. 7.
318d.

109. Selected as bright blue star in NGC 2004. Radial velocity not measured but confirms Cloud membership. Fig. 7.

110. Hen S116, within N135, but not involved in specific nebulosity. Beals' Type I, $H\beta$, γ emission.

111. Hen S117 "Emission [at Hα] is perhaps doubtful". (Near edge of N 135 but not within specific nebulosity). Narrow H lines suggest possibly Ia – O. Galactic Ca II K measured (at +33: km/s) on one plate, accompanying strong stellar K. Plate III, 9.
265c, 242: d.

112. In Hen N206. B shows extreme range of ·11. N II 3995, Si III 4567 strong. Unidentified feature at 4544 on two plates. Ca II K appears to have a weak companion (+126 km/s); the main component may be stellar or interstellar (Cloud) gas. Plate III, 3.
232c, 246c, 231d.

113. Within Hen N206A.

The only spectrum available, taken in bad seeing conditions when duplicity was suspected, shows He 4541, 4199 absorption. Emission at $H\beta$, $H\gamma$. Duplicity was confirmed visually later; the Sf component was estimated about $0^m{\cdot}4$ brighter, and the separation about 3″ of arc.
244d.

114. Within N57. The one spectrum available (untrailed) of this faint star shows He II 4686 emission, 1700 km/s wide.
Probably WN5.

115. On border of N57, within N56. He II 4686 appears as broad emission apparently shifted to red relative to other lines; N III 4634, 4640 are present weakly in emission. H and He II (Pickering) in absorption.

116. Hen S172, involved in N148C.

Code and Houck (**23**) give $V = 10{\cdot}23$, $B - V = -{\cdot}03$. The considerable difference from our V may indicate variability in this P Cyg star.

P Cyg (Beals' Type I). Weak $H\beta$ emission; $H\gamma$ absorption shifted to violet. On one plate galactic Ca II K appears to be present (+16: km/s). Classified as B2 Ia – O by Code and Houck (**23**). Plate III, 1.
269c, 213: c, 265: d.

117. Within N57A and cluster NGC 2014. See text. Plate II, 11.
308c, 311d, 340d.

118. No nebulosity but richly clustered area. $H\beta$ absorption apparently weakened by emission.

Galactic Ca II K suspected on one plate (+62: km/s) but the line is not sharp.
351c, 340c, 333c, 346d.

Remarks to Table II (continued)

119. 312d.

120. On border of N56, but no pronounced nebulosity in neighbourhood. B shows extreme range of ·13m. H and stellar Ca II provide the strongest lines. N III 4097 suspected on one plate, suggesting possibility of a composite star.
288c, 290: d.

121. On border of N56, but no pronounced nebulosity in neighbourhood. Narrow H suggests Ia–O.Sc II 4246 seems to be present. Galactic Ca II K suspected on one plate, but not measured.
319c, 318d.

122. Within N59A and doubtless an important agent in exciting this bright nebula. Nebular [O III] emission seen, plus N IV 4058 as in W stars. The HDE classification is Go. The Pickering series appears rather strongly, but nevertheless the radial velocity is reduced using the ordinary wavelengths for H lines. Plate I, 4.
255: d, 261: d, 255: d.

123. Hen S124 within N149.

H and He I emission measured, with suggestions of violet displaced absorption of He I but not H (Beals' Type I, P Cyg).
260c, 280: c.

124. Within N56.

One very weak plate shows narrow Hγ shifted about +250 km/s indicating Cloud membership.

125. Within N56. *V*, *B* show extreme ranges of ·10, ·21 respectively.
298d, 286d.

126. Hen S127 within N135 but not apparently associated with a specific nebulosity. H and Fe II present as sharp emissions; [Fe II] 4244, 4287 weakly present. Ca II absorption at +87 km/s may represent P Cyg absorption in the stellar atmosphere. Plate II, 5.
262c, 254c.

127. Hen S128. Within N135 but not associated with specific nebulosity. Densely clustered region. The P Cyg star is the following component of a 2″ of arc double, the preceding star being also a Cloud member of early type. The velocity depends only on emission of H, He I, but He II and N III emission also present. Hβ and He 4471 show P Cyg structure (Beals' Type I) with absorption displaced 240 km/s to the violet.
284c.

128. Closely follows R127 in densely clustered region. Hβ invisible on these plates, possibly incipient emission.
271d, 266d.

129. Within Hen N157, 30 Dor outskirts.
266d, 281d.

130. Within Hen N157, 30 Dor central region. Nebular emission superposed. Weak 4686, 4640 emission suspected on only plate available (rather dense in this region). HD has Oc. Fig. 8.

131. Within Hen N157, 30 Dor central region. Nebular spectrum superposed. Fig. 8.
271c, 264d.

132. Within Hen N157, 30 Dor central region. In cluster. Nebular emission superposed. Fig. 8.

133. Within Hen N157, 30 Dor central region.

4471/4541 indicates O8 but Si IV 4089 appears to be too strong for this type. This is possibly due to super-giant characteristics or to weakening of 4471 by superposed strong nebular emission. Figs. 8, 9.
219c, 266d.

134. Within Hen N157, 30 Dor central region. He I, He II, N III, N IV emission. 4471 He I and 4541 He II have absorption components of large negative displacement, (measured at about −380 km/sec with respect to Sun). Ca II Cloud interstellar absorption present. Strong nebular emission superposed. Fig. 9.

135. Within Hen N157, 30 Dor central region. H, He I, He II, N III, N IV emission. Strong superposed nebular emission. Fig. 8.

Remarks to Table II (continued)

136. Central " star " in 30 Dor but appears nebulous and is probably composite. The velocity refers to emission lines (Lick Em. Vel. +275 km/s) (**20**). Cloud interstellar Ca II K measured at +295 km/s. O type absorption (+251: km/s) plus 4686 and 4640 emission. Strong nebular spectrum superposed. Nebular He 3889 absorption (+240 km/sec) present. See Feast (**24**). Fig. 8.
276c, 280: c, 264d.

137. Within Hen N157, 30 Dor central region. Strong superposed nebular emission. Fig. 8.

138. Within Hen N157, 30 Dor central region. Strong superposed nebular emission. Figs. 8, 9.

139. Within Hen N157, 30 Dor central region. O type absorption plus weak W emission (4686, 4640). Strong superposed nebular emission. Strong Ca II absorption, presumably due to Cloud interstellar gas. Figs. 8, 9.

140. Within Hen N157, 30 Dor central region. He II, N III, N IV, N V emission. H relatively weak, masked by superposed nebular emission. Ca II absorption presumably due to Cloud interstellar gas. Fig. 8.

141. Within Hen N157; 30 Dor central region. Strong superposed nebular emission. Fig. 9.

142. Within Hen N157, 30 Dor central region. Nebular emission superposed. Little seen of stellar absorption. Fig. 9.

143. Within Hen N157, 30 Dor central region. See text for discussion of spectrum. Previously (**4**) called 30 Dor No. 50. Fig. 8. Plate II, 8.
247c, 295d.

144. Within Hen N157, 30 Dor central region. Hen S 133. H, He II, N III, N IV emission. Fig. 8.

145. Within Hen N157, 30 Dor central region. H, He II, N III, N IV emission. Nebular N1 superposed. Figs. 8, 9.

146. Within Hen N157, 30 Dor central region. Nebular emission superposed. He II, N IV emission. Fig. 8.

147. Within Hen N157, 30 Dor central region. H, He II, N III, N IV emission. Fig. 8.

148. Within Hen N159. Nebular [O III], and H emission appear, superposed on B type absorption.

149. Within Hen N159. Nebular [O III] and H emission appear, superposed on B type absorption.

Hβ stronger than N1N2 here, and therefore presumably originates mostly in a Be star.

150. B shows extreme range of ·14m. Close to Hen N 160C and lying on wisp in this bright nebula (NGC 2086 etc.) See text. Plates I, 21; II, 13.
239c, 236c, 253d.

151. Within Hen N157, 30 Dor outskirts. Plate I, 15.

152. Within N135 but not involved in pronounced nebulosity. Ca II K is probably stellar. Narrow H and strength of N II 3995 suggest Ia–O.
251c, 270c, 235:d.

153. Hen S143. Henize states " emission doubtful ". Numerous Fe II lines present, with stellar Ca II K, etc. Narrow H suggests Ia–O. Plates I, 12; III, 12.
253c, 252d.

154. In Hen N180B.
232d, 262: d.

155. 262: c, 254: c, 229d.

156, 157, 158. All three objects observed photographically or visually with the Radcliffe reflector to be compact clusters with brightest stars considerably fainter than the HDE magnitude. R158 is recorded as " neb " in CPD (−69°379). Cloud membership is evident from the cluster character and the HDE types. No Radcliffe spectra attempted.

6. *Identification of stars.*—The majority of the stars in this programme are included in the HD, HDE or CPD catalogues and we have found no great difficulty in identifying such stars at the telescope. For HDE stars, not occurring in the CPD, local charts in x, y were prepared tied in to the CPD with nearby stars. It was desirable in a few crowded areas to supplement such charts with direct photographs taken with the 74-inch reflector.

In view of such experiences it has not been felt necessary to provide identification charts for all the stars of this paper, nor when the stars are already identified by Henize (**8**) or Arp (**9**).

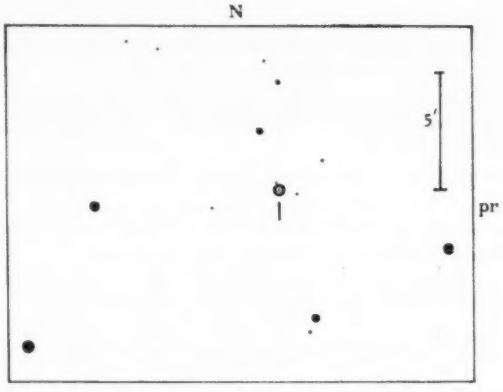

FIG. 1.—*Field of HV* 821 (*R*1) *from blue plate.*

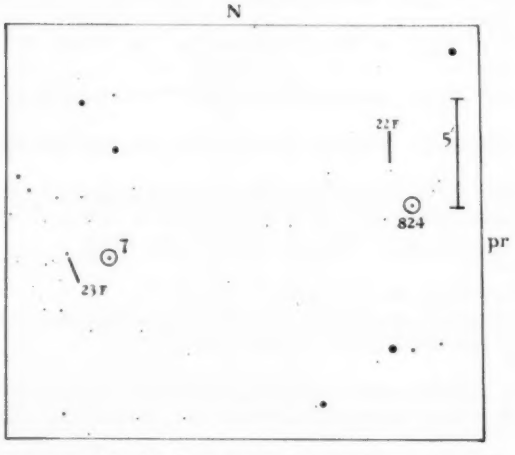

FIG. 2.—*Field of HV* 824 *and HV* 829 (*R*7) *from blue plate.*

Identification charts are, however, provided for all anonymous members of the Clouds (Figs. 1 to 10). The stars are identified by Radcliffe numbers, foreground stars (when they occur) from Table III being identified by their numbers followed by F. HV 1956 is identified in Fig. 10, together with a foreground star, although we have not as yet observed the variable spectroscopically.

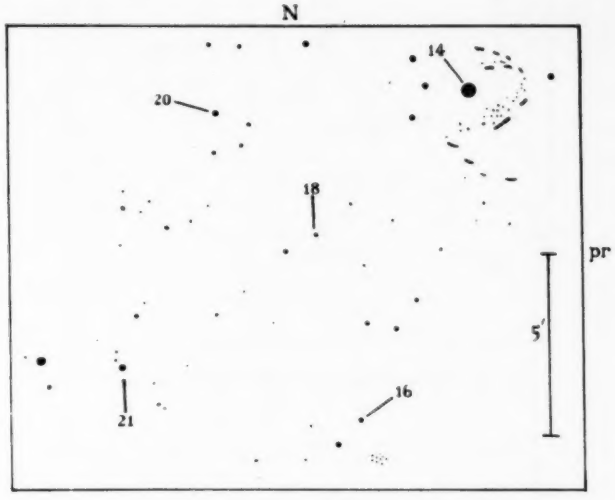

FIG. 3.—*Field of NGC 346 from red plate.*

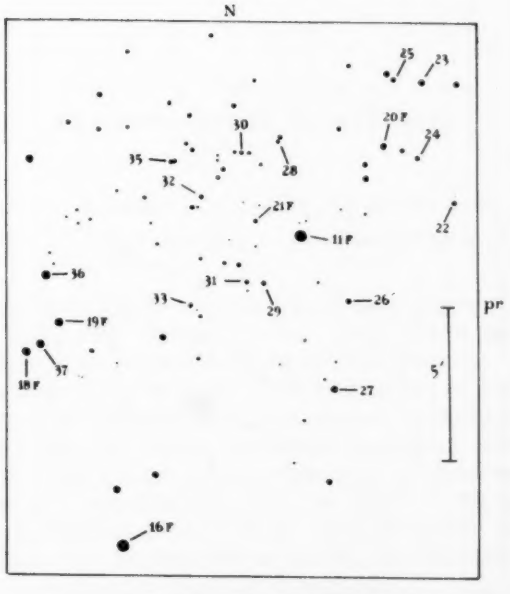

FIG. 4.—*Field of NGC 371 from yellow plate.*

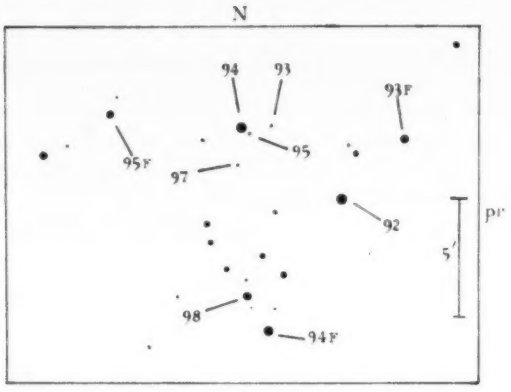

FIG. 5.—*Field of HD 271191 (R94) from red plate.*

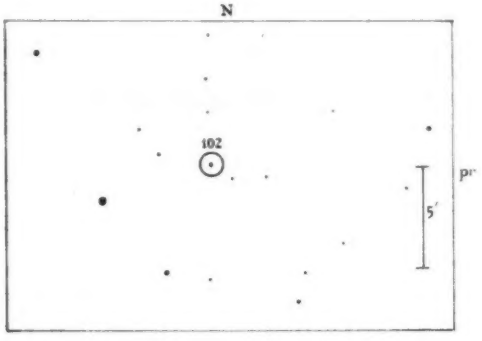

FIG. 6.—*Field of W Men (R102) from blue plate.*

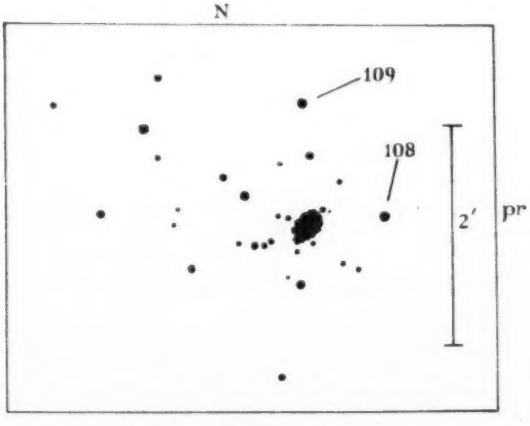

FIG. 7.—*Field of NGC 2004 from yellow plate.*

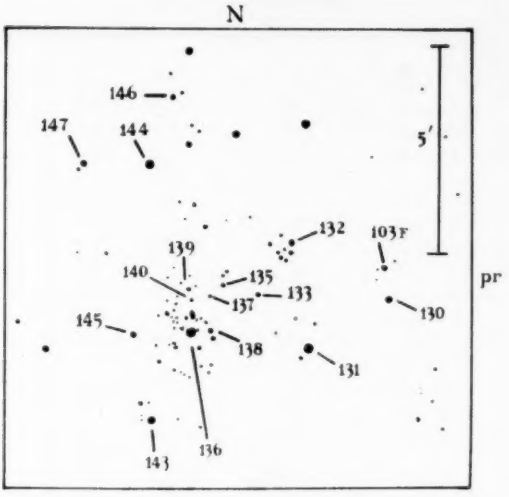

FIG. 8.—*Field of* 30 *Dor from red plate (omitting nebulosity).*

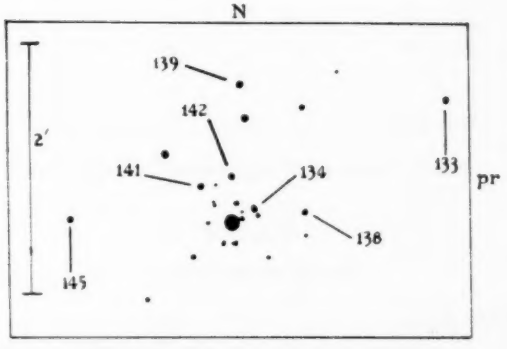

FIG. 9.—*Central region of* 30 *Dor from ultra-violet plate.*

7. *Foreground stars.*—A list of individual foreground stars is given in the accompanying Table III. Besides the star designation is quoted the photographic magnitude (from various sources) and HD spectrum. In nearly every case the observations were restricted to only one narrow or untrailed spectrum, and this was found quite adequate for the purpose of indicating non-membership of the Cloud through low velocity and lack of supergiant characteristics. A? following the star designation indicates that proof of non-membership is not quite so convincing as usual on account of low quality of the spectrum.

Remarks are added to some stars at the end of the Table. It will be noticed that a few stars have been selected because the Harvard or Potsdam classifications (28) suggested that the stars might be supergiants.

Three peculiar foreground stars are dealt with separately in Section 15.

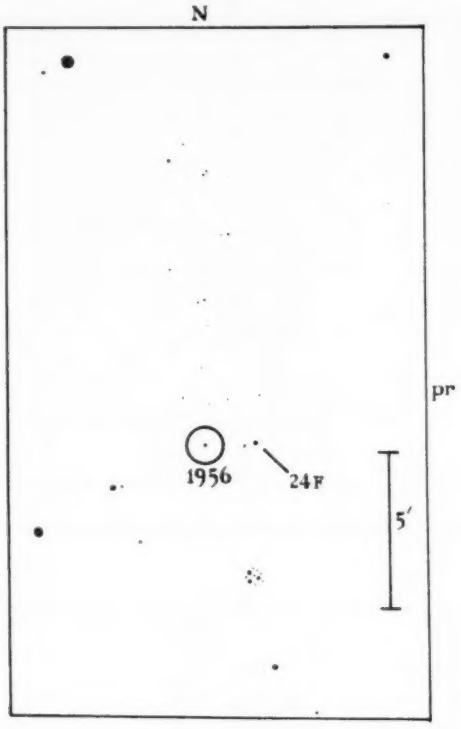

FIG. 10.—*Field of HV 1956 and 24F from blue plate.*

TABLE III

Proved foreground stars

(a) SMC Region

	Star	m_{pg}	Sp.
1F	−74°2110•	12+	
2	HD 1484•	9·1	F8
3	1755•	9·1	Fo
4	3752•	9·4	Fo
5	4512•	10·1	F2
6	4725•	10·9	A
7	4852•	10·8	G
8	5512•	10·6	G
9	5678	10·8	F2
10	6193•	10·1	A5
11	6406	10·0	F5
12	7222	11·2	B9
13	Hen S1•		
14	Hen S7•		
15	Hen S37		
16F	Arp H•	9·4	
17	Arp P•	10·4	
18	Arp U•	12·1	
19	Arp X•	10·9	
20	Anon•		
21	Anon•		
22	Anon•		
23	Anon•		
24	Anon•		

(b) LMC Region

25	HD 31722	8·9	A2
26	32762	8·4	A2
27	33148	10·1	G5
28	33486•	8·1	B9
29	33617	8·9	Go
30	33970	9·5	F2

TABLE III (*continued*)

(*b*) *LMC Region* (*continued*)

	Star	m_{pg}	Sp.
31F	HD 34651	8·6	Fo
32	35026	9·0	A3
33	35094	8·9	A2
34	35140	9·6	A2
35	35183	9·0	A2
36	35293	9·2	Ao
37	35294	8·9	F5
38	35538	10·3	A
39	35665	9·2	G5
40	35978	9·3	A2
41	36661N•	9·0	A2
42	36751?	9·6	A
43	39739	10·0	A
44	40343	10·3	A
45	41846•	8·8	A3
46	51164	10·8	A
47	HDE 268676	10·8	Mo
48	268754	10·8	Ko
49	268776	10·2	Go
50	268783	12·0	Mo
51	268799	10·4	Go
52	268812	12·1	K
53	268879	11·6	K2
54	268883?	12·2	K2
55	268943	10·2	Ao
56	269073	10·6	Ko
57	269081	10·4	Ko
58	269319	10·0	A5
59	269321f?•		
60	269410	11·7	G5
61	269434	11·0	Go
62	269438	11·0	F5
63	269447?	11·6	K5
64	269544?	11·9	Mo
65	269665	10·6	B9
66	269666	12·3	Ko
67	269669	11·2	Go
68F	HDE 269691	12·6	Ko
69	269696•	10·7	B
70	269724	12·2	K5
71	269731	12·4	Ko
72	269732	13·4	K2
73	269733	11·9	Go
74	269737	12·0	Ko
75	269746	12·6	K5
76	269767	10·8	Ko
77	269770	12·0	K5
78	269793	13·1	Ko
79	269808	12·1	G5
80	269820	11·0	Ko
81	269831	12·1	Ko
82	269836	12·2	K7
83	269849	12·4	K5
84	269862	12·1	Mo
85	269898	13·0	Mo
86	269915	12·3	Fo
87	269924	12·2	K5
88	270109	9·4	A2
89	270365•	12·0	Ko
90	271012	10·4	K7
91	271049	10·2	Ko
92	271151	9·9	Mo
93	271178	10·4	F8
94	271187	11·4	Mo
95	271204?	10·6	F2
96	271350•	10·2	Mo
97	−73°276•	10·0	
98	−74°310•	9·6	
99	−75°295•	10·5	
100	HV 2882•		
101	Anon•	10	
102	Anon•	12:	
103	Anon•		

Remarks to Table III

(*a*) *SMC Region*

1. Potsdam 200/20, G2s.
2. Potsdam 200/132, cFo.
3. Potsdam 200/147, cFo.
4. Potsdam 200/242, A5s.
5. Potsdam 200/265, A5s.
6. " Hγ, Hδ very narrow " (HD).

Remarks to Table III (continued)

7. " Hγ, Hδ narrow "; like δ CMa? (HD).
8. " Hγ, Hδ narrow "; F5? (HD).
10. Arp K (9).
13. Wide H, He absorption, Velocity −28 km/s, (2 plates).
14. Velocity +22: (1 spectrum).
16. Chart Arp (9).
17. Chart Arp (9). Harvard sequence k.
18. Fig. 4 and Arp (9).
19. Fig. 4 and Arp (9). Velocity +44 km/s (4 plates); B type but not supergiant.
20. Fig. 4.
21. Fig. 4.
22. Near HV 824. Fig. 2.
23. Near HV 829. Fig. 2.
24. Near HV 1956. Fig. 10. High velocity star. See Section (15) *a*.

(*b*) *LMC Region*

28. Henize quotes as exciting star for N23.
41. Close double, separation ~1″.
45. HD slightly pec? ?G.
59. TiO present. See note to R85 (Cloud member).
65. +40 km/s from one plate.
69. Luyten (**25**) gives proper motion ″·09. See Section 15 (*b*).
89. High velocity foreground star. See Section 15 (*a*).
97. Potsdam 201/377 B?.
98. Potsdam 201/441 cFo.
99. Potsdam 201/468 cF8.
100. Foreground Me variable. See Feast (**3**). Considered by earlier workers (**26**) to be a Cloud Cepheid.
101. Projected on Cluster NGC 1786 (HD 268823). See Thackeray (**27**).
102. Red star, np NGC 1929.
103. Near 30 Dor; Fig. 8.

DISCUSSION

8. *Interstellar absorption and the intrinsic colours of Cloud members.*—It is important to know to what extent, if any, the apparent magnitudes and colours of Cloud stars are affected by absorption. Such absorption may, of course, arise either within our Galaxy or within the Clouds themselves.

(*a*) *Intrinsic colours of early-type stars.*—In Fig. 11 our measured colours *B–V* of early-type Cloud stars are plotted against spectral type. The intrinsic colours of galactic supergiants are not well known. The best available are probably those of Johnson (**29**) and these are plotted as the continuous curve. If this represents the intrinsic colours of Cloud supergiants then the distance of a star above the curve measures its colour excess E_{B-V}.

In the range Bo to Ao the intrinsic colours cannot be much, if at all, redder than those given by Johnson. For instance, at B8 two Cloud stars fall on Johnson's curve and at Ao two stars are only $0^{m}\cdot01$ redder. Our results may be regarded as a good confirmation of Johnson's colours in this range. However, the strange dip in Johnson's curve at A3 is not reflected in our results. The four A3 Cloud stars must all suffer an abnormally large reddening if their intrinsic colours correspond to Johnson's. While of course this *might* be the case, it has been thought best to assume for these A3 stars the same average

colour excess that is found by assuming Johnson's intrinsic colours for the other early-type supergiants; the intrinsic colour thus found is +·04 (indicated in Fig. 11 by the dotted line). It will be clear that the A3 intrinsic colour could be still redder (up to $+0^{m}\cdot12$) without directly conflicting with our results (cf. Feinstein's (**38**) intrinsic colour of $+0^{m}\cdot13$ for A3 supergiants).

We have as yet too few O stars to draw any definite conclusions as to the applicability of Johnson's (**29**) intrinsic colours to these stars. The data on W stars are also too fragmentary to draw any conclusion, and in any case their colours may be affected grossly by emission bands, but they appear to lie in the range of O or early B type colours.

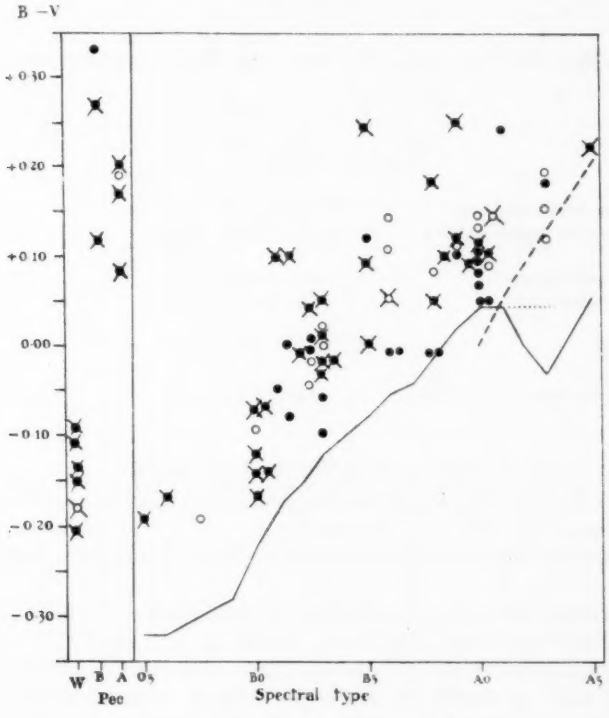

FIG. 11.—*Measured colour B−V and spectral type of Cloud stars.*

● *LMC.*
● *LMC in or near nebulosity.*
Intrinsic colours for supergiants:
. . . . . *Adopted for A3 stars.*

○ *SMC.*
○ *SMC in or near nebulosity.*
———— *Johnson* (**29**)
- - - - - *Feinstein* (**30**)

R108 (B−V=+1·19:, Pec) not plotted.

R31 (O:f:) plotted at O 7·5.

The Pec stars are all moderately red and have a considerable scatter in colour (probably affected by emission lines). They are divided in Fig. 11 into two groups A and B according to whether they show [Fe II] (Eta Car type) or He I or II emission. The two reddest Pec stars plotted both show He II emission and might therefore be considered very early type.

(*b*) *Interstellar absorption* (*early-type Cloud members*).—The scattered distribution of our Cloud stars in Fig. 11 above Johnson's curve gives evidence of reddening of variable amount in both Clouds. Table IV shows the average visual absorption $\bar{A}_V$ for Large and Small Cloud stars of type earlier than A2 which we have observed photometrically. In the Large Cloud the number of stars is sufficient to break down the material into groups of stars with or without emission lines in their spectra, or stars found within or outside Henize Hα nebulosities. At the foot of the Table we quote mean values of absorption from proved foreground stars (details of which are given in Section 14).

TABLE IV

Mean absorptions ($A_V = 3E_{B-V}$) *for stars earlier than A2* (*peculiar stars omitted*)

	LMC			SMC		
	$\bar{A}_V$	s.e.	(n)	$\bar{A}_V$	s.e.	(n)
All stars	0·33	±0·03	(48)	0·34	±0·03	(15)
Stars showing emission lines	0·40	±0·06	(9)			
Stars not showing emission lines	0·31	±0·04	(39)			
Stars within nebulosity	0·40	±0·04	(30)			
Stars not in nebulosity	0·21	±0·04	(18)			
Greatest value	0·96		(1)	0·60		(1)
Foreground absorption (see Table X)	0·21	±0·12	(5)	0·21	±0·03	(8)

Study of Table IV leads to the following conclusions:

(1) Stars in both Clouds suffer absorption of an amount that is quite small by galactic standards with very few having $A_V > 0^m{\cdot}6$. However, our selection of the apparently brightest Cloud members must favour stars suffering little absorption.

(2) The small difference in reddening between stars with and without emission lines is not statistically significant: there is no compelling evidence that emission-line stars are preferentially associated with dust or differ in intrinsic colour from stars of similar spectral types without emission lines.

(3) Stars "within" nebulae show significantly greater reddening than those outside; exclusion of cases of chance projection on nebulae would be likely to increase the difference. The greater reddening of stars within nebulae can be seen in Fig. 11 where the two groups are distinguished by symbols. Thus there is a statistical association of dust and gas in the Large Cloud.

(4) Stars outside nebulosities show essentially the same degree of reddening as our selected foreground stars.

(5) For stars within nebulosities, at least part of the reddening occurs within the Large Cloud and is not entirely due to foreground absorption.

The star with the largest observed absorption in either Cloud is R148 (−69°474). This star was selected for observation on account of its lying within an apparent absorption lane and its reddish colour on direct photographs.

(*c*) *Regional variation of absorption in the Large Cloud.*—In Fig. 12 the distribution of Large Cloud members with known colour excesses in the plane of the sky is indicated, the size of the dots increasing with the measured colour excess. There is perhaps a slight indication that large colour excesses are found preferentially in or near the main " bar " of the Cloud, and a more definite indication that small colour excesses are found preferentially in the outskirts.

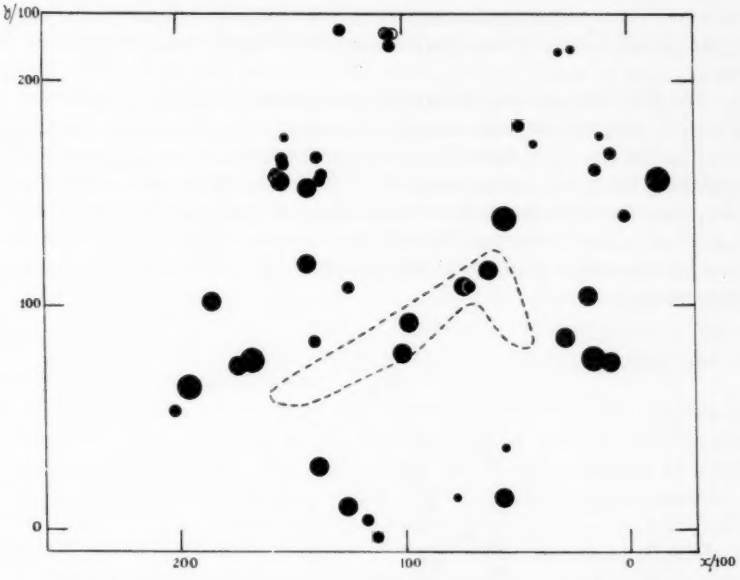

FIG. 12.—*Regional distribution of colour excesses in LMC. The position of the " bar " is outlined. The size of each dot is roughly proportional to the colour excess* E_{B-V}.

(*d*) *Intrinsic colours of late-type Cloud members.*—Data concerning colours of the few late-type Cloud members for which we have spectroscopic and photometric observations are assembled in Table V. In view of the importance of determining intrinsic colours as accurately as possible for such stars we have attempted to determine the reddening individually for each of the six stars. These late-type stars tend to occur in clustered regions. The mean colour excess of known early type stars (based on Johnson colours) in closest proximity

TABLE V

Intrinsic colours of late-type member

	Star	Sp	$B-V$	E_{B-V}	$(B-V)_0$	(30) $(B-V)_0$
R 26	Hen S40	Fo: I(e)	+0·41	·13	+0·28	+0·16
92	271182	F8 Ia	+0·57	·07	+0·50	+0·62
150	269953	Go Ia	+0·94	·18	+0·76	+0·76
117	269723	Go Ia	+1·06	·14	+0·92	+0·76
59	268757	G5 Ia	+1·55	·21	+1·34	+1·05
18	Hen S30	K5 I(a)e	+1·89	·13	+1·76	+1·65

The colour excesses E_{B-V} are mean values for early type Cloud members near each star (see text).

to each late-type star was determined and appears in the fifth column of the Table; applying this colour excess we arrive at the intrinsic colours given in the sixth column. In the last column we quote Feinstein's (**30**) intrinsic colours of galactic supergiants for the relevant spectral type.

It will be seen that the agreement with Feinstein is satisfactory, especially when it is recalled that Feinstein considers his colours to be subject to an uncertainty of $0^m.1$ which also represents the sort of uncertainty in our reddening corrections. It is of particular interest to note that the colours of the two stars from the Small Cloud (Hen S30 and 40) both agree with Feinstein's within $0^m.12$.

9. *The HR Diagram and the absolute magnitudes of Cloud supergiants.*

The HR diagram for stars with known spectral types and B, V magnitudes is shown in Fig. 13. For stars of type A1 and earlier each star has been corrected for reddening using the intrinsic colours of Johnson (**29**) as previously discussed. For the other stars the mean absorption deduced from the early-type stars has been applied. The correction applied is only $0^m.3$ ($\bar{A}_V$) and none of the discussions in this section is critically dependent on the actual amount of absorption for these stars.

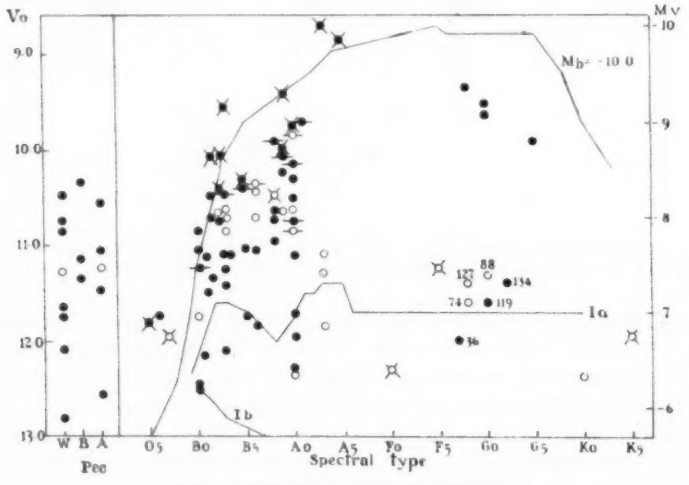

FIG. 13.—*HR Diagram of Cloud stars.*

● *LMC.* ○ *SMC.*

⊛ *LMC emission-line stars.* ⊛ *SMC emission-line stars.*

⊸● *LMC ? emission-line stars.* ⊸○ *SMC ? emission-line stars.*

*R*114 (14·5*m*, *W*) *not plotted.*

Lines corresponding to $M_{bol} = -10.0$ *and to the calibration of MK Ia and Ib supergiants* (**50**) *are shown. The periods (in days) of Cepheids are indicated by numbers.*

The absolute magnitude scale in Fig. 13 is that previously adopted (**6**). It was deduced from the apparent magnitude of the RR Lyrae variables in the Cloud ($19^m.2$) allowing $0^m.5$ (pg) for mean absorption (equivalent to 0·38 visual) and adopting $0^m.0$ for the absolute magnitude of these stars (**31**). It cannot be said that a precise distance modulus of the Clouds has yet been determined.

More accurate apparent magnitudes for the RR Lyrae members are needed and it now appears likely that the absolute magnitude of the RR Lyrae stars is $0^m.5$ or so, fainter than was previously supposed. Whilst this would decrease the distance modulus the effect is somewhat compensated by the fact that the discussion of Section 8 makes it likely that $0^m.5$ was an overestimate of the absorption correction. We have not felt therefore that a significant improvement in the distance modulus ($18^m.7$) can be made at present.

(*a*) *General features of the HR diagram.*—In general features the HR diagram is similar to that previously published (**6**) though the number of stars plotted is about doubled. Taking into account the smaller number of stars studied in the SMC and the possibility of selection differences between the SMC and LMC, the HR diagram gives no evidence for systematic differences between the two Clouds. As has been previously noted (**6**) the most striking feature of the diagram is the lack of stars in the triangular shaped region at the top left. Whilst in other parts of the diagram the absence of stars will be strongly affected by selection effects we may be tolerably certain that in that region there are no Cloud stars. The upper limit for the stars sloping from lower left to upper right is roughly parallel to the line of constant bolometric magnitude. It is interesting therefore to note that theory indicates that massive stars will evolve away from the main sequence at more or less constant bolometric magnitude.

An important feature shown by the HR diagram is that the emission line stars (mainly P Cygni type) are on the average brighter than non-emission stars of the same spectral type. The stars which have been suspected as showing emission by ourselves or by others (mainly Henize (**8**)) show the same effect but to a lesser degree. This distinctive phenomenon lends support to the belief that the great majority of our bright stars are not unresolved double or multiple stars with components of comparable brightness. There is no evidence that galactic P Cyg supergiants tend to belong to multiple systems or compact clusters that would be unresolved at the distance of the Clouds. Moreover, the rather sharp distinction between stars with and without emission lines in our HR diagram would certainly be blurred if many of our brightest "stars" at a given spectral type were in fact composite objects.

The P Cyg character of these bright stars may also be taken to indicate a definite limit for stable stars, which may probably be identified with a critical mass above which stars are unstable. This deduction is in qualitative agreement with theory but whether full quantitative agreement is obtained is rather difficult to decide. Schwarzschild and Härm (**32**) deduce that stars less massive than $60\odot$ will be stable but that over $65\odot$ they will be seriously unstable. Since it appears tolerably certain that stars up to $90\odot$ exist in the Galaxy they suggest the difficulty may be overcome by considering the stars in the range 65–$95\odot$ to be P Cygni stars but that $95\odot$ must be considered the maximum possible mass. As a test of their ideas they ask if all stars brighter than $-10^m.0$ (bolometric) ($=65\odot$) are P Cygni stars or otherwise unstable. The difficulty in deducing an answer to this question from our data is partly due to uncertainty as to the distance of the Clouds but also in large measure to the uncertainties in the bolometric conditions. The problem of bolometric corrections has recently been discussed by Popper (**33**) but the position is far from satisfactory. For our supergiants we have used the bolometric corrections applicable to main sequence stars *of the same intrinsic*

colours, taking bolometric corrections from Arp (**34**) and colours from Johnson (**29**) and Feinstein (**30**). In Fig. 13 the resulting line for $M_{bol} = -10{\cdot}0$ is shown. Clearly the occurrence of instability in the Cloud stars occurs at *about* the predicted position.

The O type stars in Fig. 13 fall in the region where evolutionary tracks have been computed for massive stars by Schwarzschild and Härm (**35**) and with the adopted bolometric corrections and distances of the Clouds these stars appear to have masses of about $120\odot$ or larger. Masses of this order were deduced by Trumpler (**36**) for certain O type stars in galactic clusters, assuming an apparent velocity difference to be due to the relativity red shift. The arguments against these large masses (e.g. Struve (**37**)) are indirect and not entirely conclusive.

All the late-type members so far discovered, lie well below the $M_{bol} = -10{\cdot}0$ line.

(*b*) *The absolute magnitudes of the W and Pec stars.*—Although most of our work on W stars concerns stars within the 30 Doradus nebulosity, for which no magnitudes are available, the few stars plotted in the HR diagram suggest that there is a big range in absolute magnitude for these stars. There are indeed probably many stars similar to R114 ($V = 14^{m}{\cdot}5$) awaiting study. These results are consistent with recent work (**38**) (**39**) which indicates a large dispersion in absolute magnitude for the W stars in the Galaxy (from about $-1^{m}{\cdot}5$ to $-5^{m}{\cdot}5$). Our results, however, indicate absolute magnitudes of the order of -7 for some WR stars. The three WN stars in 30 Dor for which magnitudes are available are arranged in a sequence with the earliest type faintest, but estimated magnitudes of the other stars suggest that this is not significant.

All 9 W stars in 30 Dor are nitrogen sequence stars whilst the others in the LMC are carbon sequence (or unknown). This may be connected with Roberts' (**40**) conclusion that WN stars are preferentially associated with clusters. The Magellanic Clouds offer an excellent opportunity to test this suggestion, but at present the data (particularly on WC stars) is too fragmentary. However, our W stars do show a strong association with nebulosity (Section 13).

Some of our W stars are given composite types (e.g. WC6 + O8). Smith (**19**) and Sahade (**41**) have argued that such stars are binaries. It should be emphasized that in writing the type as composite we are merely giving a shorthand description of the spectrum and do not wish to imply that more than one object is necessarily involved. Indeed the presence of faint W type bands in otherwise normal O type stars (**42**) (**43**) hardly lends support to a binary theory for all W stars.

The colours of the Pec stars are discussed in Section 8 (*a*) where they are divided into two classes, A (Eta Car type) and B (He emission). These two classes are plotted in the HR diagram (Fig. 13). It will be seen that the class A objects are all fainter than $10^{m}{\cdot}5$ (V_0) so that they do not seem to be associated with the normal P Cygni stars which are generally brighter than this.

(*c*) *The brightest Cloud members.*—From the present observations of Cloud members it is possible for the first time to draw fairly precise conclusions about the maximum brightnesses attained by stars in the Large Cloud.

In Table VI are listed the 18 brightest known members of the Large Cloud ordered in V. The same table lists the 18 brightest stars in B. Directly observed magnitudes, without corrections for absorption are used. In the final column are listed those of our stars which are brightest bolometrically, and for these corrections for absorption were applied.

TABLE VI

Brightest stars in the Clouds

Visual			Photographic		Bolometric	
Star		V	Star	B	Star	$(m_{bol})_0$
LMC						
R 76		9·11	R 76	9·29	R 115	7·5:
88		9·2:	88	9·4:	122	7·8:
62		9·65	62	9·75	76	8·3:
92	*	9·74	103	9·86	89	8·3:
118		9·87	118	9·94	103	8·3:
103		9·88	92 *	10·31	116	8·3:
117	*	9·91	75	10·39		
150	*	9·96	81	10·42		
94	(*)	10·03	111	10·43		
59	*	10·25	153	10·52		
153		10·28	116	10·55		
75		10·30	121	10·59		
111		10·31	73	10·61		
81		10·43	64	10·65:		
52		10·49	98	10·65		
121		10·49	52	10·67		
98		10·54	57	10·70		
116		10·55	80	10·70		
SMC						
R 45		10·13	R 45	10·27	R 42	9·2:
40		10·73	11	10·80	45	9·2:
11		10·75	40	10·81	17	9·2:
10		10·91	42	10·91		
42		10·95	9	10·98		

* red (F8–G5)

In the V ordering it will be seen that among the first 10 stars as many as *four* are red super-supergiants. (A fifth is probably present as the red component of R94). Since these stars are particularly difficult to find, it seems highly probable that there are more to be included in a final list of the 18 brightest members. If one supposes that five more such stars exist brighter than $V = 10{\cdot}3$, the visual magnitude of the 18th star would be raised only from 10·55 to 10·31.

By contrast we can be fairly certain that very few, if any, stars of type B or A brighter than $10^{m}{\cdot}6$ have been missed in our survey. (The selection of all blue HDE stars down to HDE mag. 10·7 corresponds to 11·0 on the B system.) On account of the narrowness of hydrogen lines or the presence of emission lines, such stars would stand out in the HD classification (cf. HD 33579 and 32034 classified as B and Pec respectively). Henize's Hα survey is particularly valuable in this respect. We have noticed that *all* the brightest stars in the HR diagram of type A or earlier have $H\alpha$ bright or suspected bright.

In the B ordering it will be seen that three out of the four red super-supergiants (*and* R94) drop out of the brightest 18. The one remaining late-type star (R92) remains as high as 6th in the B ordering. Discovery of more red super-supergiants will affect the B ordering far less than the V ordering. It seems

unlikely that a final listing will appreciably change our finding that the photographic magnitude of the 18th Large Cloud member

$$B_{18} = 10^{m}\cdot70.$$

This value, of course, represents a lower limit, but a final value is hardly likely to be brighter than $10^{m}\cdot5$.

It will be noticed that we find only 9 stars brighter photographically than $10^{m}\cdot50$. This may be compared with Shapley's (**44**) estimate of 152 stars brighter than 10·5 based on star counts. In an earlier analysis of star-counts Shapley and Walton (**45**) considered that there were about 20 to 30 Large Cloud members brighter than $9^{m}\cdot0$. The two most likely explanations of the great discrepancy from current findings are (*a*) underestimate of foregound stars, (*b*) inclusion of unresolved star clusters in the counts of bright Cloud members.

The six stars with apparent bolometric magnitude brighter than 8·3 are listed in the last column of Table VI. Observational selection and uncertainties in the bolometric corrections seriously affect this list. Using a distance modulus of 18·7 we find that

$(M_{bol})_{max} = -11\cdot2$, corresponding to a mass of the order of $100\odot$, (**35**), and the bolometric absolute magnitude of the sixth brightest star

$$(M_{bol})_6 = -10\cdot4.$$

The five brightest stars in the Small Cloud observed by us are also listed in Table VI, but this list is very likely to be changed by future discoveries. An objective prism survey of the Small Cloud like the HDE is very urgently required. Taken at their face value the figures suggest that the fifth brightest member (visually or photographically) has V or $B = 10\cdot95$ approximately. There can be little doubt that HD 7583 is the brightest blue member of the Small Cloud. It is interesting to note that this star lies within the 'bulge', well outside the main optical body of the Small Cloud. The three brightest stars bolometrically are listed in Table VI. It may be mentioned that since many of the brightest stars in the Large Cloud seem to be variable, any ordering such as that of Table VI must be slightly ephemeral in character.

Further, it is interesting to note that the fifth brightest star in the Large Cloud is certainly about 1 magnitude brighter than the fifth brightest star in the Small Cloud. However, there appear to be many strong arguments against a difference of more than a few tenths of a magnitude in distance moduli of the Clouds and on this basis the population of the Small Cloud is much smaller than that of the Large. Hence in the comparison of the two Clouds the magnitude of the nth brightest star must be an unreliable indicator of distance, unless both Clouds contain a considerable number of stars close to the physical upper limit of stellar luminosity.

(*d*) *Incompleteness of red survey.*—Our HR diagram is certainly affected by observational selection in the later types, as previously mentioned. Considerable efforts have been devoted towards discovering more red super-supergiants in the Large Cloud, but without success. Stars selected for investigation have mostly been in the region of clusters and nebulae, and this criterion has indeed been successful in the discovery of the five known Cloud members.

As an alternative approach, *all* stars classified as K or M in the HDE (268601 to 270500) with $m \geqslant 12\cdot0$ have been plotted. The region of greatest crowding

was found near the Sf end of the 'bar' ($x = 14{,}000$–$16{,}000$, $y = 5{,}600$–$8{,}500$). In this region of 0·448 square degrees, there are 12 faint K and M stars, corresponding to a density of 27 per square degree. This is about three times the density of such stars in a region of the HDE outside the Cloud at the same galactic latitude. All 12 K–M stars in the crowded area were investigated, and *no Cloud members were found.*

In a statistical investigation of spectral types in the bar of the Cloud Shapley and Nail (**46**) have concluded "Probably only the O, B and perhaps some of the fainter K's are Cloud members. Other preliminary studies of spectral class and colour have indicated that the spectral types of these supergiants range from the extreme blue to the extreme red"; and further "more than half the approximately 150 non-variable stars which have apparent magnitudes between 13 and 14 (scattered along the bar) are superposed galactic stars".

These quotations reflect the situation as we find it, but it would appear that the true red super-supergiants whose existence seemed probable from the small statistics of Nail and Shapley (**47**) are in fact very rare objects.

In the Small Cloud we have found a few red members at about 13^m, from Henize's Catalogue. Whether more such stars exist at a brighter level cannot be determined at present; without a general objective prism classification of Small Cloud stars down to 13^m, an investigation such as we have carried out in the Large Cloud would be most unprofitable.

10. *Comparison of Cloud members with galactic standards.*

(*a*) *Early-type stars.*—The spectra have been examined as carefully as possible with a view to detecting differences between the Cloud stars and galactic standards. Arp (**48**) has suggested that the SMC may be a metal-poor system. Though we believe that it is possible to interpret Arp's photometry without the hypothesis of metal-poorness (**49**) we have obtained greatly widened spectra of selected stars in both Clouds to make the detection of small peculiarities easier. A study of the remarks of Table II will reveal that peculiarities have been found in certain stars, most of which can certainly be attributed to causes other than metal-poorness. We have found no evidence of any *general* peculiarities for the stars in either Cloud.

All the stars studied show, as might be expected, signs of extremely high luminosity. The narrowness of the hydrogen lines, without a marked maximum at Ao, is clear in the sequence of types illustrated in Plate I, consisting solely of Cloud members. In a good many cases in both Clouds the luminosity criteria, e.g. extreme narrowness of hydrogen, especially in the A stars, indicate the star to be more luminous than galactic MK Ia standards. Details of such cases are given in the Remarks to Table II and reference should be made to Plate III which also illustrates MK standards. We have, as explained earlier, used the class Ia-O for such stars of extreme luminosity; their occurrence is not surprising when one compares their position in the HR diagram (Fig. 13) relative to Johnson and Iriarte's calibration (**50**) of the MK Ia stars.

(*b*) *Comparison of IC* 1644 *and* 30 *Dor.*—From the point of view of possible abundance differences between the two Clouds an interesting comparison can be made between the two gaseous nebulae 30 Dor (LMC) and IC 1644 (SMC). The spectrum of IC 1644 is compared with that of a portion of the 30 Dor nebulae in Plate II, 1, 2. The 30 Dor spectrum is one of a series of different parts of the nebula, which will be discussed in a later paper. The match between

the emission lines (H, He I, [O II], [O III], [Ne III]) is good and suggests no significant abundance differences. The ratio 3726/3729 [O II] is similar for the two nebulae indicating comparable (low) electron pressures.

(*c*) *The red super-supergiants in the LMC.*—The discovery of five late-type stars of extremely high luminosity in the LMC was reported in a previous paper (**4**). A few details of the spectra were then given. The spectra of these stars, especially at 49A/mm, contains a great wealth of sharp absorption lines and a detailed analysis of these plates is clearly desirable. Until this can be carried out we shall briefly note in this section some of the outstanding features of the spectra. This is necessary since, although a moderately good match for these stars can be found with MK standards, there are definite discrepancies which are probably due to the exceptional luminosities of these stars. These discrepancies are mainly noticeable at 49A/mm and might perhaps have been overlooked at 86A/mm (a dispersion closer to that used by the Yerkes observers for spectral type work). Comparison of the types given previously (**4**) with those of Table II will show some slight changes but in view of the following discussion it will appear that these are not significant. In what follows reference should be made to Plates I and II.

HD 271182 (R92) is classified as F8 Ia. At 86A/mm the match with an F8 Ia standard is good. At 48A/mm whilst the general match with this type is reasonable, the H lines are too weak. This would indicate a slightly later type for HD 271182. On the other hand the general run of intensities of all the lines except hydrogen, indicates a type between F5 Ia and F8 Ia. The ratio Mg II 4481/Ti II, Fe II 4488–9, also places the star slightly earlier than F8. Some lines, notably Fe I 4118·5 (E.P. 3·56V) are weak in the star compared with δCMa(F8 Ia). Other lines involving the same lower state are not suitable for examination of a similar effect on our plates.

HD 269953 (R150) is classified as G0 Ia. At 86 A/mm the general match with F8 Ia or G0 Ia is good but the strength of the H lines indicates a type close to F8 Ia. However at 49A/mm the metal lines are seen to be somewhat stronger than in HD 271182 (F8 Ia, previous paragraph) and the ratio Mg II 4481/Ti II, Fe II 4488–9 indicates G0 Ia or even slightly later (Mg II 4481 too weak for F8 Ia). Comparison of standard stars shows that La II 4334 is a rather sensitive criterion for type at 49A/mm and this line also indicates G0 Ia or slightly later for HD 269953.

HD 269723 (R117) is classified G0 Ia. However most metal lines (including La II 4334 and Sr II 4215 are stronger and Mg II 4481 is slightly weaker than in a G0 Ia standard. This would indicate a slightly later type and (perhaps a higher luminosity) for 269723. On the other hand a direct comparison with 269953 (G0 Ia, previous paragraph) shows that whilst La II 4334, Mg II 4481 indicate an earlier type of 269723 than 269953 (La II weaker, Mg II stronger in 269723), the general strength of the metal lines is greater in 269723 suggesting it to be the later of the two stars.

The various effects described above may be tentatively attributed to the extremely high luminosity of these stars (Ia–O character). We may also note that effects due to dilution of radiation may be important as they apparently are in HD 33579 (R76) (see note to Table II).

R143 (Anon in 30 Dor region) is classified F7 Ia. The H lines are filled in by nebular emission and so cannot be used in the determination of spectral type. The plate at 86A/mm matches F8 Ia well but the plate at 49A/mm indicates a

distinctly earlier type (near F5 Ia). It appears probable that there has been a real change of type between the epochs of these two plates.

HD 268757 (R59), (G5 Ia), the star of latest type found in the LMC, has been discussed previously (**4**). (See Plate I, 22, 23.) The type is certainly later than G0 Ia but the absence of MK standards for late G Ia stars makes classification less certain.

(*d*) *The spectra of the Cloud Cepheids.*—The spectral types of the Cepheid variables and of the R Cr B variable W Men have been discussed previously (**3**). Slight revision of the types have been made in a few cases. In the case of HV 821 (R1) (SMC) three spectra all in one cycle have been obtained since those listed in (**3**). It seems likely from the exposure times and densities of the spectra that the first of these three (F8 Ia or slightly earlier, calculated phase 0·83) was obtained nearest maximum light and the other two (F8 Ia or slightly later, at 0·95 and G1 Ib at 0·11) on the declining branch. In the first two of these spectra it was noted that the H lines were slightly strong for the adopted type. This is in accord with the observations of galactic Cepheids near maximum light (**51**) (**52**) and hence somewhat strengthens the case of similarity of Cepheids in the SMC and in the Galaxy. The ratio 4395/4400 progressively decreases in the sequence for these three spectra, indicating increasingly later type, as expected, on the declining branch. Spectra of HV 821 in the Small Cloud at different phases are reproduced in Plate I, 19, 20.

It is interesting to note that some of the Cepheid spectra away from maximum light indicate lower luminosity than Ia (e.g. G1 Ib in HV 821, see Plate I, 20). These are the only cases of stars classified of Ib luminosity in the present paper.

The velocities determined from the Cepheid spectra all clearly indicate Cloud membership for these stars. They will be published when more extensive observations have been carried out.

Photometric work on the Cepheids in the SMC has led some workers to believe that there exist essential differences between these stars and galactic Cepheids. No such differences are apparent in the spectroscopic results. The whole problem has recently been reviewed (**53**). Recent work on galactic Cepheids has shown them to be more complicated a group than was at one time thought. It appears possible that there is a considerable spread in absolute magnitude and colour at any given period (**54**) with the brighter variables bluer. These will be the ones preferentially selected for observation in the early work on the Clouds and the difference between the galactic and SMC Cepheids reported by Kron and Svolopoulos (**55**) may arise partly from this cause. Furthermore, despite Kron's extensive observations there is still considerable uncertainty in the intrinsic colours of the galactic Cepheids. Finally the reddening correction of $0^{m}\cdot09$ applied by Kron and Svolopoulos to the SMC Cepheids may be invalid. It is true that we find for our early type stars a mean excess of about $0^{m}\cdot1$ in the Clouds, but Fig. 11 shows that the range extends down to zero excess. For stars like Cepheids which are present in considerable numbers in the Clouds it may be argued that the ones preferentially chosen for observation will be mainly unreddened stars (see also Section 13). We do not consider therefore that any difference between Cepheids in the Galaxy and in either Cloud has yet been established beyond reasonable doubt.

(*e*) *Representation of the elements in the Magellanic Clouds.*—This spectroscopic material provides numerous examples of lines and elements which have

never before been detected anywhere outside our own Galaxy. The accompanying Table VII lists 23 elements certainly and 3 doubtfully identified in Magellanic Cloud objects. It is possible that a more detailed examination of some of the spectra would add a few more elements to the list.

TABLE VII

Elements identified in the Large (L) *and Small* (S) *Clouds*

Element	Absorption	Emission	
		Nebulae	e stars
H	LS	LS	LS
He	LS	LS	LS
C	LS?		L
N	LS	L	L
O	LS	LS	
Ne		LS	
Na	L		
Mg	LS		
Al	LS		
Si	LS		
S			L?
Ca	LS		
Sc	LS		
Ti	LS		
V	L		
Cr	L		
Mn	LS		
Fe	LS		LS
Ni	L		L?
Sr	LS		
Y	L		
Zr	L		
Ba	LS		
La	L		
Eu	L?		
Gd	L?		

Fewer elements have been identified in the Small Cloud simply because we have had fewer bright stars, especially of the later types, to observe.

Identification of the heavier elements rests largely on measures of an excellent spectrum of R92 (49A/mm); La II is certainly represented by the line 4334A (see Plate II, 13) and a few others, while Eu II and Gd II probably contribute to blends at 4205 and 4184A respectively.

11. *U, B, V photometry.*—The discussions of our three-colour photometry is obviously affected adversely by the fact that it was conducted with a silvered primary mirror. Though we consider our conversion to Johnson's V and $B-V$ as entirely satisfactory, the ultra-violet results can be considered as no more than provisional.

Previously (6) we gave an approximate relation between our ultra-violet colours and Johnson's $U-B$; it has been found since that a satisfactorily accurate conversion is not possible. The present discussion is therefore based on U_R-B_R and $B-V$.

Primarily due to the revision of the $U_R - B_R$ system (see Section 4), the present slope of the reddening line is considerably smaller than found originally (**6**). We took

$$E_{U-B}/E_{B-V} = 0{\cdot}26$$

as a preliminary new value for this slope. We denote by Q, as is customary, the intercept of the reddening line with the line $B-V=0$. The importance of Q is that it is independent of interstellar reddening but for a given luminosity is only dependent on the spectral type. Q was calculated from the formula:

$$Q_R = (U_R - B_R) - 0{\cdot}26\,(B-V).$$

In Fig. 14 Q_R is plotted against the Radcliffe spectral types for both LMC and SMC supergiants. The diagram is based on considerably more data than the corresponding figure in (**6**). In spite of the considerable scatter, a significant correlation between Q_R and spectral type can be discerned. The diagram is of importance as it does not show a significant difference between the two Clouds.

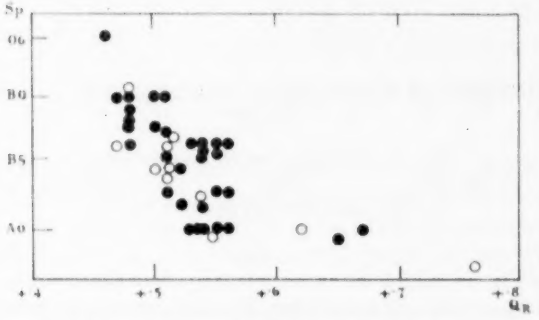

FIG. 14.—*Correlation of Q_R and spectral type.*
● *LMC.* ○ *SMC.*

It is now known that reddening lines are not quite straight. The curvature has been established by several authors and has been explained (by others) as due to the finite bandwidths of the photometries and is undoubtedly real. The effect naturally becomes important only in cases of very heavy absorption; for the present study it seems entirely justified to neglect the curvature. We therefore confined ourselves to the more simple straight reddening lines.

In Fig. 15 the final reddening line for Bo supergiants is shown. Abscissae are $B-V$ and ordinates are $U_R - B_R$. The figure combines Cloud stars with reddened galactic supergiants which have been observed at the Radcliffe Observatory with the same equipment. In order to strengthen the determination of the line, not only Bo stars but also stars of other spectral types to B6 were used, appropriately reduced to Bo stars suffering the same absorption. To this end the difference in intrinsic colour index from that of a Bo star was applied to both observed colour indices. The corrections $\Delta(B-V)$ depend on the relation between colour index and spectral type for supergiants (**29**) whereas the corrections $\Delta(U_R - B_R)$ were derived from Q_R and $\Delta(B-V)$ using the relation

$$\Delta(U_R - B_R) = \Delta Q_R + 0{\cdot}26 \quad \Delta(B-V)$$

never before been detected anywhere outside our own Galaxy. The accompanying Table VII lists 23 elements certainly and 3 doubtfully identified in Magellanic Cloud objects. It is possible that a more detailed examination of some of the spectra would add a few more elements to the list.

TABLE VII

Elements identified in the Large (L) *and Small* (S) *Clouds*

Element	Absorption	Emission	
		Nebulae	e stars
H	LS	LS	LS
He	LS	LS	LS
C	LS?		L
N	LS	L	L
O	LS	LS	
Ne		LS	
Na	L		
Mg	LS		
Al	LS		
Si	LS		
S			L?
Ca	LS		
Sc	LS		
Ti	LS		
V	L		
Cr	L		
Mn	LS		
Fe	LS		LS
Ni	L		L?
Sr	LS		
Y	L		
Zr	L		
Ba	LS		
La	L		
Eu	L?		
Gd	L?		

Fewer elements have been identified in the Small Cloud simply because we have had fewer bright stars, especially of the later types, to observe.

Identification of the heavier elements rests largely on measures of an excellent spectrum of R92 (49A/mm); La II is certainly represented by the line 4334A (see Plate II, 13) and a few others, while Eu II and Gd II probably contribute to blends at 4205 and 4184A respectively.

11. *U, B, V photometry.*—The discussions of our three-colour photometry is obviously affected adversely by the fact that it was conducted with a silvered primary mirror. Though we consider our conversion to Johnson's V and $B-V$ as entirely satisfactory, the ultra-violet results can be considered as no more than provisional.

Previously (**6**) we gave an approximate relation between our ultra-violet colours and Johnson's U–B; it has been found since that a satisfactorily accurate conversion is not possible. The present discussion is therefore based on $U_R - B_R$ and $B-V$.

Primarily due to the revision of the $U_R - B_R$ system (see Section 4), the present slope of the reddening line is considerably smaller than found originally (**6**). We took

$$E_{U-B}/E_{B-V} = 0{\cdot}26$$

as a preliminary new value for this slope. We denote by Q, as is customary, the intercept of the reddening line with the line $B-V=0$. The importance of Q is that it is independent of interstellar reddening but for a given luminosity is only dependent on the spectral type. Q was calculated from the formula:

$$Q_R = (U_R - B_R) - 0{\cdot}26\,(B-V).$$

In Fig. 14 Q_R is plotted against the Radcliffe spectral types for both LMC and SMC supergiants. The diagram is based on considerably more data than the corresponding figure in (**6**). In spite of the considerable scatter, a significant correlation between Q_R and spectral type can be discerned. The diagram is of importance as it does not show a significant difference between the two Clouds.

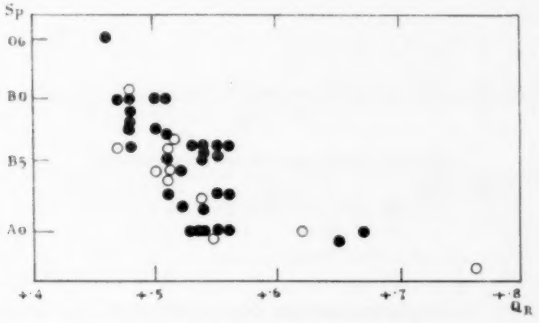

FIG. 14.—*Correlation of Q_R and spectral type.*
● *LMC.* ○ *SMC.*

It is now known that reddening lines are not quite straight. The curvature has been established by several authors and has been explained (by others) as due to the finite bandwidths of the photometries and is undoubtedly real. The effect naturally becomes important only in cases of very heavy absorption; for the present study it seems entirely justified to neglect the curvature. We therefore confined ourselves to the more simple straight reddening lines.

In Fig. 15 the final reddening line for Bo supergiants is shown. Abscissae are $B-V$ and ordinates are $U_R - B_R$. The figure combines Cloud stars with reddened galactic supergiants which have been observed at the Radcliffe Observatory with the same equipment. In order to strengthen the determination of the line, not only Bo stars but also stars of other spectral types to B6 were used, appropriately reduced to Bo stars suffering the same absorption. To this end the difference in intrinsic colour index from that of a Bo star was applied to both observed colour indices. The corrections $\Delta(B-V)$ depend on the relation between colour index and spectral type for supergiants (**29**) whereas the corrections $\Delta(U_R - B_R)$ were derived from Q_R and $\Delta(B-V)$ using the relation

$$\Delta(U_R - B_R) = \Delta Q_R + 0{\cdot}26 \;\; \Delta(B-V)$$

never before been detected anywhere outside our own Galaxy. The accompanying Table VII lists 23 elements certainly and 3 doubtfully identified in Magellanic Cloud objects. It is possible that a more detailed examination of some of the spectra would add a few more elements to the list.

TABLE VII

Elements identified in the Large (L) *and Small* (S) *Clouds*

Element	Absorption	Emission	
		Nebulae	e stars
H	LS	LS	LS
He	LS	LS	LS
C	LS?		L
N	LS	L	L
O	LS	LS	
Ne		LS	
Na	L		
Mg	LS		
Al	LS		
Si	LS		
S			L?
Ca	LS		
Sc	LS		
Ti	LS		
V	L		
Cr	L		
Mn	LS		
Fe	LS		LS
Ni	L		L?
Sr	LS		
Y	L		
Zr	L		
Ba	LS		
La	L		
Eu	L?		
Gd	L?		

Fewer elements have been identified in the Small Cloud simply because we have had fewer bright stars, especially of the later types, to observe.

Identification of the heavier elements rests largely on measures of an excellent spectrum of R92 (49A/mm); La II is certainly represented by the line 4334A (see Plate II, 13) and a few others, while Eu II and Gd II probably contribute to blends at 4205 and 4184A respectively.

11. *U, B, V photometry.*—The discussions of our three-colour photometry is obviously affected adversely by the fact that it was conducted with a silvered primary mirror. Though we consider our conversion to Johnson's V and $B-V$ as entirely satisfactory, the ultra-violet results can be considered as no more than provisional.

Previously (**6**) we gave an approximate relation between our ultra-violet colours and Johnson's $U-B$; it has been found since that a satisfactorily accurate conversion is not possible. The present discussion is therefore based on U_R-B_R and $B-V$.

Primarily due to the revision of the $U_R - B_R$ system (see Section 4), the present slope of the reddening line is considerably smaller than found originally (**6**). We took

$$E_{U-B}/E_{B-V} = 0{\cdot}26$$

as a preliminary new value for this slope. We denote by Q, as is customary, the intercept of the reddening line with the line $B-V=0$. The importance of Q is that it is independent of interstellar reddening but for a given luminosity is only dependent on the spectral type. Q was calculated from the formula:

$$Q_R = (U_R - B_R) - 0{\cdot}26\,(B-V).$$

In Fig. 14 Q_R is plotted against the Radcliffe spectral types for both LMC and SMC supergiants. The diagram is based on considerably more data than the corresponding figure in (**6**). In spite of the considerable scatter, a significant correlation between Q_R and spectral type can be discerned. The diagram is of importance as it does not show a significant difference between the two Clouds.

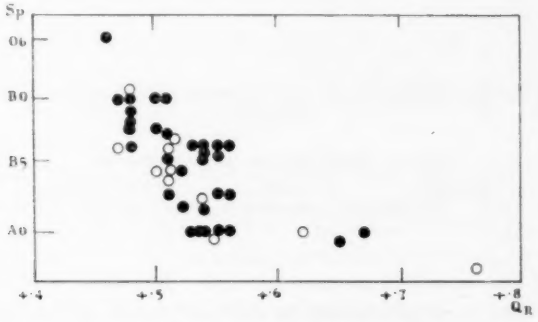

FIG. 14.—*Correlation of Q_R and spectral type.*
● *LMC.* ○ *SMC.*

It is now known that reddening lines are not quite straight. The curvature has been established by several authors and has been explained (by others) as due to the finite bandwidths of the photometries and is undoubtedly real. The effect naturally becomes important only in cases of very heavy absorption; for the present study it seems entirely justified to neglect the curvature. We therefore confined ourselves to the more simple straight reddening lines.

In Fig. 15 the final reddening line for Bo supergiants is shown. Abscissae are $B-V$ and ordinates are $U_R - B_R$. The figure combines Cloud stars with reddened galactic supergiants which have been observed at the Radcliffe Observatory with the same equipment. In order to strengthen the determination of the line, not only Bo stars but also stars of other spectral types to B6 were used, appropriately reduced to Bo stars suffering the same absorption. To this end the difference in intrinsic colour index from that of a Bo star was applied to both observed colour indices. The corrections $\Delta(B-V)$ depend on the relation between colour index and spectral type for supergiants (**29**) whereas the corrections $\Delta(U_R - B_R)$ were derived from Q_R and $\Delta(B-V)$ using the relation

$$\Delta(U_R - B_R) = \Delta Q_R + 0{\cdot}26 \;\; \Delta(B-V)$$

where ΔQ_R was read off from Fig. 14 and $\Delta(B-V)$ is the correction applied to the abscissae. The spectral types are all from Radcliffe determinations for the Cloud stars and for most of the galactic stars used. Among the latter group we made use of a few MK determinations by Hiltner (**56**). The Magellanic Cloud stars all lie on the upper left hand side of Fig. 15 because of the smaller absorption suffered by them.

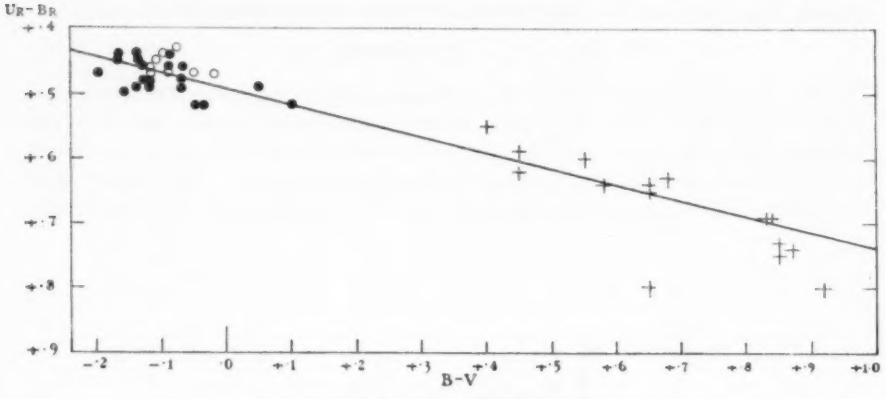

FIG. 15.—*Reddening line for Bo supergiants.*
● *LMC.* ○ *SMC.* + *Galactic stars.*
O to B6 types, reduced to Bo, have been used.

The data of Fig. 15, which are more extensive than those of (**6**), are consistent with the view that a single reddening line represents adequately Magellanic Cloud and galactic supergiants of the same type. We deduce $E_{U-B}/E_{B-V}=0{\cdot}25$ which is very close to the provisional result 0·26 used above.

Fig. 16 shows the unreddened positions of the member stars of both Clouds with spectral types earlier than Ao. The ordinates were found from the observed U_R-B_R, reduced by means of the blue colour excess E_{U-B} derived from the relation

$$E_{U-B}=0{\cdot}25\ E_{B-V}$$

whereas the abscissae are the intrinsic colours according to Johnson. We have excluded the stars of type Ao and later, on account of the difficulties with Johnson's intrinsic colours in this range (see Section 8). The interest in the diagram is to show the similarity of LMC and SMC as regards the intrinsic line.

The general conclusion of these photoelectric observations is thus to reinforce arguments of earlier sections that no pronounced differences between the bright stars in the two Clouds and the Galaxy have been detected, nor between the absorbing properties of the interstellar dust.

12. *Interstellar lines in the spectra of Cloud members.*—In Table VIII is summarized the available evidence for the existence of interstellar lines in the spectra of Cloud members. Some of these lines are of low velocity indicating that they originate from gas within our Galaxy and others have velocities characteristic

of the Clouds. Since distant B type stars at high galactic latitudes show interstellar lines (**57**), it is not surprising that we should detect such lines in our spectra. The interstellar lines, both of galactic and Magellanic Cloud origin, are generally weak and can only be measured on a small number of our plates with suitable exposures. A galactic interstellar line in R62 (HD 32034) is reproduced in Plate II, 7a.

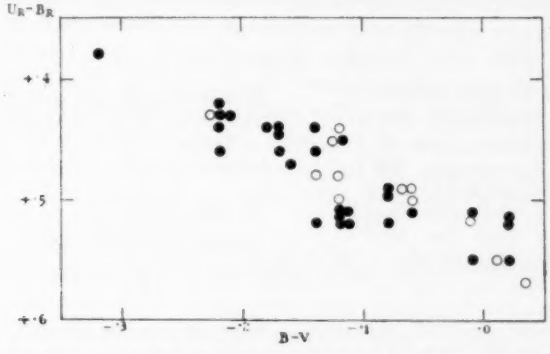

FIG. 16.—*Intrinsic line shown by unreddened positions for* O5 *to B9 supergiants in LMC* (●) *and SMC* (○).

In the lists of Marshall (**58**) and Kühlborn (**59**) there are a few unidentified faint lines in B type stars which might be confused or blended with galactic interstellar K (due to velocity shifts) on some of our spectrograms. However, we do not think that they will be major contributors to the measured line in our stars.

In the case of interstellar lines due to gas within the Magellanic Clouds, it will be seen that Table VIII contains only a few stars. Only stars for which the K line shows a fairly large difference in velocity from the star, or stars of very early type (about Bo or earlier) have been included. It is not known with any

TABLE VIII

Cloud members with interstellar lines

(a) Galactic interstellar lines

	Star	RV(Ca II)	Sp		Star	RV(Ca II)	Sp
			LMC				
R 53	HD 268605	+2:(1)	Bo Ia:	R 101	HD 269547	+21 (1)	B3 Ia:
62	32034	+6 (2)	B9 Ie	111	269661	+33:(1)	B9 Ia–O:
73	268907	+18 (1)	B8 Ia	112	269660	+126 (1)	B2 Ia:
81	269128	0 (1)	B2·5 Ieq	116	269700	+16:(1)	B1·5 Iaeq
85	269321	−9:(1)	B5 Iae	121	269801	suspected	B9 Ia–O:
87	269333	+43:(1)	W+B1:I				
			SMC				
30	Anon	+74:(1)	Be	Doubtful measure. Cloud or galactic interstellar ?			
37	Arp b		B6 I	Line in correct position for low velocity K but seems too strong for interstellar line at this latitude.			
40	6884	−17 (1)	B8 Ie				
45	7583	−13:(2)	Ao Ia–O				

TABLE VIII (*continued*)

(*b*) *Cloud interstellar lines*

LMC

	Star	RV(Ca II)	Sp	
R 78	269050	+207: (1)	Bo Ia	Central star N100
103	269546	+206 (1)	B3 Ip	Velocity differs from star. In N144

Also the following WN stars in the 30 Doradus region show Cloud interstellar lines: R 134, 136, 139, 140.

SMC

R 4	Hen S6	+121: (1)	$(A-B)_0$.	At edge of N19. Possibly P Cygni stellar.
11	5291	+146 (2)	B6 Ia	At edge of N50. Too strong to be entirely stellar.
14	5980	+153 (1)	Wp	In N66.
17	Arp h	+112 (1)	Bo I	
18	Anon	+112: (1)	Bo·5 I	At edge of N66.
36	Arp e	+152 (1)	B3 I	Velocity differs from star.

Note.—The number of plates contributing to each velocity is given in parenthesis.

certainty at what spectral type among supergiants the *stellar* K line attains appreciable strength. It may be that it remains relatively weak at later types than Bo in which case we could find many more examples of Cloud interstellar absorption. For instance Code and Houck (**23**) consider the high velocity K line in HDE 269700 (R116) to be Cloud interstellar. The line is clearly present on our spectrograms but we have been in some doubt as to the possible effect of a stellar K component in a B2 supergiant and the star does not appear in Table VIII. In many later B and early A stars the observed K line is probably a blend of stellar and interstellar components.

Table VIII also includes remarks on the situation with regard to Henize nebulosities for stars suspected of showing the Cloud interstellar K line. In each case in the LMC there is clear involvement in a Cloud nebula; in the SMC, too, nearly all stars are either within or near the edge of a nebula. This supports the conclusion that most of these observed lines originate in Cloud interstellar gas.

13. *Involvement in nebulosity.*—In addition to the foregoing conclusion that Cloud stars apparently involved in nebulosity tend to show interstellar lines due to Cloud gas, we find some other interesting properties of stars within and without Cloud nebulosities. We have already seen (Table IV) that stars within nebulosity tend to suffer greater absorption and have concluded that this points to a *statistical* association of Cloud dust and gas. It is also of interest to enquire into the association of stars of different spectral types with nebulosity. Table IX shows the distribution among spectral types in the Large Cloud. In this Table we have excluded a few border-line cases (e.g. stars lying within the vast Henize N135 but not apparently associated with specific nebulosity) and those stars classed as B or A without sub-classification.

TABLE IX

Distribution of spectral types among LMC stars within and without Cloud nebulosity

Type	W	Pec	O5	6 8	Bo	o·5	1	1·5	2	2·5	3 5	B6–A5	F8–G5	Cep.
Within	13	5	1	2 1	7	3	1	1	1	0	2 2	5	4	1
Without	0	4	0	0 0	0	0	1	2	1	2	5 2	18	1	5

This tabulation shows clearly that

(*a*) stars of type O to Bo·5 are associated in every case with nebulosity, while those of later type (to A5) are commonly found outside nebulous regions. This is just the situation found by Hubble (**60**) for galactic nebulae, and strongly points to the stars of type earlier than B1 as active agents in exciting the nebulosity.

It should be noted that although our HR diagram proves the existence of many Cloud stars of type later than B1 which are brighter, visually, than the O – B1 stars, the latter will be far more effective, as stronger sources of radiation beyond the Lyman limit, in exciting Hα regions. The radii of Strömgren spheres are not nearly so sensitive to visual luminosity as to spectral type. Hubble (**60**) did in fact remark that there were some supergiants of α Cyg type in the Galaxy, involved in nebulosity. We find the same situation in the LMC but there is no reason to suppose that such stars are primary agents in exciting, the nebulosity. The brightest star in the LMC (HD 33579, R76) appears to be in a region devoid of nebulosity.

In passing we may note that reference to Fig. 11 shows that stars of type O to B1 appear to be reddened more than those of later types and this is fully borne out by detailed examination. This conclusion, of course, rests on the validity of Johnson's intrinsic colours throughout the range of types O5 to A0; but assuming these colours we have some evidence for an association of the stars of earliest type not only with nebulosity, but also with dust.

Table IX also shows that

(*b*) Our W stars are *all* associated with nebulosity (9 out of the 13 occur in the 30 Dor region).

(*c*) The red super-supergiants (F8 to G5) tend to be associated with nebulae. The one exception (R92) lies close to but just outside the faint Hen N43. For 3 out of the 5 certain cases the involvement with nebulosity is particularly striking on direct photographs.

If this connection is established it might imply that these interesting stars have actually been born within these nebulae in astronomically recent times. However, it must be remembered that these objects were selected for observation mainly just because they were in regions of clusters or nebulae, and at present little can be said about the possible existence of other such stars outside nebulae.

(*d*) There is apparently no correlation between the bright Cepheids that we have observed and nebulosity. The association of galactic Cepheids with nebulosity also appears to be slight.

14. *Foreground absorption in the direction of the Magellanic Clouds.*—A list of proved foreground stars has been given above (Table III). Spectral types have been determined for only those few stars with photometric data available in order to obtain some idea of the galactic absorption in the direction of the Clouds. Table X lists 9 such stars in the field of the SMC and 5 in the field of the LMC. The spectral types are in general less accurate than those of Cloud members since a star was usually dropped from the spectroscopic programme once a spectrum had shown it to be a foreground object. We may note that the radial velocity of the B type star 19F (+44 km/s) supports the luminosity classification in making the star a foreground object. Using the intrinsic colours of Johnson and Morgan (**10**), we obtained the colour excesses E_{B-V} listed.

The two cases of negative colour excess probably result from inaccuracies in the types and the fairly rapid change of intrinsic colour with type. If

TABLE X

Selected foreground stars for absorption

Radcliffe No.	Type	V	$B-V$	E_{B-V}	Distance (psc)
			SMC		
6F	F2: V:	10·74	+0·45(10)	+0·08	300
10F	F0: V:	9·77	+0·34(3)	+0·04	220
11F	F5 V:	9·57	+0·50(4)	+0·06	160
12F	A1 V(?III)	10·60	+0·06(5)	+0·01	1000
13F	B5 V:(e)	11·71	−0·10(4)	+0·06	3800
16F	K2 III	8·40	+0·98(4)	−0·18	500
17F	A2: V	10·25	+0·18(2)	+·011	580
18F	K1 III	10·83	+1·20(1)	+0·12	1200
19F	B3 V(?III)	11·01	−0·09(3)	+0·11	3630
				$\bar{E}_{B-V}$ = +0·04 ± 0·03 (s.e.)	
			(16F omitted)	$\bar{E}_{B-V}$ = +0·07 ± 0·01 (s.e.)	
			LMC		
25F	A3 V	8·44	+0·21(3)	+0·12	190
26F	A3 V	8·07	+0·20(3)	+0·11	160
28F	A0 V	7·86	−0·04(3)	−0·04	350
31F	A5 V	8·37	+0·33(3)	+0·18	140
35F	A4: V	9·17	+0·12(3)	+0·00	290
				$\bar{E}_{B-V}$ = +0·07 ± 0·04 (s.e.)	

Note.—The Radcliffe numbers are from Table III. The number of photoelectric observations is given in brackets. The photometry of 16F and 17F is by Arp (**9**).

HD 33486 (28F) were B9 rather than A0, it would have a positive excess (though A0 is still regarded as the most probable type). 16F gives a fairly large negative colour excess (−0·18) but the intrinsic colours vary rapidly with type in the early K's (see (**10**), Fig. 13) and there is also a dependence on luminosity.

Mean values of E_{B-V} are shown in the Table. Clearly the absorption is relatively small. The LMC might be expected to show greater field absorption than the SMC being at a lower galactic latitude but in fact the difference between the means is practically removed if 16F is omitted. Distances for the stars are also given in Table X (absolute magnitudes from (**34**)). The magnitudes were corrected for reddening in deriving the distance; the two stars with negative excesses being considered unreddened. The stars lying in front of the SMC at distances greater than 1 kpc do not show a significantly greater mean absorption than the nearer stars.

The more distant stars are presumably well beyond the bulk of the galactic absorbing layer and the results give an indication of the galactic absorption applicable to Cloud members.

15. *Peculiar foreground stars*

(*a*) *Two high velocity foreground stars.*—Two stars (one in the direction of each Cloud) have been found to show dwarf characteristics but about the same radial velocity as if they were Cloud members. Detailed examination of their spectra shows them to be high velocity galactic objects. They have been classified using the criteria of Keenan and Keller (**61**).

Anon 24F in the field of the SMC is classified as G2V from the ratio Hγ/4325 and, to a much lesser extent, from the strength of the G band. Sr II 4077 is used for luminosity classification. It is just possible that the type is as late as G5 and the star as bright as luminosity Class III. However Sr II 4215 is decidedly weak for the type and 4172 is strong. This is a known high velocity characteristic resulting from the weakening of CN (**61**). The effect in 24F is considerably more marked than in the high velocity star ε And. The metal/metal type adopted by Kinman (**62**) (4226/4325) indicates a type in the early K's. The velocity from one plate is +177 : km/sec.

HDE 270365 89F is in the field of the LMC and is classified as Go III from Hγ/4325 and Sr II 4077. It could just possibily be as late as G2. 4216/4172 indicates high velocity characteristics (CN weak), the effect being more marked than in ε And. The metal/metal ratio 4226/4325 again indicates a type in the early K's. The velocity from one plate is +250 : km/sec.

Three-colour photometry of HDE 270365 gives V 11·43, $(B-V)$ +0·98, (U_R-B_R)+1·23, which converts approximately into the U, B, V system as $(U-B)$+0·58. These observations confirm and strengthen the spectroscopic conclusions. Unless the reddening is large which is very unlikely, the $(B-V)$ colour is too red for a Go star. This is expected for a metal-poor star (cf. (**63**), (**64**)) with a type determined from Hγ/4325. Furthermore the star has an ultraviolet excess of $0^m{\cdot}22$ ($\delta(U-B)$) compared with the Hyades intrinsic line and lies close to the M3 intrinsic line (cf. (**64**) and (**65**)).

It is not too surprising that the velocities of these two stars agree quite closely with that expected for Cloud members since it is known that the major part of the velocity of each Cloud is merely the reflection of galactic rotation.

(*b*) *A peculiar early-type foreground star.*—HD 269696 (69F = CPD −69°389) was discovered to have appreciable proper motion by Luyten (**66**) who reported that Miss Cannon found the spectrum to vary between B5 and "almost as late as Ao". The HD classification is "B", but it is the only star so classified that we have found to be a foreground star. Lourens (**67**) who specifically requested spectroscopic observations, has recently measured the proper motion as $0''{\cdot}044$ p.a.

Seven Radcliffe spectra have been secured (6 at 86A/mm, 1 at 49A/mm) which agree with Miss Cannon's finding that the spectrum is variable. One plate shows prominent He I and a good general match with η Hya (B3 V) for the strength of H and He; however, the comparison is vitiated by the presence of Ca II K (about as strong as in B9 V) and Mg II 4481 is also stronger than in η Hya. None of the other 6 plates shows He I or the other lines certainly; H alone is clearly seen, but with widths remaining much as in B3 V, i.e. very much narrower than Ao V. Thus Ca II K, observed once, cannot be interstellar.

Radcliffe photometry gives $V=11{\cdot}15$, $B-V=-0{\cdot}28$ (3 measures), the colour corresponding to B1 V, i.e. much earlier than observed.

No velocity measures have yet been made, but visual inspection shows that the radial velocity is low and not subject to a wide range of variation, if at all.

Luyten (**66**) has suggested that the star might be a white dwarf. The narrow hydrogen lines need not necessarily rule out this possibility. Clearly a trigonometrical parallax is very urgently required. Observations of the star are being continued.

16.—The spectroscopic programme has been carried out almost entirely by Feast and Thackeray, the photoelectric by Wesselink. Thanks are due to Mr N. J. Woolf (Radcliffe Student) for obtaining a few spectra; to Messrs J. Bentley, J. Jooste and R. Smith for some assistance at the telescope during photoelectric observations; to H.M. Astronomer (Cape), Dr R. H. Stoy, for the use of some electronic equipment and its maintenance under the supervision of Dr A. W. J. Cousins; and finally to Mrs S. M. Blore for typing the MS.

Radcliffe Observatory,
Pretoria:
1960 *March.*

References

(1) M. W. Feast, A. D. Thackeray and A. J. Wesselink, *Obs.*, **75,** 216, 1955.
(2) A. J. Wesselink, *M.N.*, **116,** 3, 1956.
(3) M. W. Feast, *M.N.*, **116,** 583, 1956.
(4) M. W. Feast and A. D. Thackeray, *M.N.*, **116,** 587, 1956.
(5) A. D. Thackeray, *Stellar Populations, Spec. Vaticana, Ric. Ast.*, **5,** 195, 1958.
(6) M. W. Feast, A. D. Thackeray and A. J. Wesselink, *Obs.*, **78,** 156, 1958.
(7) A. J. Cannon, *H.A.*, **100,** 205, 1936.
(8) K. G. Henize, *Ap. J. Supp.*, No. 22, 1956.
(9) H. C. Arp, *A.J.*, **63,** 118, 1958.
(10) H. L. Johnson and W. W. Morgan, *Ap. J.*, **117,** 313, 1953.
(11) J. K. McDonald, *J.R.A.S. Canada*, **XLII,** 220, 1948, D.A.O. Contrib. No. 12.
(12) R. M. Petrie, D. M. Andrews and J. K. McDonald, *Pub. D.A.O.*, **X,** 415, 1958.
(13) M. W. Feast and A. D. Thackeray, *M.N.*, **120,** 463, 1960.
(14) *Cape Mimeogram* No. 5, 1958.
(15) S. C. B. Gascoigne, *Aust. J. Phys. Supp.*, **17,** No. 3, 1954.
(16) A. J. Wesselink, *M.N.*, **119,** 576, 1959.
(17) C. S. Beals, *Pub. D.A.O.*, **IX,** 1, 1950.
(18) E. M. Lindsay, *M.N.*, **116,** 649, 1956.
(19) H. J. Smith, *Harvard Thesis*, 1955.
(20) R. E. Wilson, *Lick Obs. Pub.*, **13,** Pt. 5, 1918.
(21) R. A. Rossiter, *Pub. Michigan Obs.*, **XI,** 1955.
(22) O. Struve and K. Wurm, *Ap. J.*, **88,** 84, 1938.
(23) A. D. Code and T. E. Houck, *P.A.S.P.*, **70,** 261, 1958.
(24) M. W. Feast, *Obs.*, **73,** 255, 1953.
(25) W. J. Luyten, *A search for Faint Blue Stars*, **IX,** Minneapolis, 1957.
(26) H. Shapley, V. McK. Nail and W. G. Tifft, *A. J.*, **56,** 1939, 1951.
(27) A. D. Thackeray, *M.N.A.S.S.A.*, **16,** 3, 1957.
(28) F. Becker, *Pub. Astrophysical Obs. Potsdam*, **27,** Pt. 1, 1929.
(29) H. L. Johnson, *Lowell Bull.*, **90,** 1958.
(30) A. Feinstein, *Zs. f. Astrophys.*, **47,** 218, 1959.
(31) A. D. Thackeray and A. J. Wesselink, *Obs.*, **75,** 33, 1955.
(32) M. Schwarzschild and R. Härm, *Ap. J.*, **129,** 637, 1959.
(33) D. M. Popper, *Ap. J.*, **129,** 647, 1959.
(34) H. C. Arp, *Encyclopedia of Physics*, **51,** 75, 1958.
(35) M. Schwarzschild and R. Härm, *Ap. J.*, **128,** 348, 1958.
(36) R. J. Trumpler, *P.A.S.P.*, **47,** 249, 1935.
(37) O. Struve, *Stellar Evolution*, Princeton University Press, 1950, pp. 18–20.
(38) Y. Andrillat, *Etoiles à Raies d' Emission:* Liège Colloquium, 1957, p. 61.
(39) B. Onderlicka, *Etoiles à Raies d' Emission:* Liège Colloquium, 1957, p. 68.
(40) M. S. Roberts, *Etoiles à Raies d' Emission:* Liège Colloquium, 1957, p. 76.
(41) J. Sahade, *Etoiles à Raies d' Emission:* Liège Colloquium, 1957, p. 46.
(42) R. Wilson, *Etoiles à Raies d' Emission:* Liège Colloquium, 1957, p. 85.
(43) A. B. Underhill, *Etoiles à Raies d' Emission:* Liège Colloquium, 1957, p. 91.

(44) M. Shapley, *H.B.*, 886, 9, 1932.
(45) H. Shapley and M. L. Walton, *H.C.*, **288**, 1925.
(46) H. Shapley and V. McK. Nail, *Proc. Nat. Acad. Sci.*, **41**, 185, 1955; H.R. 407.
(47) V. McK. Nail and H. Shapley, *Proc. Nat. Acad. Sci.*, **39**, 358, 1953; H.R. 373.
(48) H. C. Arp, *A.J.*, **64**, 175, 1959.
(49) M. W. Feast, *Obs.*, **80**, 104, 1960.
(50) H. L. Johnson and B. Iriarte, *Lowell Bull.*, **91**, 1958.
(51) O. Struve, *Obs.*, **65**, 257, 1944.
(52) A. D. Code, *Ap. J.*, **106**, 309, 1947.
(53) *Joint Discussion on Luminosity of Cepheids*, Trans. I.A.U., **X**, 680, 1960.
(54) A. R. Sandage, *Ap. J.*, **127**, 513, 1958.
(55) G. E. Kron and S. N. Svolopoulos, *P.A.S.P.*, **71**, 126, 1959.
(56) W. A. Hiltner, *Ap. J.*, Sup. No. 24, 1956.
(57) G. Munch, *P.A.S.P.*, **64**, 312, 1952.
(58) R. K. Marshall, *Publ. Michigan Obs.*, **V**, 137, 1934,
(59) H. Kühlborn, *Veröff. Berlin-Babelsberg*, **XII**, Pt. 1, 1938.
(60) E. Hubble, *Ap. J.*, **56**, 162, 400, 1922.
(61) P. C. Keenan and G. Keller, *Ap. J.*, **117**, 241, 1953.
(62) T. D. Kinman, *M.N.*, **119**, 538, 1959.
(63) J. L. Greenstein, *Third Berkeley Symposium on Mathematical Statistics & Probability*, University of California, 1955; Mt. Wilson Reprint 202.
(64) A. R. Sandage and O. J. Eggen, *M.N.*, **119**, 278, 1959.
(65) H. L. Johnson and A. R. Sandage, *Ap. J.*, **124**, 379, 1956.
(66) W. J. Luyten, *H.B.*, **858**, 13, 1928.
(67) J. v. B. Lourens, *M.N.A.S.S.A.*, **17**, 138, 1958.

AN ANALYSIS OF THE RADIAL VELOCITIES OF GALAXIES IN THE VIRGO CLUSTER

Sidney van den Bergh

(Communicated by C. S. Beals)

(Received 1960 July 25)*

Summary

It is found that the radial velocities in the Virgo cluster do not deviate significantly from a Gaussian distribution. However, reasonable assumptions regarding the mass to luminosity ratios of galaxies indicate that there is no equipartition of energy between the cluster members. Stable binary and multiple systems appear to exist within the cluster. The velocity differences of members of close pairs may indicate mass to light ratios smaller than those obtained from the virial theorem.

Introduction.

Humason, Mayall and Sandage (1956) have obtained radial velocities for 95 galaxies in the region of the Virgo cluster†. With the exception of NGC 4902 (van den Bergh 1960a) all objects within this area were assumed to be physical cluster members. In analysing the data, equal weight was assigned to the Lick and Mount Wilson values of the radial velocities. Due to the very irregular surface distribution of nearby galaxies it is not possible to estimate the number of non-cluster members which have been included in the sample. However, the distribution of distance moduli obtained from the luminosity classifications of galaxies in the region of the Virgo clusters (van den Bergh 1960c) suggests that the number of non-cluster members included is probably quite small.

Analysis of the data.

A mean radial velocity, corrected for solar motion, of 1175 ± 64 (m.e.) km/sec and a velocity dispersion of 615 ± 45 km/sec were obtained for the cluster members. The observational errors of individual radial velocities are smaller than the observed velocity dispersion by one order of magnitude. Their influence on the data has therefore been neglected. The distribution of the radial velocities in intervals of 200 km/sec is given in Table I.

TABLE I

Velocity distribution in the Virgo cluster

$V_e - \overline{V}_e$ (km/sec)	n	$V_e - \overline{V}_e$ (km/sec)	n
−1700 to −1500	1	+ 100 to + 300	10
−1500 −1300	1	+ 300 + 500	9
−1300 −1100	3	+ 500 + 700	6
−1100 − 900	2	+ 700 + 900	4
− 900 − 700	6	+ 900 +1100	7
− 700 − 500	3	+1100 +1300	1
− 500 − 300	10	+1300 +1500	1
− 300 − 100	13	+1500 +1700	0
− 100 + 100	17		

* Received in original form 1960 May 30.

† The cluster was assumed to occupy the region: $11^h\,50^m < \alpha(1855) < 12^h\,25^m$, $-1° < \delta(1855) < +20°$ and $12^h\,25^m < \alpha(1855) < 13^h\,05^m$, $-15° < \delta(1855) < +16°$.

To test the assumption that the observed distribution of radial velocities is Gaussian the moments about the mean (in units of 200 km/sec) were computed from the data in Table I and are given below:

$$\mu_1 = 0{\cdot}0 \qquad \mu_3 = -4{\cdot}3$$

$$\mu_2 = 9{\cdot}2 \qquad \mu_4 = 243{\cdot}7.$$

From these moments one obtains

$$\gamma_1 = -\sqrt{\frac{\mu_3^2}{\mu_2^3}} = -0{\cdot}15 \pm 0{\cdot}25 \tag{1}$$

and

$$\gamma_2 = \frac{\mu_4}{\mu_2^2} - 3 = -0{\cdot}11 \pm 0{\cdot}51 \tag{2}$$

in which γ_1 is a measure of whether or not the distribution is symmetrical γ_2 measures departures of a symmetrical nature from a Gaussian distribution. The fact that both γ_1 and γ_2 are smaller than their respective mean errors shows that the observed distribution of the radial velocities in the Virgo cluster does not depart significantly from a Gaussian distribution. Application of the χ^2 test to the data of Table I also shows that the observed distribution does not deviate significantly from a Gaussian distribution. Within the accuracy of the data there is no indication that the velocity dispersion depends on position within the cluster or that the cluster as a whole is rotating.

The equipartition of energy.

The fact that the *velocity* distribution of the cluster members is Gaussian does not imply that equipartition of energy prevails among the cluster members. After assigning, more or less arbitrarily, mass to light ratios 40, 30, 20, 10 and 5 to E, Sa, Sb, Sc and Ir galaxies respectively, the observational data were divided into two groups. The first group contained only galaxies with $m > 1 \times 10^{11}\, m_\odot$, the second group only galaxies with $m < 1 \times 10^{11}\, m_\odot$. The velocity dispersion, σ, and the mean distance from the cluster centre, $\bar{R}$, for these two groups are given in Table II.

TABLE II

*Velocity dispersion and mean mass of cluster galaxies**

	$\bar{m}$	σ	$\bar{R}$
$m > 1 \times 10^{11}\, m_\odot$	$22 \times 10^{10}\, m_\odot$	635 ± 68 (m.e.) km/sec	$6^\circ{\cdot}9$
$m < 1 \times 10^{11}$	5×10^{10}	600 ± 67	$7^\circ{\cdot}5$

* Cluster centre assumed to be at $\alpha\,(1855) = 12^h\,24^m$, $\delta\,(1855) = +13^\circ$.

The data in the table indicate that equipartition of energy does not prevail in the Virgo cluster. This probably implies that the age of the cluster is smaller than its time of relaxation. This conclusion is supported by the observation that the surface distribution of galaxies over the cluster area is highly irregular.

The possible existence of binary galaxies.

It is of some interest to enquire whether stable binary or multiple systems exist in a relatively dense cluster of galaxies like the Virgo cluster. In an attempt to answer this question all pairs of galaxies in the Virgo cluster with separations smaller than 10′·0, for which radial velocity data are available, were selected and are listed in Table III. If all the pairs of galaxies in Table III were optical then the dispersion of the velocity differences of the members of pairs should be $\sigma\sqrt{2}$ where σ is the velocity dispersion in the cluster. A χ^2 test on the velocity differences in Table III shows that the velocity differences have a distribution which differs significantly, at the 5 per cent level, from the theoretical distribution with a dispersion $\sigma\sqrt{2}$. In Fig. 1 the observed distribution of the velocity differences of the pairs listed in Table III is compared with a Gaussian curve with a dispersion of $\sigma\sqrt{2}$. The figure indicates that the observed velocity differences between members of pairs are smaller than would be expected if all pairs were optical. It therefore appears that many of the pairs listed in the table probably form physical systems.

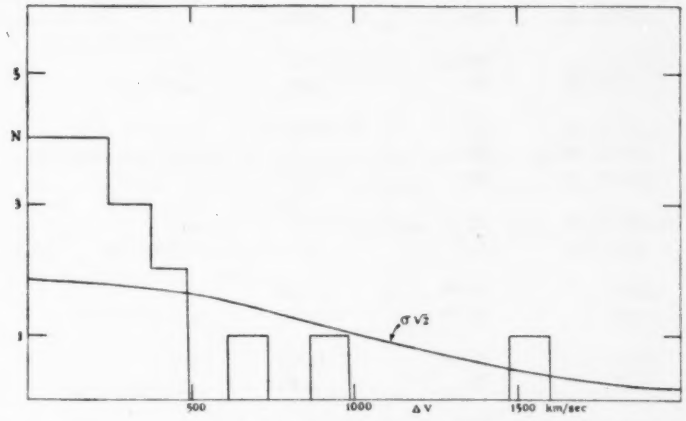

FIG. 1.—*The observed distribution of the 16 velocity differences of pairs of galaxies with separations smaller than 10′·0 is compared with the expected distribution for a similar number of optical pairs. The figure indicates that many of the close pairs of galaxies in the Virgo cluster possibly form physical binary systems.*

The mass to light ratio of cluster galaxies.

The data in Table III may be used to obtain an approximate upper limit to the mean mass of the galaxies in the Virgo cluster. It has been shown by Page (1952) that one can define a double-angled mass function F, analogous to the mass function derived for spectroscopic binaries, which is defined as

$$F \equiv CS(\Delta v)^2 = mf \qquad (3)$$

in which Δv is the velocity difference of the two members of a pair, S their separation in minutes of arc, m the mean mass of the two members of the pair and f a projection factor. Adopting a Hubble constant $H = 120$ km/sec/Mpc (van den Bergh 1960b), a mean cluster velocity $\bar{V}_e = 1175$ km/sec, and expressing ΔV in km/sec and m in solar masses one obtains for the constant in equation (3) a value of $3{\cdot}3 \times 10^5$. Adopting this value of C and counting triple systems with all

TABLE III

Possible multiple galaxies in the Virgo Cluster

NGC	V_e km/sec	DDO type and class	m_{pg}	Separations and velocity differences
4270	2236 ± 50	Sa	13·13	7′·0, 7′·3, 9′·2
4273	2191 ± 40	Sc*t III:	12·35	301, 45, 256 km/sec.
4281	2492 ± 50	E5	12·32	
4382	721 ± 30	Ep or Et	10·05	7′·6
4394	720 ± 150	SBb⁻ II	11·81	1 km/sec
4435	796 ± 100	E4	11·86	4′·4
4438	−105 ± 75	Snntt	10·92	901 km/sec
4458	309 ± 250	[Eo]	13·1	3′·8
4461	1813 ± 40	Sa	12·0	1504 km/sec
4464	1104 ± 50	[E3]	13·6	4′·0, 9′·8
4467	1379 ± 300	[E2]	15·6	461, 275 km/sec
4472	918 ± 50	E4	9·33	
4477	1195 ± 75	S(B)a	11·4	5′·5
4479	753 ± 100	So	13·6	442 km/sec
4478	1410 ± 75	E1	12·3	7′·3, 8′·6, 9′·3:
4486	1218 ± 20(1)	E1	9·56	196, 192, 4 km/sec
Anon	1414 ± 50	[Eo]	14·5	
4550	280 ± 50	E7	12·6	3′·3
4551	908 ± 300	[E4]	13·0	628 km/sec
4567	2206	Sc**t	11·98	1′·3
4568	2335	Sc**t	11·66	129 km/sec (2)
4647	1379	Sc**	12·05	2′·6
4649	1248	E1	9·88	131 km/sec (3)
4809	870	[Ir]	13·3	0′·7
4810	810	[Ir]	11·7	60 km/sec (4)

Notes to Table III

Classification types in square brackets are due to Hubble
(1) Only Mount Wilson velocity used
(2) Page (1952) obtains $\Delta V = 56 \pm 25$ km/sec
(3) Page (1952) obtains $\Delta V = 260 \pm 90$ km/sec
(4) Data from Page (1952).

separations smaller than 10′·0 as three pairs one obtains $F = 3{\cdot}73 \times 10^{11} m_{\odot}$. Adopting $f = \frac{1}{4}$, equation (3) yields a mean mass $\overline{m} = 1{\cdot}5 \times 10^{12} m_{\odot}$. It should be emphasized that this value is an upper limit since it is based on the assumption that *all* the galaxies in Table III form permanent physical binary systems. In reality a number of the pairs in the table are probably optical or pairs moving in hyperbolic orbits. In both cases the mean square velocity difference of the components will, for reasonable mass to light ratios, be considerably larger than it would be if all the pairs formed stable physical binary systems. Observational

errors will also, in the mean, tend to increase the dispersion in the observed velocity differences of those pairs which form physical binary systems. The true mean mass of the galaxies in Table III is therefore probably considerably smaller than $1{\cdot}5 \times 10^{12}\, m_{\odot}$.

Assuming a galactic absorption of 0·25 magnitudes one obtains a mean photographic luminosity of $5{\cdot}4 \times 10^{9}\, L_{\odot}$ for the galaxies in Table III and hence $m/L \ll 280$. The application of the virial theorem in the form given by King (1959) to the Virgo cluster yields a rather uncertain mass to light ratio

$$m/L \approx 700.$$

This result depends on the assumption that the radial density distribution in the cluster is that of a polytrope of index $n = 5$. The rather extreme assumption that the cluster has a uniform density distribution throughout would lead to a mass to light ratio which is 50 per cent smaller than the value which is quoted above.

Although the number of multiple galaxies in the Virgo cluster for which velocity data are available is small, the difference between the mass to light ratios obtained from multiple galaxies and from the virial theorem is possibly significant.

David Dunlap Observatory,
Richmond Hill,
Ontario, Canada:

1960 *July.*

References

van den Bergh, S., 1960a, *Publ. David Dunlap Obs.* Vol. 2, No. 6.
——— 1960b, *J. Roy. Astr. Soc. Can.*, **54**, 59.
——— 1960c, *Ap. J.*, **131**, 558.
Humason, M. L., Mayall, N. U., and Sandage, A. R., 1956, *A. J.*, **61**, 97.
King, I., 1959, *A. J.*, **64**, 351.
Page, T., 1952, *Ap. J.*, **116**, 63.

NOTE ON MAGNETIC INSTABILITIES IN STELLAR STRUCTURE

T. G. Cowling

(Received 1960 July 13)

Summary

A particular model of a magnetic star, found by Prendergast to be unstable if the magnetic field is sufficiently great, is shown to be unstable for all magnitudes of the field. The bearing of this result on the general problem of magnetic instabilities is discussed, and it is indicated that such instabilities lead to a readjustment in the field rather than to an explosion of the star as a whole.

---

1. The magnetic field which can exist in a star in equilibrium is limited by a number of considerations. Chandrasekhar and Fermi (1953) showed that the magnetic energy $\mathfrak{M}$ and the gravitational energy Ω in equilibrium are connected by the equation

$$3P + \mathfrak{M} = |\Omega| \tag{1}$$

where P denotes the volume-integral of the material pressure, integrated over the volume of the star. For a gaseous star, if the ratio γ of specific heats is constant throughout the star, P is connected with the total heat energy Q of the star by

$$P = (\gamma - 1)Q. \tag{2}$$

Thus equation (1) can be written

$$3(\gamma - 1)Q = |\Omega| - \mathfrak{M}. \tag{3}$$

Since P and Q are both essentially positive, it follows from either of equations (1) and (3) that $\mathfrak{M} < |\Omega|$. This imposes an upper limit on the average magnetic field which can exist in the star.

The significance of the condition $\mathfrak{M} < |\Omega|$ is roughly as follows. Equation (1) expresses, in an integrated form, the fact that gravitational forces in the star are balanced by the material pressure and magnetic stresses acting jointly. The condition $\mathfrak{M} = |\Omega|$ could be realized only if gravity could be balanced everywhere by magnetic stresses alone, the material pressure being negligible. Such a state of affairs is unlikely in practice to be approached; thus the inequality $\mathfrak{M} < |\Omega|$ gives an upper limit to the magnetic field which is also unlikely to be approached. In fact Prendergast (1958) showed that for a uniform liquid star, with an appropriate type of magnetic field, the condition that the material pressure is positive everywhere imposes the more restrictive condition

$$\mathfrak{M} < 0{\cdot}5069|\Omega|. \tag{4}$$

The magnitude of the magnetic field may be further restricted by stability considerations. Radial oscillations of a star are slowed down by a magnetic

field; an approximate equation giving the principal period $2\pi/\sigma$ in a gaseous star is

$$I\sigma^2 = (3\gamma - 4)(|\Omega| - \mathfrak{M}) \tag{5}$$

where I is the polar moment of inertia about the star's centre (Chandrasekhar and Limber 1954). Thus, in a stable star ($\gamma > 4/3$), σ^2 is decreased by the presence of the magnetic field, in so far as $|\Omega|$ is decreased by $\mathfrak{M}$ on the right of equation (5); this may be regarded as implying a reduction of stability. This implication is, however, a little equivocal; equation (5) can be written in the alternative form

$$I\sigma^2 = 3(3\gamma - 4)P \tag{6}$$

in which the magnetic field does not appear explicitly. It is, in fact, only in so far as the magnetic field reduces the contribution of the material pressure to supporting gravity that σ^2 is reduced.

A less equivocal indication of instability due to a magnetic field was given by Prendergast (1958). He showed that, for his type of magnetic field in a uniform liquid star, certain non-radial displacements indicate instability if

$$\mathfrak{M} > 0{\cdot}4068|\Omega|. \tag{7}$$

These displacements need not be those most likely to yield instability; thus states of equilibrium exist, not violating the pressure condition (4), which are none the less ruled out because unstable.

2. In this note it will be shown that Prendergast's type of magnetic field in a uniform liquid star is always unstable, however small the field may be. The line of argument is roughly as follows. Prendergast expresses the change in energy due to a small displacement as the sum of two parts, one gravitational, and the other magnetic. The first is essentially positive; the second turns out to be negative for the displacement considered. Instability is inferred if the second is greater in magnitude than the first.

However, Prendergast's field vanishes at the surface of the star, and is small in a sufficiently shallow layer directly below the surface. We consider, therefore, a displacement differing from Prendergast's only within this shallow surface layer, and such that the radial displacement becomes zero at the star's (spherical) surface. Thus with the modified displacement the star retains its spherical form, and its gravitational energy is unaltered by the displacement. On the other hand, since the magnetic field is small in the surface layer, and this layer is thin, the modification of the displacement in the surface layer does not affect the change $\delta\mathfrak{M}$ in magnetic energy, and $\delta\mathfrak{M}$ is, as in Prendergast's discussion, negative, however weak is the field. It follows that the modified displacement leads to a reduction in the total energy below that in the equilibrium state, which accordingly is unstable for all values of the magnetic field.

3. We proceed to the detailed discussion. Prendergast considers an equilibrium configuration in which the magnetic forces do not alter the spherical form $r = R$ of the free surface. The magnetic field $\mathbf{H}$ is one axially symmetric about a diameter, given by

$$\mathbf{H} = \alpha R^{-1}\tilde{\omega}S\mathbf{1} + \operatorname{curl}(\tilde{\omega}S\mathbf{1}). \tag{8}$$

Here α is a certain numerical constant, $\tilde{\omega}$ the distance from the axis of symmetry,

and $\mathbf{1}$ a unit vector in the azimuthal (ϕ) direction; S is a function of r which, together with its first derivative, vanishes on the surface $r=R$ of the star.

Prendergast then considers a displacement $\boldsymbol{\xi}$ from equilibrium of the form

$$\boldsymbol{\xi}=\operatorname{curl}(\tilde{\omega}U\mathbf{1}). \tag{9}$$

Let r, θ, ϕ be polar coordinates with the axis of the field a polar axis (so that $\tilde{\omega}=r\sin\theta$). Then the form adopted for the function U is

$$U=\epsilon r\cos\theta\equiv\epsilon r\mu \quad (\mu=\cos\theta) \tag{10}$$

where ϵ is an arbitrary small constant. The change $\delta\mathbf{H}$ in the field produced by the displacement (9) is given by

$$\delta\mathbf{H}=R^{-1}\tilde{\omega}T\mathbf{1}+\operatorname{curl}(\tilde{\omega}P\mathbf{1}) \tag{11}$$

where

$$r^2\tilde{\omega}^2P=\frac{\partial(\tilde{\omega}S,\tilde{\omega}^2U)}{\partial(r,\mu)} \tag{12}$$

$$r^2T=\alpha\frac{\partial(S,\tilde{\omega}^2U)}{\partial(r,\mu)}. \tag{13}$$

As noted earlier, Prendergast expresses the change in potential energy due to the displacement $\boldsymbol{\xi}$ as the sum of two parts (see his equation (82), the right-hand side of which gives twice the change in potential energy). The first part is the change $\delta\Omega$ in the gravitational energy; since the star is a uniform liquid one, this depends only on the distortion of the surface. The second is the change $\delta\mathfrak{M}$ in the magnetic energy, given by

$$\delta\mathfrak{M}=\frac{1}{8\pi}\int\{\tilde{\omega}^2T^2+|\operatorname{curl}(\tilde{\omega}P\mathbf{1})|^2-2\alpha\tilde{\omega}^2PT\}\,d\tau \tag{14}$$

the integral being over the star's volume. Prendergast found that, with the assumed displacement, $\delta\Omega>0$, $\delta\mathfrak{M}<0$; for a sufficiently large initial magnetic field $\delta\mathfrak{M}$ is greater in magnitude than $\delta\Omega$, this implying instability.

We shall modify Prendergast's analysis as follows. The displacement $\boldsymbol{\xi}$ will still be taken to be given by (9); equation (10) will, however, be modified to read

$$U=f(r)\cos\theta\equiv f(r)\mu \tag{15}$$

where $f(r)$ is a continuous and twice differentiable function of r. The function $f(r)$ is chosen to equal ϵr, as before, in the range $0<r<R-\delta$, where δ is small; in the range $R-\delta<r<R$, $f(r)$ becomes rapidly smaller, dropping to zero at $r=R$. This choice of U makes the radial component of $\boldsymbol{\xi}$ vanish at $r=R$; that is, the displacement becomes one which leaves the spherical form of the free surface unaltered, so that $\delta\Omega=0$. On the other hand we can show that, because the displacement differs from Prendergast's value only in the small range $R-\delta<r<R$, $\delta\mathfrak{M}$ is not appreciably different from Prendergast's value.

To establish this last result, we need simply to consider orders of magnitude of the different terms in equation (14). Because of the rapid reduction of U to zero in the small range $R-\delta<r<R$, we must regard $\partial U/\partial r$ as large, of order δ^{-1}, in this range; $\partial^2U/\partial r^2$ will be large of order δ^{-2}. On the other hand, $S=0$ and $\partial S/\partial r=0$ when $r=R$; thus S must be small of order δ^2 in the same range. It follows from equations (12) and (13) that P and T are of order δ in the range, and that $\partial P/\partial r$ is finite (i.e. proportional to the zero power of δ).

This implies that the terms $\tilde{\omega}^2T^2$, $-2\alpha\tilde{\omega}^2PT$ in the integrand on the right-hand side of (14) are both small in the range $R-\delta<r<R$. The term $|\mathrm{curl}\,(\tilde{\omega}P\mathbf{l})|^2$ involves $\partial P/\partial r$, and so is finite. However, because the range $R-\delta<r<R$ is small, the total contribution of this range to the integral in (13) is small (of order δ). The same was true before the modification of U from Prendergast's form; thus the modification in U introduces no sensible change in $\delta\mathfrak{M}$. Thus with the modified displacement $\delta\Omega=0$, while $\delta\mathfrak{M}$ has virtually the same negative value as in Prendergast's work. That is, as stated earlier, a displacement exists which reduces the total potential energy below the equilibrium value, and the equilibrium is unstable. This result is true however weak is the magnetic field.

4. The significance of this result is in indicating what consequences may follow from the instability. The instability is one in the field by itself, and does not depend on the relative magnitudes of the magnetic and gravitational forces. If the magnetic forces are small, clearly the instability must relieve itself by a readjustment of the field in the star, this not excluding departures from axial symmetry and (possibly) the extrusion of lines of force through the surface; the spherical form of the star will thereby be hardly affected. If the magnetic forces are increased, and become comparable with gravity, a continuity argument suggests that a similar readjustment is likely to occur, the only difference being that the star's surface will depart more from the spherical form. It is possible, of course, that the field will be unable to reach stable equilibrium without passing through a discharge phase like that considered by Dungey (1958) in connection with the theory of flares, the discharge enabling lines of force to become unfrozen from the material. But there is no reason to expect, as has been suggested in connection with supernovae (Oort and Wahlraven 1956, note 3 on p. 304) that magnetic instability may be able to blow up the star.

This conclusion might be thought to depend on the artificial assumption of a uniform liquid star. The gravitational energy of such a star is not altered by any internal displacement which leaves the form of the surface unaffected; this is why instability is possible even when the magnetic forces are small compared with the gravity. In a more normal, stably-stratified, star no similar result can hold. Virtually any internal displacement must lead to an increase in the gravitational energy; instability can arise only if the magnetic field is sufficiently strong for this increase to be offset by the decrease in magnetic energy. Thus instability might be expected to arise only when the magnetic forces have become large enough also to be able to explode the star.

A result obtained by Chandrasekhar and Fermi (1953) shows that this is not the case. A star can undergo complete disintegration due to magnetic instability only if its total energy $\Omega+\mathfrak{M}+Q$ in the unstable equilibrium is positive. Since $\Omega<0$, this can be written

$$\mathfrak{M}+Q>|\Omega|$$

or, using equation (3),

$$(4-3\gamma)Q>0. \tag{16}$$

Since Q is essentially positive, this condition is realized only if $\gamma<4/3$, however great the magnetic field may be.

In a uniform expansion, in fact, magnetic stresses vary as the 4/3 power of the density, just like radiation pressure does. Their effect is accordingly, like

that of radiation pressure, to dilute the effect of gas pressure and make the state approach one of neutral equilibrium. This is the significance to be attached to the reduction in stability indicated by equation (5). This refers to the overall effect in a *uniform* expansion; of course, in other displacements the variation in the magnetic stresses may be more conducive to instability than would be the variation of radiation pressure.

We conclude, then, that magnetic instabilities cannot cause the explosion of a star as a whole. Instability due to a magnetic field is such that the most unstable parts of the field are able to relieve themselves of their instability by a redistribution of the lines of force through the mass. Such a redistribution may be violent, as the example of solar flares indicates; but it cannot explode the whole star.

Dept. of Applied Mathematics,
The University,
Leeds:
1960 *July* 11.

References

Chandrasekhar, S., and Fermi, E., 1953, *Ap. J.*, **118**, 116.
Chandrasekhar, S., and Limber, N., 1954, *Ap. J.*, **119**, 10.
Dungey, J. W., 1958, *Cosmic Electrodynamics* (Cambridge University Press), Chapters 3 and 6.
Oort, J. H., and Wahlraven, Th., 1956, *B.A.N.*, **12**, No. 462, p. 285.
Prendergast, K. H., 1958, *Ap. J.*, **128**, 361.

COMPUTING PRECISE STAR CO-ORDINATES

A. J. Wickens and Harold E. Jones

(Communicated by the Dominion Astronomer)

(Received 1960 May 2)

Summary

The Geodetic Survey of Canada has found it feasible to use the IBM 650 computer to determine precise apparent star co-ordinates without the use of precomputed tables or punch cards of Besselian or Independent Star Numbers and Annual Variation, etc. Corrections for precession, proper motion, nutation, aberration and parallax are applied to the positions from the basic catalogues. Newcomb's precession constants are used; nutation is computed using the formulae of the Improved Lunar Ephemeris; aberration is computed following the method described by Porter and Sadler. The resulting programme requires an average of about ten seconds per star and will preserve the accuracy of FK_3 star co-ordinates for many years from the catalogue epoch.

The Geodetic Survey of Canada has devised a programme for the IBM 650 computer to give precise apparent star co-ordinates at upper or lower transit with a minimum of input. The advantages of this programme over the more conventional programmes arise from the fact that it starts from the co-ordinates of any fundamental catalogue. A single set of star cards will suffice for many decades except for very high circumpolars which should not be updated more than ten or fifteen years. Cards or tables of mean places for each year are not required, nor are cards or tables of day numbers. Each star card contains mean co-ordinates, and proper motion for the epoch, with the parallax and a time T_0, the fraction of a Julian century from 1900 January 0·5 to the epoch. To find the apparent co-ordinates of a group of stars observed on one evening it is only necessary to punch one card with the date, approximate local time, and longitude, and then pick out the respective star cards. The programme is convenient for updating *General Catalogue* stars. Its precision is adequate to preserve the accuracy of FK_3 co-ordinates for many decades.

Preliminary analysis of the problem showed that the fundamental variable throughout is a time T, the fraction of a Julian century from 1900, January 0·5, to the instant of observation. The problem thus reduced to finding T, applying the precession and proper motion from T_0 to T to give the mean place at the instant of observation, and to this applying the nutation, aberration, and parallax for the time T to give the apparent place.

Since the apparent place for upper or lower meridian transit is required, the local sidereal time is taken as the right ascension α of the star or, for lower transit, α plus twelve hours. The fraction of a Julian century to the Greenwich midnight of date T_m is computed first. Then, the Greenwich mean sidereal time for that midnight S is computed using Newcomb's formula for the right ascension of the mean Sun (**8**) plus twelve hours.

$$S = 6^h\,38^m\,45^s{\cdot}836 + 8640184^s{\cdot}542\,T_m + 0^s{\cdot}0929\,T_m^2.$$

By comparing S with α plus the longitude and by using the approximate input time to indicate upper or lower transit, a correction ΔT is found such that

$$T = T_m + \Delta T.$$

The corrections for precession and proper motion combined are computed as outlined by Doolittle (**2**) using the Taylor's series

$$\Delta_1\alpha = \frac{d\alpha}{dt}(T-T_0) + \frac{1}{2!}\frac{d^2\alpha}{dt^2}(T-T_0)^2 + \frac{1}{3!}\frac{d^3\alpha}{dt^3}(T-T_0)^3 + \frac{1}{4!}\frac{d^4\alpha}{dt^4}(T-T_0)^4 + \dots$$

and a similar series for $\Delta_1\delta$. The first and second derivatives only are expanded completely in terms of the independent partial derivatives in precession and proper motion. The expansions used are:

$$\frac{d\alpha}{dt} = \frac{\partial_\rho\alpha}{\partial t} + \frac{\partial_\mu\alpha}{\partial t}$$

$$\frac{d^2\alpha}{dt^2} = \frac{\partial_\rho{}^2\alpha}{\partial t^2} + 2\frac{\partial_\rho\partial_\mu\alpha}{\partial t^2} + \frac{\partial_\mu{}^2\alpha}{\partial t^2}$$

$$\frac{d^3\alpha}{dt^3} = \frac{\partial_\rho{}^3\alpha}{\partial t^3} + \text{neglected terms}$$

$$\frac{d^4\alpha}{dt^4} = \frac{\partial_\rho{}^4\alpha}{\partial t^4} + \text{neglected terms}$$

with similar expansions for declination. It was found necessary to use the fourth derivatives to preserve accuracy for stars of high declination such as Polaris. The partial derivatives with respect to precession are:

$$\frac{\partial_\rho\alpha}{\partial t} = m + n\sin\alpha\tan\delta$$

$$\frac{\partial_\rho\delta}{\partial t} = n\cos\alpha$$

with corresponding higher order derivatives. Newcomb's values of the precession constants m and n as cited by Kopff and Gondolatsch (**6**) were used.

$$m = 4608''\cdot506 + 2''\cdot7945\,T + 0''\cdot00012\,T^2$$

$$n = 2004''\cdot685 - 0''\cdot8533\,T - 0''\cdot00037\,T^2.$$

The partial derivatives with respect to proper motion are shown by Doolittle (**2**) to be:

$$\frac{\partial_\mu\alpha}{\partial t} = \mu_\alpha \qquad \frac{\partial_\mu{}^2\alpha}{\partial t^2} = 2\mu_\alpha\mu_\delta\tan\delta$$

$$\frac{\partial_\mu\delta}{\partial t} = \mu_\delta \qquad \frac{\partial_\mu{}^2\delta}{\partial t^2} = -\tfrac{1}{2}\mu_\alpha{}^2\sin 2\delta$$

where μ_α and μ_δ are the proper motions in right ascension and declination respectively. The cross terms are shown to be:

$$\frac{\partial_\rho\partial_\mu\alpha}{dt} = n\mu_\alpha\cos\alpha\tan\delta + n\mu_\delta\sin\alpha\sec\delta^2$$

$$\frac{\partial_\rho\partial_\mu\delta}{\partial t} = -n\mu_\alpha\sin\alpha.$$

The application of $\Delta_1\alpha$ and $\Delta_1\delta$ to the preliminary co-ordinates gives the mean place of instant and these mean place coordinates are used in computing the other corrections.

The corrections used for nutation are given by Smart (**11**) as:

$$\Delta_n\alpha = \Delta\psi\,(\cos\epsilon + \sin\epsilon\sin\alpha\tan\delta) - \Delta\epsilon\cos\alpha\tan\delta$$
$$\Delta_n\delta = \Delta\psi\sin\epsilon\cos\alpha + \Delta\epsilon\sin\alpha$$

where $\Delta\psi$ and $\Delta\epsilon$, the nutation in longitude and obliquity respectively, are computed using all terms of the formulae in the *Improved Lunar Ephemeris* (**5**). The obliquity of the ecliptic ϵ, is equal to the mean obliquity ϵ_m, plus $\Delta\epsilon$, and the mean obliquity is computed by Newcomb's formula (**8**).

$$\epsilon_m = 23^\circ\,27'\,08''{\cdot}26 - 46''{\cdot}845\,T - 0''{\cdot}0059\,T^2 + 0''{\cdot}00181\,T^3.$$

The corrections for annual aberration are computed following the method described by Porter and Sadler (**10**). The formulae used are:

$$\Delta_a\alpha = -1189''{\cdot}80\sec\delta\,[-(y' + 0''{\cdot}0000553)\cos\alpha + (x' + 0''{\cdot}0002815)\sin\alpha]$$
$$\Delta_a\delta = -1189''{\cdot}90\,[(y' + 0''{\cdot}0000553)\sin\alpha\sin\delta + (x' + 0''{\cdot}0002815)\cos\alpha\sin\delta - (z' + 0''{\cdot}0000240)\cos\delta]$$

where x' y' and z' are the three components of the Earth's velocity with respect to the centre of gravity of the solar system. These velocity components are computed by a numerical differentiation over a 2·4 hour period of the functions:

$$-X = R\cos\beta\cos\lambda$$
$$-Y = R\,(\cos\beta\sin\lambda\cos\epsilon - \sin\beta\sin\epsilon)$$
$$-Z = R\,(\cos\beta\sin\lambda\sin\epsilon + \sin\beta\cos\epsilon)$$

where X, Y and Z are the rectangular co-ordinates of the Earth with respect to the centre of the Sun, β and λ being the Sun's true latitude and longitude with respect to the Earth. The latitude is assumed to be zero. The mean longitude of the mean Sun is computed by Newcomb's formula (**8**)

$$L = 279^\circ\,41'\,48''{\cdot}04 + 100^{\text{rev.}}\,00^\circ\,46'\,08''{\cdot}13\,T + 1''{\cdot}090\,T^2.$$

This is reduced to the mean longitude of the true Sun by using the larger terms of Newcomb's equation of centre formula (**8**)

$$\Delta L = (6910''{\cdot}057 - 17''{\cdot}24\,T)\sin g + 72''{\cdot}338\sin 2g$$

where g, the Earth's mean anomaly, is computed using the formula from the *Improved Lunar Ephemeris* (**5**).

$$g = 358^\circ\,28'\,33''{\cdot}00 + 99^{\text{rev.}}\,359^\circ\,02'\,59''{\cdot}10\,T - 0''{\cdot}54\,T^2 - 0''{\cdot}0120\,T^3.$$

Neglecting the perturbations of the longitude by the Moon*, the true longitude of the true Sun is thus given by

$$\lambda = L + \Delta L + \Delta\psi.$$

The radius vector in astronomical units is computed using a formula given by Danjon (**1**)

$$R = 1{\cdot}00014018_0 - 0{\cdot}0167283848\cos g - 0{\cdot}00013992\cos 2g$$

* See note at end of paper.

The perturbations of R due to the Moon are allowed for by the expression

$$\Delta R = -0{\cdot}0000307621\, R\cos D$$

which is derived from Newcomb (**8**) where D, the mean elongation of the Sun from the Moon is computed using the formula from the *Improved Lunar Ephemeris* (**5**):

$$D = 350^\circ\,44'\,14''{\cdot}95 + 1236^{\text{rev.}}\,307^\circ\,06'\,51''{\cdot}18\,T - 5''{\cdot}17\,T^2 + 0''{\cdot}0068\,T^3.$$

The result of this numerical differentiation, giving velocity components X' Y' and Z' with respect to the Sun's centre, is corrected for the effects of Jupiter and Saturn as described by Plummer (**9**) to get the velocity with respect to the centre of mass of the solar system. The velocity corrections used are:

$$\frac{\Delta X'}{2} = -0{\cdot}0000036\sin\lambda_J - 0{\cdot}0000008\sin\lambda_S$$

$$\frac{\Delta Y'}{2} = 0{\cdot}0000033\cos\lambda_J + 0{\cdot}0000007\cos\lambda_S$$

$$\frac{\Delta Z'}{2}\ \text{(assumed)} = \text{zero}$$

where λ_J and λ_S, the longitudes of Jupiter and Saturn respectively, are computed by approximate formulae derived from a study of Hill (**4**) and the current *American Ephemeris*.

$$\lambda_J = 237^\circ\,30' + 8^{\text{rev.}}\,154^\circ\,54'\,T$$
$$\lambda_S = 268^\circ\quad\ + 3^{\text{rev.}}\,142^\circ\,07'\,T.$$

The required velocity components are:

$$x' = X' - \Delta X'$$
$$y' = Y' - \Delta Y'$$
$$z' = -Z' - \Delta Z'.$$

The corrections used for parallax as given by Smart (**11**) are:

$$\Delta_p\alpha = \pi\sec\delta\,(\cos\alpha\cos\epsilon\sin\lambda - \sin\alpha\cos\lambda)$$
$$\Delta_p\delta = \pi\,(\cos\delta\sin\epsilon\sin\lambda - \cos\alpha\sin\delta\cos\lambda - \sin\alpha\sin\delta\cos\epsilon\sin\lambda)$$

where π is the parallax of the star.

In the above computations the complete formulae for $\Delta\psi$, $\Delta\epsilon$, λ, R and ϵ are not used for each star in a set. These variables are computed for the starting time of the set and for a time twelve hours later. The value at each individual star time is interpolated linearly within the twelve hour interval.

The corrections for nutation, aberration and parallax are combined in the following manner to give the total difference between mean and apparent co-ordinates:

$$\Delta_a\alpha = \Delta_n\alpha + \Delta_a\alpha + \Delta_p\alpha + \Delta\alpha\,\Delta\delta\tan\delta$$

$$\Delta_a\delta = \Delta_n\delta + \Delta_a\delta + \Delta_p\delta \pm \frac{\Delta\alpha^2}{2}\cos\delta$$

where the last terms are approximate corrections to the differential formulae used to compute the individual corrections, $\Delta\alpha$ and $\Delta\delta$ being the sum of the individual corrections.

The accuracy is high. In order to check the programme, apparent places computed by it were compared with positions supplied to the Dominion Observatory by the U.S. Naval Observatory. Thirty-four FK_3 (3, 7) stars observed during 1959 were checked. Updating the 1950 values of the fundamental catalogue (an average interval of 9·5 years) the maximum discrepancy in declination was 0″·02 in one case; most discrepancies were zero. In right ascension the maximum discrepancy for stars below 80° declination was 0ˢ·002; for those above 80° it was 0ˢ·005 (for Polaris).

The limiting factors of the programme are the interval of updating and the declination of the star. This is because of the instability of the Taylor's series used in computing precession which involves tangents and secants of the declination to the same power as the order of the derivative. In order to study the limitations, twenty-four of the previous test stars for which 1925 co-ordinates are given (3) were updated from 1925 (an average interval of 34·5 years). In the comparison the maximum discrepancy in declination was 0″·05 (for Polaris). In right ascension, for stars below 83° declination, the maximum discrepancy was 0ˢ·007; for stars up to 87° declination, the maximum discrepancy was 0ˢ·026; and for two stars at 89° 04′ declination, the discrepancies were 0ˢ·566 and 0ˢ·312. A further study of the magnitude of the derivatives indicates that for Polaris a safe maximum of updating interval would be 15 years and that the allowable interval increases very fast as the declination decreases. Therefore, the epoch of star cards for the few very high polars should be advanced every decade or so. With this precaution, it is clear that the programme is adequate for updating over any interval that the Geodetic Survey can expect to require.

Revisions of the programme are being considered. A few more terms to the corrections may be added. The time required, which now averages about ten seconds per star, can be reduced. Apparent places at any sidereal time, not necessarily meridian transits, can be computed with a minor modification. Because of the basic approach revisions are simple and the programme very versatile.

The assistance given to the writers by Mr G. A. Corcoran and Mr N. E. Cleary of the Geodetic Survey, Mr M. M. Thomson and Mr R. W. Tanner of the Dominion Observatory and Mr F. P. Scott of the U.S. Naval Observatory, is greatly appreciated.

Note.—The perturbations of the longitude were omitted from the original programme due to demands for space when numerical checks indicated the effect was small.

As suggested by Mr D. H. Sadler we include the following function for the lunar perturbations of the Sun's longitude :

$$dL = 6''\cdot454 \sin D \text{ (8)}.$$

We, therefore, must include the term of long period given by

$$\delta L = 6''\cdot40 \sin (231^\circ 19 + 20^\circ\cdot20\, T) \text{ (8)}.$$

Dominion Observatory,
Ottawa,
Canada:

1960 *April* 19.

References

(1) Danjon, André. *Astronomie Générale.* Paris: J. & R. Sennac, 1952–3.
(2) Doolittle, C. L. *Practical Astronomy.* New York: Wiley, 1896.
(3) " Dritter Fundamentalkatalog des Berliner Astronomischen Jahrbuchs, I Teil, Die Auwers-Sterne für die Epochen 1925 und 1950." *Veröffentlichungen des Astronomischen Rechen-Instituts.* Berlin, 1937.
(4) Hill, G. W., " A New Theory of Jupiter and Saturn." *Astronomical Papers of the American Ephemeris,* Vol. IV, Washington, 1890.
(5) *Improved Lunar Ephemeris* 1952–1959. A Joint Supplement to the American Ephemeris and the (British) Nautical Almanac, Washington, 1954.
(6) Kopff, A. and Gondolatsch, F. " Grundbegriffe der Sphärischen Astronomie." *Astronomisch-Geodatischen Jahrbuch,* 1951.
(7) Kopff, A. " Dritter Fundamentalkatalog des Berliner Astronomichen Jahrbuchs, II Teil, Die Zusatzsterne für die Epoche 1950." *Abhandlungen der Preussischen Akademie der Wissenschaften.* Berlin, 1938.
(8) Newcomb, Simon. " Tables of the Sun ". *Astronomical Papers of the American Ephemeris,* Vol. VI. Washington, 1898.
(9) Plummer, H. C. " Note on the Calculation of Stellar Aberration ", *M.N.,* **69,** 414, 1909.
(10) Porter, J. G., and Sadler, D. H. " Stellar Aberration ", *M.N.,* **110,** 467, 1950.
(11) Smart, W. M. *Spherical Astronomy.* Cambridge University Press, 1956.

THE RADIO TELESCOPE FOR 7·9 METRES WAVELENGTH AT THE MULLARD OBSERVATORY

C. H. Costain and F. G. Smith

(Received 1960 June 24)

Summary

This pencil-beam radio telescope, which uses the principle of aperture synthesis, has a resolution of $0{\cdot}8° \times 0{\cdot}8°$ at a wavelength of 7·9 m. A survey of the sky between R.A. 05^h and 17^h, Dec. $+10°$ to $+50°$, has proved the performance of the instrument. The map of this region, which is presented in this paper, shows detail of the spur of radio emission at galactic longitude $l' = 0°$; it also shows some discrete sources, including the Coma cluster.

---

1. *Introduction.*—The construction of a radio telescope with high resolving power at a long wavelength involves large apertures, but not necessarily the large collecting areas which correspond to filled apertures. The present instrument was designed to have a beamwidth of about $0{\cdot}8° \times 0{\cdot}8°$, which requires an aperture about 1700 ft across at $\lambda = 8$ m. A square of this side would have an area of about 60 acres, while a much smaller collecting area is sufficient for the detection of the radio waves emitted from many features which can be resolved with a 1° beam. It is therefore possible to use an aerial system which has a large linear extent without a commensurate area, as for example in the Mills Cross instruments. The principle of aperture synthesis is employed in this instrument, the extension of the aerial in one direction being achieved by the combination of recordings made at successive positions of a movable aerial. The first survey with this instrument has covered the sky from R.A. 05^h to 17^h between Dec. $+10°$ and $+50°$, with a resolution of approximately $0{\cdot}8°$ by 2°. An extension of the present observations will allow a resolution of $0{\cdot}8°$ by $0{\cdot}8°$ if this proves desirable.

2. *Aperture synthesis.*—The principle was first used by Blythe (1957), whose instrument was a direct forerunner of the present one. A general discussion has been given by Ryle and Hewish (1960). The arrangement of the present instrument is shown in Fig. 1. It consists of a fixed East–West aperture 128λ long, together with a small mobile aerial on a track bisecting the fixed aerial and extending about 60λ to the north of it. The fixed aerial is at any time observing a narrow strip of sky along the meridian, and the combination of the two aerials as an interferometer at successive North–South spacings on successive days of observation makes a Fourier analysis of the brightness distribution along this strip. The brightness distribution is subsequently reconstructed by a Fourier synthesis in a computing machine.

In this process of synthesis, the full resolving power of the 50-acre area is built up. The sensitivity is less than that of a full aperture by a factor of $D/(3d_1d_2)^{1/2}$, where D is the side of the equivalent aperture, d_1 is the North–South

aperture of both aerials, and d_2 is the East–West aperture of the mobile aerial (Ryle and Hewish). The excitation of the fixed aerial, and the weighting of the Fourier components in the North–South direction, determine the shape of the final polar diagram, which without any grading would be the product of the voltage polar diagrams of the two arms of a cross aerial each $2D$ long.

The design of the instrument turns mainly on the choice of the North–South aperture (d_1) of both aerials, and on the East–West aperture (d_2) of the mobile aerial. The latter was fixed at 4λ, approximately 100 ft, which was the largest conveniently movable array. With an effective North–South aperture of $1\frac{1}{2}\lambda$, which is obtained with a simple corner reflector, the sensitivity is about 1/16th that of the full square aperture with side $D = 1650$ ft. The effective collecting area of the instrument is therefore about 4 acres.

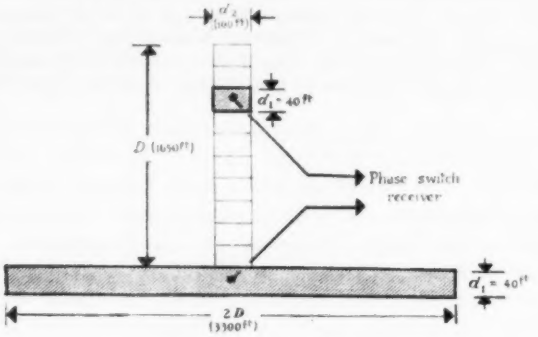

FIG. 1.—*Arrangement of the two aerials.*

The grading of excitation chosen for both arms approximated to a Gaussian curve rather than to the triangular grading which would give a precise equivalence to a uniformly filled aperture. This allowed a reduction of the near sidelobes and a slight increase in sensitivity. The moving aerial was uniformly excited East–West, and correspondingly the excitation of the 128λ aperture could be graded in uniform sections 4λ in length.

3. *The construction of the aerial system.*—Both aerials are in the form of corner reflectors fed by a linear array of full-wave dipoles. It has been shown by Moullin (1949) that a right-angled corner with sides $1\frac{1}{4}\lambda$ wide has a high gain and a polar diagram nearly free from sidelobes. The sides were here made 27 ft, or $1{\cdot}1\lambda$, using 23 SWG steel wire at a spacing of 1 foot. With the feed at $\lambda/2$ from the apex a very similar polar diagram was obtained, with half-power points at $\pm 25°$.

The mobile aerial consists of four full-wave dipole elements, each complete in its own portion of corner reflector one wavelength long. The four portions are mounted together on tripods with guy lines to set towards any declination $\pm 45°$ from the zenith. Each dipole, which presents an impedance of about 500 ohms, is separately matched to a balanced-to-unbalanced transformer through $\lambda/2$ of twin feeder whose spacing may be suitably adjusted, and the four are connected in parallel through equal lengths of coaxial feeder. No adjustment was made for mutual impedances, which were found to be negligible.

The fixed aerial is 3300 ft long, and contains 128 dipoles. Each is connected by a $\lambda/2$ twin feeder to a branching system of twin feeders which provides an equal electrical path to each group of four dipoles. This feeder system has an arrangement of $\lambda/4$ transformers at each junction, so that the feeders are matched throughout with the relative excitation of different parts of the aerial determined by the ratios of the transformers on the two feeders which join at each branch of the feeder. By choosing a grading approximating to a truncated Gaussian distribution, in which the end dipoles had 10 per cent of the excitation of the centre dipoles, a smooth polar diagram was obtained, with sidelobes less than 3 per cent and decreasing away from the main lobe.

The adjustment of the transformers was made in the first instance by measurements of impedance using an admittance bridge; final adjustments were made by comparing the voltages on each dipole when the aerial was excited by a signal generator. A portable battery receiver was used for this measurement, which included a phase comparison between adjacent dipoles. The grading was found to be stable over a period of several months, although it was found to be sensitive to moisture on the open wire feeder lines.

Mechanically, the construction of both aerials is very simple. At each dipole of the long aerial a frame of Dexion angle supports the centre of the dipole and also the reflecting screen. Each frame is guyed separately, so that the declination setting of the whole aerial may be changed by a progressive alteration of successive frames, the aerial being flexible enough to allow a 30° twist in a length of about 150 ft. The mobile aerial is a stiffer structure, separating into 25 ft lengths weighing about 200 pounds each. A move of the four sections involves at least four people and takes about 40 minutes.

Over 5 miles of aluminium angle and 35 miles of reflector wire were used in the construction.

4. *The receiver and recording arrangements.*—A phase-switching receiver with 100 kc/s bandwidth is connected to the two aerials through similar sets of coaxial cables and pre-amplifiers. To provide electrically equal paths an extra 1600 ft of open feeder is included in the transmission line from the mobile aerial, equal to that in the feeder system of the fixed aerial. When observations are made far from the zenith and at large aerial spacings, extra cable may have to be inserted in one aerial connector to keep the relative phases correct over the whole receiver bandwidth.

With equal cables the receiver output is proportional to a cosine Fourier component, and the sine component must be recorded by the insertion of a quarter-wavelength of cable in one aerial connector. The cycle of recording is determined by a motor driven from a sidereal time supply. For four consecutive quarters of each sidereal minute the receiver is connected to the two aerials with (*a*) equal cables, (*b*) an extra quarter wave (*c*) an extra three-quarter wave (*d*) an extra half wave. The output, smoothed by a time constant of 0·1 sec, is fed into an integrator which measures sucessively the difference (*a*)–(*d*) and (*b*)–(*c*) each integrated over 15 seconds. The form of the record is seen in Fig. 2. It would be possible to record such information directly in digital form, but it has been found relatively easy to transfer the present records to punched tape via a record reader and manual perforator.

The gain of the receiver is stabilized by an automatic gain control, which determines the gain according to the total noise level at the input of the pre-amplifiers. The effective aerial temperature varies between about 7000 °K and 20000 °K. The feeders of the fixed aerial have an attenuation of 8·1 db, so that the noise level reaching the preamplifier has a minimum temperature of about 1350 °K, considerably greater than the excess noise of the preamplifier, which is about 200 °K. By injecting a correlated noise signal via equal cables into the preamplifier inputs, this excess noise could be measured along with the phase calibration of the receiver; a regular check was made in this way to ensure that the gain was controlled almost entirely by the galactic background. One record of aerial temperature through 24 hours suffices to define the gain of the whole system through all subsequent measurements at the same declination setting.

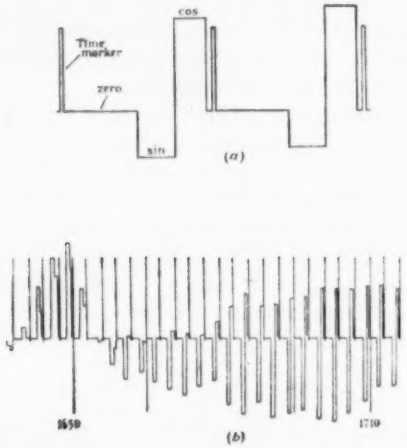

FIG. 2.—(*a*) *Idealized form of record. The time marks are at intervals of* 1 *sidereal minute.* (*b*) *Portion of record at* 5λ *spacing.*

5. *Observations at small aerial spacings.*—Although the North–South aperture of the moving aerial was 1½λ, the separate stations at which it was placed were only 1λ apart. This has the effect of reducing the grating sidelobes in the declination pattern. A spacing of 1λ between the centres of the fixed and moving aerials is physically impossible, so that the components of this spacing and of zero spacing must either be omitted or specially recorded. Omission of these components would mean that the map would not show the mean level or the correct average gradient of temperature over the whole declination range.

The component with 1λ spacing, which involves a small overlap of the two aerials, was recorded with only one of the four moving aerial sections, so that a small part only of the fixed aerial was obscured. A small error in the gradient of temperature will result from this overlap.

The component with zero spacing, corresponding to physical superposition of the aerials, was recorded in two parts. The centre four sections of the fixed aerial were isolated electrically, and these four were first used instead of the moving aerial as an interferometer with the remainder of the fixed aerial.

Secondly, the four centre sections were connected to a receiver which measured the total power received. Combination of the two recordings according to their sensitivities can reproduce exactly the zero spacing component.

The largest component is that recorded as the total power from the four centre sections, since this represents the average brightness temperature over the beam of the moving aerial. Since it is a slowly varying function of time, it is convenient to omit it from the Fourier synthesis, and to add it at the stage when a final map is drawn only if it is necessary to use the correct zero level of temperature on the map.

The computations were performed on the Cambridge electronic computor EDSAC II.

6. *Observations.*—The first synthesis observations were made in 1958, with the aerials set at a declination of 30° N. The separate spacings were one wavelength apart as seen from this direction, up to 30λ maximum. The useful observing time was limited by:

(i) Long-distance propagation of commerical broadcasts *via* ionospheric reflections. This was observed regularly in the day time from October to March.

(ii) Enhanced solar radiation, which occasionally completely swamped daytime records.

(iii) Scintillation, occurring mostly at night.

(iv) Wet weather. The open twin-wire feeder used throughout proved to be sensitive to moisture. The velocity of propagation down a thoroughly wet feeder is about 1/3 per cent below normal, which is a serious change in 1500 feet length. The balance between the feeders to the two aerials was often not exact, since wetting was often uneven. This is a more serious limitation than had been anticipated.

These disturbing effects are all easily detected in the traces made by a series of radio stars on each record. These radio stars provided an excellent calibration every few hours in both amplitude and phase, and the selection of records was made by using these calibrations. The variation of phase through 24 hours in acceptable records was usually about 10°.

7. *The results.*—Twelve hours of R.A. were covered, from $05^h\,00^m$ to $17^h\,00^m$. Fig. 3 shows the sections of sky obtained over one hour, from $16^h\,00^m$ to $17^h\,00^m$, omitting the background level. Sections from R.A. $12^h\,30^m$ to $17^h\,00^m$ were combined with the background level to provide the contour map of Fig. 4. Most of the detail from the sections appears in this map, but some is lost in the process of drawing contours. The contour interval is 1000 °K of brightness temperature.

The most prominent feature is the spur of radio emission at galactic longitude $l' = 0°$. This now shows a remarkable sharp northern edge between Dec. = 20° and Dec. = 25°, with a more irregular southern limit. The northern edge is in places quite unresolved with the 2° beam, and may be less than ½° in extent. At higher declinations the background is flat and relatively featureless. Several discrete sources are to be seen, for example at R.A. $15^h\,03^m$, Dec. = 26°. In the area R.A. 05^h to 17^h, $10° < \text{Dec.} < 50°$, there are 17 clearly defined sources,

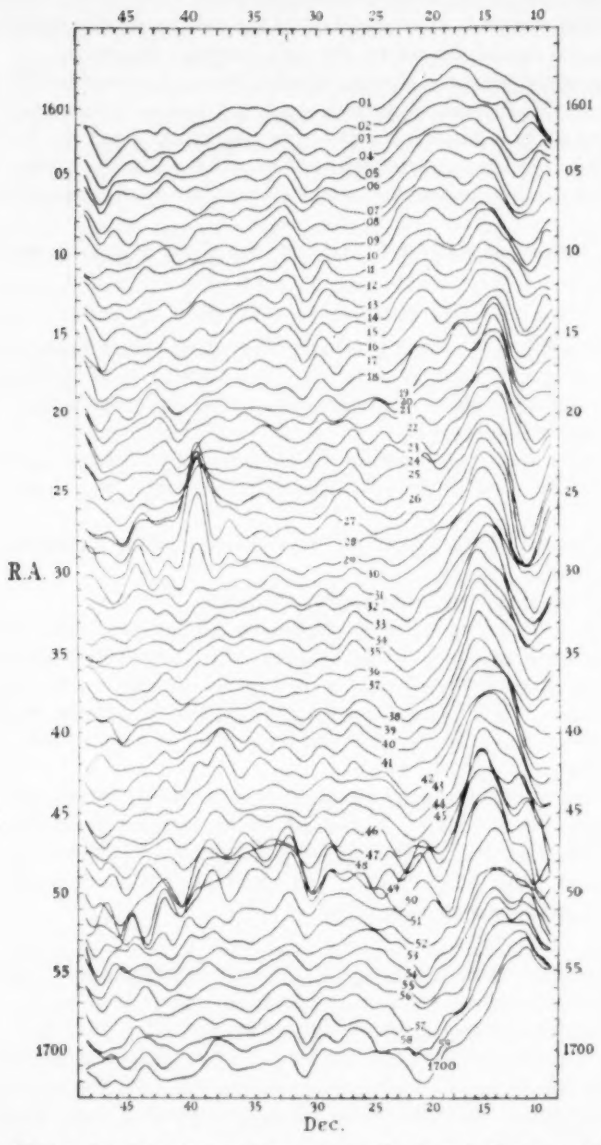

FIG. 3.—*Section of the sky brightness, between R.A.* $16^h\ 00^m$ *and* $17^h\ 00^m$, *omitting the background level.*

16 of which prove to correspond closely in position with previously known sources (as in the 3C catalogue, 1959). Information about more known sources can be found by inspecting the detailed sections of sky, and it is hoped in this way to investigate the spectra of a large number of sources. First inspection suggests that all 3C sources with flux greater than about 10×10^{-26} w.m.$^{-2}$(c/s)$^{-1}$ at 178 Mc/s will appear on the 38 Mc/s survey.

The Coma cluster shows clearly on the map at R.A. $12^h\ 57^m{\cdot}7$, Dec. $= +28°\ 20'$. The total flux, which must be somewhat indeterminate for an extended source, is about 50×10^{-26} w.m.$^{-2}$ (c/s)$^{-1}$ at 38 Mc/s. This value, combined with that of Seeger, Westerhout and Conway (1957) of 11×10^{-26} w.m.$^{-2}$ (c/s)$^{-1}$ at 408 Mc/s, gives a spectral index of $-0{\cdot}65$.

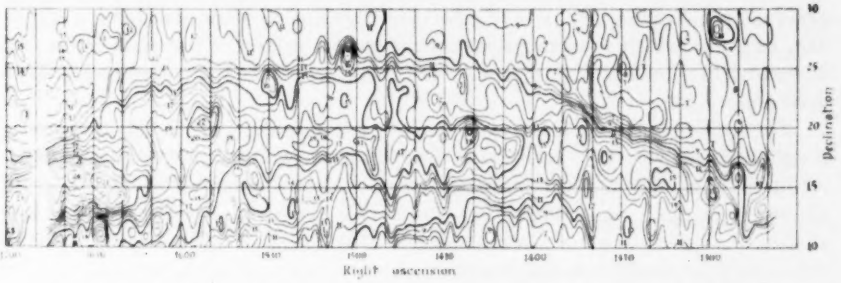

FIG. 4.—*Map of the sky brightness at 38 Mc/s, between R.A.* $12^h\ 20^m$ *and* $17^h\ 00^m$ *Dec. between* 10° *and* 30°.

8. *The Accuracy of the survey.*—From the intensities and positions of the radio stars, and from the general form of the background level, it is evident that the system is behaving generally as expected.

There are several factors influencing the reliability of the results. Random errors in amplitude on the individual records, and random errors in phase between the interferometer aerials, produce side lobes analogous to those produced by errors in excitation in a broadside array. Similarly the noise level on each record will be combined in the synthesis to provide a random fluctuation level on each sky section. Finally there are some systematic errors which affect this particular survey.

9. *Errors in measurement.*—The largest error in measurement is that of the relative phase of the different Fourier components. From the measured range of phase errors it is to be expected that the side lobes in declination will be about 4 per cent r.m.s. The near side lobes in R.A. are determined by the excitation of the fixed aerial, and are about 3 per cent. Far side lobes in R.A. are less than 1 per cent.

The declination side lobe error will be expected to give spurious features with an intensity of the order of 500 °K over most of the present map.

10. *Random noise level.*—The combination of 60 Fourier components, each with the observed noise level, will be expected to provide a random noise level of 600 °K on the map. This value increases to 1200 °K at the declination limits of the survey at Dec. $= 10°$ and 50° where the primary aerial gain is reduced to one half.

11. *Systematic errors.*—There are three effects producing systematic errors in the present survey. The first arises from the difficulty already mentioned of obtaining the Fourier component at a spacing of one wavelength. This results in an error in the North–South slope of temperature over the whole map. It

appears from inspection of the map that the general gradient of temperature from North down to South over the spur at Dec. $\simeq 20°$ may be due to this systematic error.

The secondary grating response depends on the interval between stations of the movable aerial. Very intense features outside the declination range covered by the map may contribute to the observed temperature at any point. For observed points near Dec. $= +10°$ the map contains a component from a secondary response which reaches 12 per cent of the sensitivity of the main beam, but at declinations between $+15°$ and $+50°$ there is no secondary response greater than 4 per cent.

Finally a small systematic error is due to a simplification in the computing programme, in which the declination polar diagram was assumed to be symmetrical in the sine of the zenith angle, although in fact the survey was not centred about the zenith. As a result the sensitivity varies from about 7 per cent low at Dec. $= +50°$ to about 7 per cent high at Dec. $= +10°$. This defect has been eliminated in subsequent computations.

12. *Conclusions.*—The aperture synthesis system has been proved to work satisfactorily. The most serious practical difficulty of the present system has been the sensitivity of the feeder lines to moisture. Remaining limitations are concerned with the ionosphere; long distance propagation may be expected to become less troublesome during sunspot minimum, but scintillation will remain as an obstacle to the development of the full resolving power, as indeed it must for any high resolution instrument on a long wavelength.

The value of the observations lies in the detail that may be observed at a long wavelength in the spur and other features of the Galaxy. Some hundreds of radio stars will be observable, allowing a considerable extension of spectrum measurements. The results of these observations will be published separately.

Mullard Radio Astronomy Observatory,
Cavendish Laboratory,
Cambridge:
1960 *June* 23.

References

Blythe, J. H., 1957, *M.N.*, **117**, 644.
Moullin, E. B., 1949, *Radio Aerials*, Oxford, 1949.
Ryle, M. and Hewish, A., 1960, *M.N.*, **120**, 220.
Seeger, C. L., Westerhout, G., and Conway, R. G., 1957, *Ap. J.*, **126**, 585.

THE RADIO SPECTRUM OF THE ANDROMEDA NEBULA

J. E. Baldwin and C. H. Costain

(Received 1960 July 1)

Summary

Some new observations of the Andromeda nebula have been made at frequencies of 38 and 178 Mc/s. At 178 Mc/s both fan-beam and interferometric measurements have allowed a number of point sources superimposed on the nebula to be distinguished; a comparison of the number of these sources with those found in neighbouring areas of sky suggests that they are not related to the nebula.

By comparing the observations at 38 and 178 Mc/s with those previously made at Jodrell Bank at 408 Mc/s, it has been possible to show that all parts of the nebula have a similar spectrum, the brightness temperature varying at $\nu^{-2.5\pm0.1}$ a figure close to that for the Galaxy.

Introduction

A number of observations of the radio emission from the Andromeda nebula have been made in the frequency range 81·5–408 Mc/s (**1**, **2**, **3**, **4**, **5**). The overall distribution of emission from the nebula is now well established, most of the radiation originating in an extended halo about $10^\circ \times 6^\circ$ in size. On the other hand, no satisfactory value has been obtained for the spectrum of the radiation, mainly because of the difficulty of separating the radiation from M31 from the superimposed galactic emission. Different observers have subtracted the galactic emission in differing arbitrary ways and the resulting flux densities cannot usefully be compared. Values of the spectral index ranging from $-0{\cdot}6$ (**6**) to $-1{\cdot}1$ (**5**) have been quoted. A more reliable way of deriving the spectral index, and one which shows up clearly the probable errors of the determination, is to compare scans across M31 over a range of frequencies using beams of similar shapes. Recent measurements at Cambridge at frequencies of 38 Mc/s and 178 Mc/s combined with the observations of Large, Mathewson and Haslam (**4**), enable this procedure to be used, giving the spectral index of the radiation from M31 over the range 38–408 Mc/s. The 178 Mc/s observations also provide new information concerning the distribution of brightness over the nebula, particularly with regard to the 'point' sources of radio emission in this region of the sky.

178 Mc/s observations

Recordings of the total power received by one element of the 178 Mc/s interferometric radio telescope at Cambridge have been made with the aerial beam centred on $\delta = +40^\circ{\cdot}0$. The beam widths to half power points are $4^\circ{\cdot}6$ in δ and $13'{\cdot}5$ in α. Fig. 1 shows the mean of two recordings on successive days. From measurements of the polar diagram, the aerial efficiency is known to be 0·75 and the observed temperatures have therefore been multiplied by 1·33 to give true brightness temperatures. The halo of M31 extends from 00^h25^m to 00^h57^m, superimposed on which there are several features whose

width in right ascension is that expected for a radio source $\leqslant 13'{\cdot}5$ in diameter. Many of these sources appear on an interferometric record made using both portions of the radio telescope at an E–W spacing of 465λ, and are therefore $\leqslant 3'$ arc in size. In particular the sources at right ascensions $00^h\,28^m$, $00^h\,31^m\,45^s$, $00^h\,46^m$, $00^h\,52^m$, $00^h\,54^m$ are all of small angular size. Part of the area of sky close to M31 has recently been surveyed at 178 Mc/s using the aperture

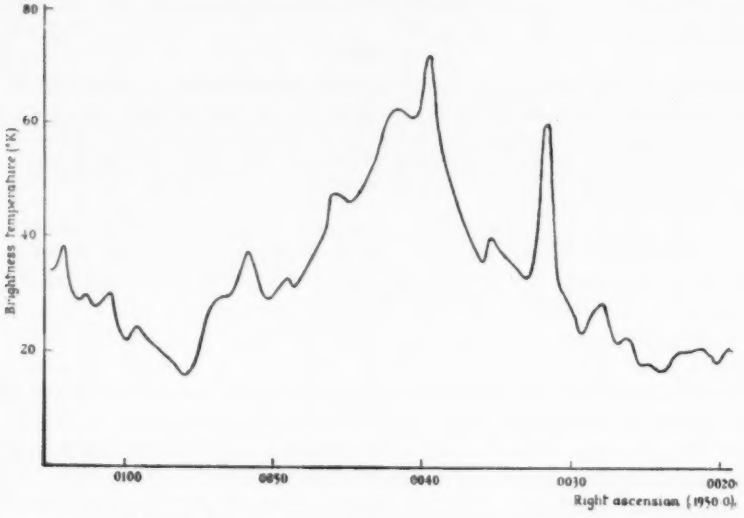

FIG. 1.—*Drift curve of the variation of brightness temperature at 178 Mc/s across the Andromeda nebula. The aerial beam was centred on* $\delta = +40°$. *The plotted curve is the mean of two readings.*

synthesis technique (7), giving positions of sources of small angular size down to flux densities of about $2{\cdot}10^{-26}$ w.m.$^{-2}$(c/s)$^{-1}$. In the region of sky $44° < \delta < 39°30'$, $0020 < \alpha < 0100$ the following sources have been located by P. F. Scott and D. R. Marks, who have kindly allowed us to make use of the information.

α			δ		S ($\times 10^{-26}$ w.m.$^{-2}$(c/s)$^{-1}$)
h	m	s	°	′	
00	28	07	+40	53	2·5
00	33	56	+42	36	1·9
00	39	34	+39	48	2·3
00	41	55	+42	30	1·9
00	45	26	+40	06	3·1
00	46	07	+43	56	1·6
00	51	39	+40	26	3·1
00	53	59	+43	58	2·4

Two of these sources are probably the same as those observed by Large, Mathewson and Haslam (4) at $00^h\,46^m\,15^s$, $+40°\,24'$ and $00^h\,52^m\,00^s$, $+40°\,30'$. The source at $00^h\,39^m\,34^s$, $+39°\,48'$, lying just over 1° south of the centre of M31, appears on the total power curve (Fig. 1) with a flux density of 4×10^{-26} w.m.$^{-2}$ (c/s)$^{-1}$, but its flux density is too small for a reliable angular

diameter to be quoted for it. No source has been detected coinciding with the optical nucleus of M31.

The average density of radio stars down to flux densities of

$$2 \times 10^{-26} \text{ w.m.}^{-2} (\text{c/s})^{-1}$$

over the area of M31 is not significantly different from the density in other samples of sky nearby. Most of the radio sources superimposed on M31 are thus not physically connected with it but remain as a confusing feature in the determination of the spectral index.

38 Mc/s observations

The 38 Mc/s interferometer at Cambridge, employing the principle of aperture synthesis, has been used to observe the region in the vicinity of M31 with a beam width of $0^\circ{\cdot}8$ in α and $4^\circ{\cdot}4$ in δ. The beam width in δ is determined by the total North–South movement of the small section of the interferometer; observations at this declination using spacings up to 12λ are at present available.

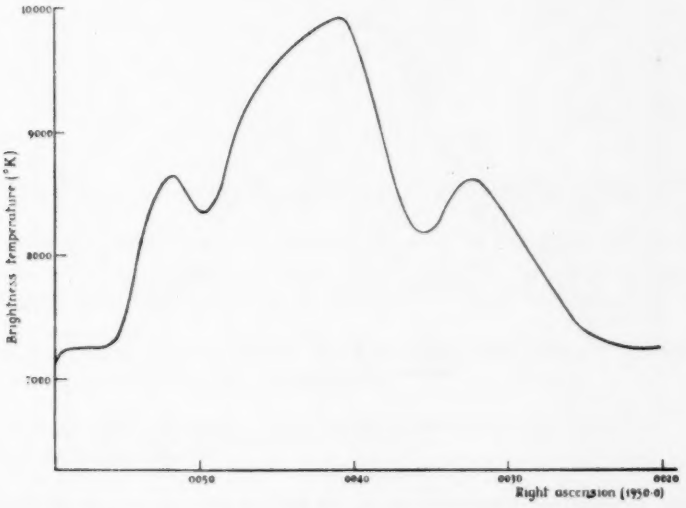

FIG. 2.—*Synthesised distribution of brightness at 38 Mc/s across the Andromeda nebula at* $\delta = +40°$.

The results obtained are in the form of scans in declination at successive minutes of right ascension with a declination beam width of $4^\circ{\cdot}4$ to half power points. The values at $\delta = +40^\circ{\cdot}0$ are plotted in Fig. 2. Examination of the scans in δ suggests that the feature in Fig. 2 at $\alpha = 00^h\,52^m$ is associated with the 178 Mc/s source at $\delta = +40°26'$.

The radio spectral index of M31

The radio data provide two distinct kinds of information relating to the spectrum of M31 which are affected in different ways by errors in measurement:

(i) The spectral index of the radiation from the whole of M31. The accuracy of this determination depends on the accuracy of the absolute scales of temperature employed by different observers and an accurate knowledge of the aerial efficiency.

(ii) The variation of spectral index across M31. This depends only on a comparison of the shapes of the scans at different frequencies and is independent of any assumed scale of temperature.

To reduce the observations at 38 Mc/s and 178 Mc/s and the Jodrell Bank observations at 408 Mc/s to a common beam width, the 178 Mc/s observations have been smoothed in right ascension to give an effective $40' \times 4°{\cdot}6$ beam whilst the 408 Mc/s observations have been smoothed in declination to give a similar beam. The beam width of $48' \times 4°{\cdot}4$ at 38 Mc/s is sufficiently similar for the present discussion.

The three curves derived in this way are shown together in Fig. 3, the scales of temperature having been chosen to give the best overall fit between the curves. There is good general agreement between the curves except at $\alpha = 00^h 32^m$ and $\alpha = 00^h 52^m$ where it is evident that the radio sources at these right ascensions have flux densities falling off more steeply towards higher frequencies than M31 itself.

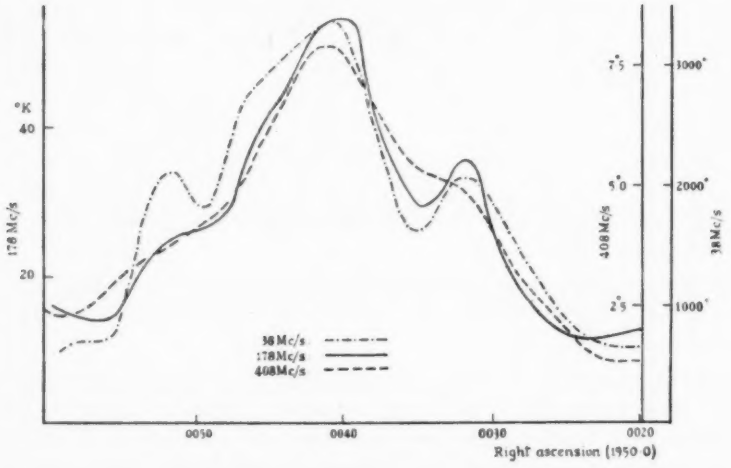

FIG. 3.—*Brightness temperatures at* 38, 178 *and* 408 *Mc/s scaled to give the best overall fit between the curves. All the observations have been smoothed to a beam width of* 40′ *in right ascension by* 4°·6 *in declination.*

Brightness temperatures taken from the temperature scales in Fig. 3 are plotted in Fig. 4. These points define the mean spectral index of M31. The slope of the line is $-2{\cdot}5 \pm 0{\cdot}1$. The flux density of M31 thus varies with frequency, ν, as $\nu^{-0{\cdot}5}$ i.e. the spectral index of M31 is $-0{\cdot}5$. For the spectral index of the galactic radiation Adgie and Smith (**8**) obtained a value of $-0{\cdot}5 \pm 0{\cdot}1$, in good agreement with the result for M31. More recent measurements by Costain (**9**) on the galactic radiation have given a spectral index of $-0{\cdot}37 \pm 0{\cdot}04$, which is just consistent with the M31 value.

Adgie and Smith (**8**) and Costain (**9**) also found that, except in regions of sky very close to the galactic plane, the spectral index of the galactic radiation is independent of direction. Examination of Fig. 3 suggests that, within the

errors of measurement, the spectral index of M31 is constant across the nebula. Using the 178 Mc/s and 408 Mc/s results, the variation in spectral index between $00^h\,30^m$ and $00^h\,50^m$ is $\gtrsim 0{\cdot}2$. Similarly using the 38 Mc/s and 408 Mc/s results together, the variation in spectral index between $00^h\,30^m$ and $00^h\,50^m$ is $\gtrsim 0{\cdot}15$.

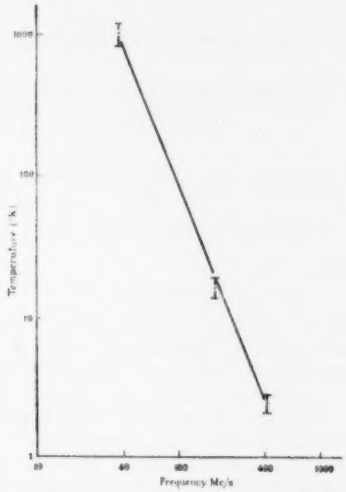

FIG. 4.—*Plot of the mean spectrum of M31 derived from the relative temperature scales in Fig. 3.*

The close agreement between the spectral index of the radio emission from the Galaxy and M31 and the constancy of this spectral index throughout each galaxy suggests that these may be typical features of the radio emission from normal galaxies.

We should like to thank Professor M. Ryle for his help with the observations and his continued interest in the investigation.

Mullard Radio Astronomy Observatory,
Cavendish Laboratory,
Cambridge:
1960 *June* 24.

References

(1) Brown, R. Hanbury, and Hazard, C., *M.N.*, **111**, 357, 1951.
(2) Baldwin, J. E., *Nature*, **174**, 320, 1954.
(3) Seeger, C. L., Westerhout, G., and Conway, R. G., *Ap. J.*, **126**, 585, 1957.
(4) Large, M. I., Mathewson, D. S., and Haslam, C. G. T., *Nature*, **183**, 1250, 1959.
(5) Brown, R. Hanbury, and Hazard, C., *M.N.*, **119**, 297, 1959.
(6) Whitfield, G. R., *M.N.*, **117**, 680, 1957.
(7) Ryle, M., and Hewish, A., *M.N.*, **120**, 220, 1960.
(8) Adgie, R., and Smith, F. G., *Observatory*, **76**, 181, 1956.
(9) Costain, C. H., *M.N.*, **120**, 248, 1960.

Summary of Edinburgh paper

SPECTROPHOTOMETRIC MEASUREMENTS OF EARLY-TYPE STARS*

VI. Results and Discussion for 25 Stars of MK Type B3

H. E. Butler and H. Seddon

Summary

Equivalent widths are given for 80 absorption and emission lines in the spectra of 25 stars of MK type B3. These have been reduced in a way comparable with that used for the B2 stars in the previous paper of this series.

As compared with the B2 stars, the strength of the hydrogen lines has increased while there is an indication that the strength of the He I lines has slightly decreased. The absorption lines of N II, O II, Si III, and S III are decreasing in strength as we move to later types, but within the B3 subtype their dependence on luminosity is unaltered. There is no change in the C II lines although the behaviour of 6578–6583 seems anomalous. The lines of Mg II and Si II in the dwarfs do not appear to have altered but the amount in the supergiants may have increased by as much as 100 per cent over that of the B2 supergiants. The Fe II emission is still present in those dwarfs that show Hα emission and there is the first suspicion of Fe II absorption in the supergiants.

The measured interstellar lines and bands now include the region 4890 which is assumed interstellar from the similarity of its behaviour to that of the other bands. Analysis of these data does not amplify the conclusions already reached in earlier papers.

The amount of Hα emission in two of the dwarf stars changed while the sequence of spectra were being photographed. Spectra taken before and after the change have been analysed: it appears that only the Balmer lines were affected.

* The full text of this paper appears in *Publications of the Royal Observatory, Edinburgh*, **2**, No. 5, 1960.